

dissertation, December 2007

Odd frequency superconductivity in
symmetry breaking systems

Takehito Yokoyama

Department of Applied Physics,
Nagoya University

Contents

1	Introduction	1
1.1	Superconductor —history and classification	1
1.2	Mesoscopic superconductivity	9
1.2.1	Proximity effect	11
1.2.2	Josephson effect	19
1.3	Vortex	20
1.4	Nonequilibrium Green’s functions formalism	24
1.4.1	Keldysh formalism	27
1.4.2	Gor’kov equation	29
1.4.3	Quasiclassical approximation	31
1.5	Purpose and outline of this thesis	35
2	Resonant proximity effect in normal metal / diffusive ferromagnet / superconductor junctions	45
2.1	Introduction	45
2.2	Formulation	47
2.3	Results	51
2.3.1	Conditions for the formation of zero-energy peak in DOS	52
2.3.2	Junctions with s -wave superconductors	58
2.3.3	Junctions with d -wave superconductors	66
2.4	Conclusions	71
3	Manifestation of the odd-frequency spin-triplet pairing state in diffusive ferromagnet/superconductor junctions	79
3.1	Introduction	79
3.2	Formulation	81
3.3	Results	87
3.3.1	Spin singlet s -wave superconductor junctions	88
3.3.2	Spin-triplet p -wave superconductor junctions	90
3.3.3	Relevance of the odd-frequency component to ZEP of LDOS	96

3.4	Conclusions	96
4	Odd-frequency pairing state inside the Abrikosov vortex core	103
4.1	Introduction	103
4.2	Formulation	104
4.3	Results	105
4.4	Conclusions	113
5	Chirality sensitive effect on surface state in chiral p-wave superconductors	119
5.1	Introduction	119
5.2	Formulation	120
5.3	Results	122
5.4	Conclusions	129
5.5	Appendix: Basic properties of Riccati parameters from the Eilenberger equations	129
6	Summary and outlook	135

Chapter 1

Introduction

1.1 Superconductor — history and classification

In 1957, Bardeen, Cooper and Schrieffer (BCS) completed the microscopic theory of the superconductivity.[1] According to their theory, the phonon-mediated electron-electron interaction leads to the formation of Cooper pair below the transition temperature. Since this interaction is isotropic, the pairing state is also isotropic *s*-wave symmetry and spin-singlet. This theory successfully explains the energy gap in the density of states. The kind of superconductors described by the BCS theory are dubbed *conventional* superconductors.

A new paradigm has come in 1986, the discovery of the cuprate high-temperature superconductors.[2] Remarkably, these superconductors have a high transition temperature which can exceed even 100 K. The discovery of high-temperature superconductivity in the cuprates caused a flurry of activity in various subfields of condensed-matter research, stimulating not only studies of the basic mechanisms leading to this phenomenon, but also a widespread search for new technological applications. An essential difference of the cuprates from conventional superconductors is the symmetry of the Cooper pairs: they have *unconventional d*-wave symmetry. In addition to the cuprates, exotic superconductors have been discovered to this date, such as heavy-fermion and organic superconductors, and Sr_2RuO_4 . For many of these superconductors, the pairing symmetry is no longer *s*-wave and they are known to have unconventional superconductivity.

Sr_2RuO_4 discovered in 1994 [3] is believed to have chiral *p*-wave pairing. It has a layered perovskite structure common to ruthenate and cuprate superconductors as shown in Fig. 1.1. Let us introduce *d*-vector, a useful

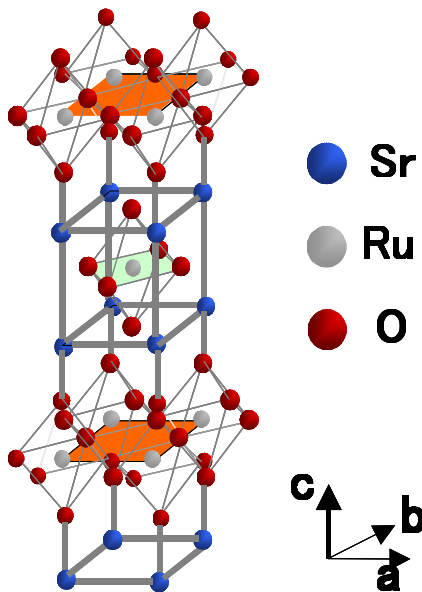


Figure 1.1: Crystal structure of Sr_2RuO_4 .

representation of pair potential. Below, $\hat{\cdot}$ means 2×2 matrices in spin space. Pair potential has the form in general:

$$\hat{\Delta}(\mathbf{k}) = i [\Delta_{\mathbf{k}} \hat{\sigma}_0 + \mathbf{d}_{\mathbf{k}} \cdot \hat{\boldsymbol{\sigma}}] \hat{\sigma}_2 \quad (1.1)$$

where $\hat{\sigma}_j$ ($j=0, 1, 2, 3$) are Pauli matrices. For spin-singlet pairing, $\Delta_{\mathbf{k}}$ is nonzero and $\mathbf{d}_{\mathbf{k}}$ is zero. For spin-triplet pairing like Sr_2RuO_4 , $\mathbf{d}_{\mathbf{k}}$ is nonzero while $\Delta_{\mathbf{k}}$ becomes zero. In this way, $\mathbf{d}_{\mathbf{k}}$ features the pair potential in triplet superconductors where the spin of Cooper pair is perpendicular to $\mathbf{d}_{\mathbf{k}}$. To unveil the d -vector of Sr_2RuO_4 , NMR Knight shift[4](see Fig. 1.2), μSR [5] or other experiments[6] have been performed. As a result, it is now believed that the d -vector of Sr_2RuO_4 is given by

$$\mathbf{d} = z \Delta_0 (\bar{k}_x \pm i \bar{k}_y), \bar{k}_j = \frac{k_j}{k_F}. \quad (1.2)$$

This pairing is called chiral p -wave pairing due to the chirality of the d -vector.

Now, for a general classification of the unconventional superconductors, we will discuss the symmetry in the superconducting states. According to the Landau theory, the symmetry breaking is often accompanied with a phase transition, which means when the system undergoes a phase transition, some symmetries possessed by the system before can be lost. For the

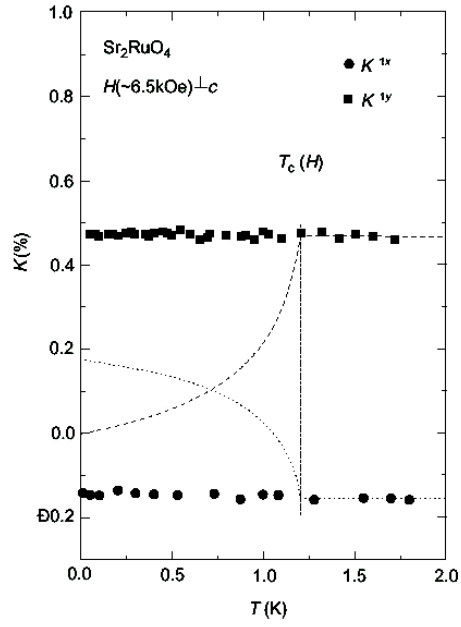


Figure 1.2: Knight shift data of Sr_2RuO_4 which supports triplet pairing [4].

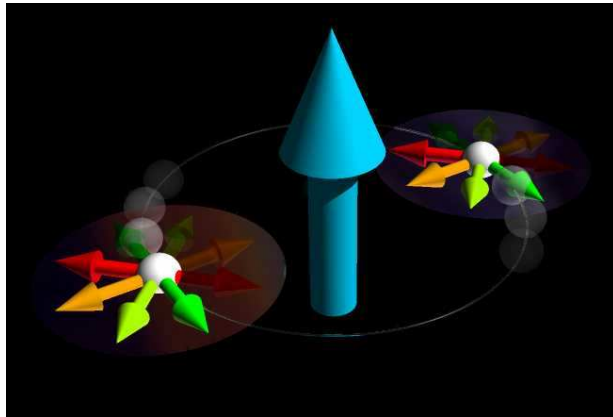


Figure 1.3: Sketch of d -vector in Sr_2RuO_4 . [6]

second-order phase transition, the symmetry breaking across the transition is continuous and thus the symmetry group after the breaking becomes a subgroup of the full symmetry group. The full symmetry group \mathcal{G} is given by $\mathcal{G} = G \times R \times U(1) \times T$ where G is the point group symmetry of the crystal lattice, R is the symmetry of spin rotation, $U(1)$ is the one-dimensional global gauge symmetry, and T is the time-reversal symmetry. Consider symmetry group \mathcal{G}_1 which is reduced to symmetry group \mathcal{G}_2 ($\mathcal{G}_2 \subset \mathcal{G}_1$) by a symmetry breaking. Then, quotient space $\mathcal{G}_1/\mathcal{G}_2$ represents the order parameter space. The $U(1)$ symmetry is broken spontaneously by the phase coherence in the superconducting state. Hence, in a superconducting transition, we have $\mathcal{G}_1 = G \times R \times U(1) \times T$ and $\mathcal{G}_2 = G \times R \times T$ and therefore the order parameter space is $\mathcal{G}_1/\mathcal{G}_2=U(1)$. In a conventional superconductor, symmetries other than $U(1)$ are kept, but more detailed symmetry classification is required in general. By determining the symmetry properties of the order parameter besides $U(1)$, we can classify the unconventional superconductors in a transparent manner.

A simple classification of the superconductors can be made based on the parity of the pairing state in space. Since in the superconducting state, the electrons form the Cooper pairs whose total spin S is an integer. Therefore, we have the spin-singlet ($S = 0$) with even parity or the spin-triplet ($S = 1$) with odd parity. When S is fixed, the total orbital angular momentum L of the Cooper pair is determined according to the Fermi statistics. For spin-singlet, L should be an even integer, while for spin-triplet, L should be an odd integer. In conventional superconductors, both S and L are zero and the pairing is known as s -wave in analogy to atomic orbitals. It is believed that the pairing in the high-Tc cuprate has d -wave symmetry ($S = 0$ and $L = 2$), and Sr_2RuO_4 favors the p -wave symmetry ($S = 1$ and $L = 1$).

In addition to the above-mentioned superconductors, disordered superconductors are also of great interest for theoretical reasons, because they represent new symmetry classes in disordered non-interacting fermion problems that are not realized in metals.[7] The study of symmetry classes in disordered or chaotic systems dates back to 1962. In 1962, following the early work of Wigner[8], Dyson classified complex many-body systems such as atomic nuclei according to their fundamental symmetries.[9] Arguing on mathematical grounds, he proposed the existence of three symmetry classes, which are distinguished by their behavior under reversal of the time direction and by their spin. The statistical properties of these classes are described by three random-matrix models, called the Gaussian orthogonal, unitary, and symplectic ensembles. The Wigner-Dyson statistics of disordered or chaotic single-particle systems applies to the ergodic limit, i.e., to times long enough for the degrees of freedom to equilibrate and fill the available phase space

uniformly. More specifically, in the context of disordered mesoscopic systems, the ergodic limit is reached for times larger than the diffusion time L^2/D , where D is the diffusion constant and L the linear extension of the system. By the uncertainty relation, the ergodic limit corresponds to the energy range below the Thouless energy D/L^2 .

However, the symmetry classes in Wigner-Dyson statistics do not exhaust the number of possible universality classes in disordered single-particle systems; new universality classes are found out in dirty superconductors. In dirty superconductors, the momentum k of a single particle is no longer a good quantum number. The plain-wave eigenfunctions with momentum k should be replaced by position-dependent functions and pairing is between time-reversed states. To find these functions, one needs to set up equations for them. This is achieved by generalizing the Hartree-Fock equations to include the pairing potential of the superconducting state. The resulting equations are called Bogoliubov-de Gennes (BdG) equations. These equations are widely applied to more general situations with order parameter varying in space (such as the normal metal/superconductor junction or vortex state). Since the elementary excitation (quasiparticle) of superconductors can be viewed as destroying a Cooper pair from the condensate and creating an electron in the vacancy, the BdG equations are often used to describe the behavior of the quasiparticles in the superconductors. At the same time, the properties of the dirty superconductor and its classification will be determined by the BdG equations, where pairing symmetry is reflected. A classification of the symmetry classes in dirty superconductors have been advanced recently. Depending on the existence (or the lack) of time reversal and spin rotation symmetries, dirty superconductors can be classified into four symmetry classes, CI, DIII, C, and D in Cartan's classification scheme (Table 1.1). Hence, the situation is different from the Wigner-Dyson scenario[8, 9] where only three distinct classes -the Gaussian orthogonal, unitary, and symplectic ensembles- exist. These classes are believed to complete the possible universality classes in disordered single-particle systems.

Table 1.1: Symmetry classes of dirty superconductors.[7]

Class	Time reversal	Spin rotation	Symmetric space
D	No	No	SO(4N)
C	No	Yes	Sp(2N)
DIII	Yes	No	SO(4N)/U(2N)
CI	Yes	Yes	Sp(2N)/U(N)

The interplay of superconductivity and disorder has also triggered an interesting subject of superconductor-insulator transition. Disorder is expected to enhance the electrical resistance of a system, while superconductivity leads to a zero-resistance state. Although superconductivity has been predicted to persist even in the presence of disorder,[10] experiments performed on thin films have demonstrated a transition from a superconducting to an insulating state with increasing disorder or magnetic field.[11] However, the mechanism of this transition is still under debate.[12]

By now, we have discussed superconductors where symmetries other than $U(1)$ are kept. Other kinds of superconductors with multiple broken symmetry ($U(1)$ plus other symmetries) also show rich physics. Let us first consider Cooper pairs with a nonzero total momentum, where translational symmetry is broken. This situation arises when we turn on the magnetic field H and split the Fermi surfaces of the spin-up and -down electrons apart, which leads to a finite center of mass momentum. In this case, we have the BCS state, the spin polarized state (normal state), and possibly more states to compete for the ground state. When the magnetic field H is strong (weak) enough, the spin polarized (BCS) state will be favored. In the intermediate region of H , it is suggested by Fulde and Ferrell,[13] and Larkin and Ovchinnikov[14] that pairing electrons of opposite spins located close to their own Fermi surfaces may lower the energy (see Fig.1.4). Since the paired electrons have different momenta, there will be a net momentum in the Cooper pair and it causes the oscillation of the order parameter. This state is now known as the Fulde-Ferrell-Larkin-Ovchinnikov (FFLO) state. It breaks both translational and rotational symmetries. Though the FFLO state was studied theoretically in an earlier time, lack of experimental support in the conventional superconductors has made it overlooked for a long time. The situation has been changed by experimental results suggestive of the FFLO state in heavy fermions, quasi-1D organic, or high-Tc superconductors.[15] Recent experimental results in CeCoIn₅, a quasi-2D d -wave superconductor, are particularly encouraging. This subject is also of interest to the nuclear and particle physics communities because of the possible realization of the FFLO state in high density quark matter and nuclear matter, as well as in cold fermionic atom systems.[16] On the theoretical side, more suggestions dealing with the pairing between unbalanced fermions are also proposed, such as the deformed Fermi surface pairing and the breached pairing states. To classify and discuss the relation between these different phases, more classification schemes beyond the Landau theory are necessary and this will serve to enhance our understanding of the quantum phases and the phase transitions.[17]

Besides the FFLO states, there are other types of intriguing superconductors with multiple broken symmetry, like ferromagnetic superconductors

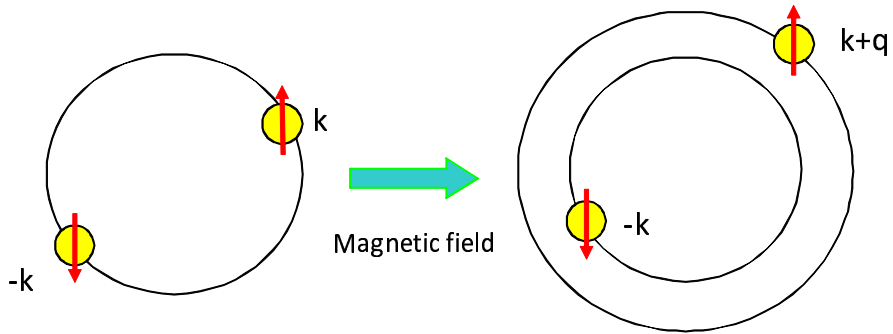


Figure 1.4: Schematic of the formation of FFLO state. The Cooper pairs in the FFLO state have a finite center of mass momentum.

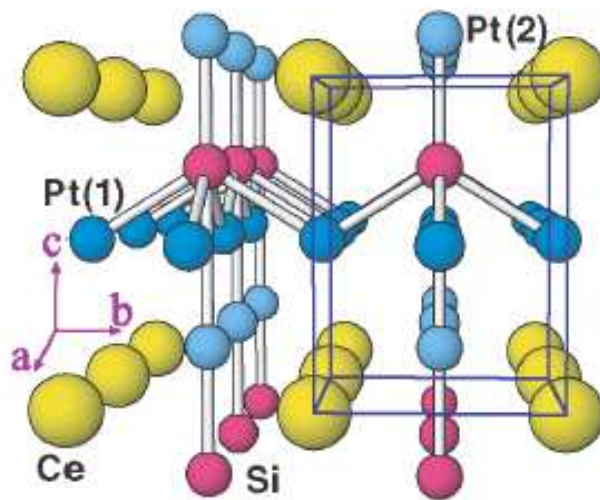


Figure 1.5: Crystal structure of CePt₃Si.[25]

or noncentrosymmetric superconductors, which have received a tremendous interest. Magnetism and superconductivity have long been under intensive pursuit in the field of low temperature physics. After the advent of the BCS theory, it became clear that superconductivity in the singlet state could also be destroyed by an exchange field. The exchange field, in a magnetically ordered state, tends to align spins of Cooper pairs in the same direction, thus preventing a pairing effect. This is the so-called paramagnetic effect which demonstrates that ferromagnetic ordering is unlikely to appear in the superconducting phase. In such a situation the energy for ferromagnetic ordering decreases and, instead of ferromagnetic order, nonuniform magnetic ordering should appear. Anderson and Suhl called this state *cryptoferromagnetic*. [18]

Meanwhile, superconductivity and antiferromagnetism can coexist quite peacefully because, on average, the exchange and orbital fields are zero at distances of the order of the Cooper pair size or superconducting coherence length. Actually experimental evidences of magnetism and superconductivity coexisting in some ternary rare-earth compounds were reported. [19] However, the interplay of ferromagnetism and superconductivity, albeit antagonistic orders, has recently attracted much attention because nontrivial phenomena are predicted or found experimentally. Such phenomena are expected to occur in ferromagnet/superconductor junctions [20, 21] and also in ferromagnetic superconductors. Ferromagnetic superconductors are likely to have triplet pairings since triplet pairings and ferromagnetism can coexist. Up to now, several bulk materials, e.g., UGe_2 [22], ZrZn_2 [23] and URhGe [24], are identified as ferromagnetic superconductors.

Recent discovery of heavy fermion superconductor CePt_3Si has also opened up a new field of the study of superconductivity. [25] This is because this material does not have inversion center (see Fig.1.5). After this discovery, other novel heavy fermion superconductors without inversion symmetry such as UIr , CeRhSi_3 , and CeIrSi_3 have been discovered. [26, 27, 28] Also, in non- f -electron systems, new noncentrosymmetric superconductors such as $\text{Cd}_2\text{Re}_2\text{O}_7$, $\text{Li}_2\text{Pd}_3\text{B}$, and $\text{Li}_2\text{Pt}_3\text{B}$ have been discovered. [29, 30, 31, 32] Because of the broken inversion symmetry, Rashba type spin-orbit coupling is induced, [33, 34] and hence different parities, spin-singlet even-parity pairing and spin-triplet odd-parity pairing, can be mixed in superconducting state. [35] From a lot of experimental and theoretical studies, it is believed that the most possible candidate of superconducting state in CePt_3Si is $s+p$ -wave pairing. In general, $d+f$ -wave pairing or other mixtures are allowed in noncentrosymmetric superconductors depending on material parameters. [36]

All the superconductors mentioned above are even-frequency superconductors. Recently, there has been a growing attention to the so-called *odd-frequency* pairing, which means that the Cooper pair wavefunction is sym-

metric under exchange of spatial- and spin-coordinates, but antisymmetric under exchange of time-coordinates (see Table 1.2 for a general classification of superconductors). This exotic state had been theoretically proposed to exist by Berezinskii a few decades earlier in the context of liquid ^3He . [37] Recently, the presence of odd-frequency pairing was predicted in ferromagnet/conventional superconductor junctions due to the breakdown of symmetry in spin space. [21] Consequently, strong experimental evidence of the existence of odd-frequency pairing has been reported. [38, 39] Motivated by this, it is found that odd-frequency pairing exists near the interface in normal metal/superconductor junctions due to the violation of translational symmetry. [40] Hence, we see that symmetry breaking more than $U(1)$ is an important ingredient for the presence of odd-frequency pairing.

Table 1.2: Symmetry classifications of superconductors. Generally, superconductors are classified into four classes.

Spin	Orbit	Matsubara frequency
Singlet	Even	Even
Triplet	Odd	Even
Singlet	Odd	Odd
Triplet	Even	Odd

The study of multiple symmetry breaking systems may be related to the emerging field of complexity in strongly correlated electronic systems. [41] A wide variety of recent intensive studies have convincingly demonstrated that several transition metal oxides and other materials have dominant states that are not spatially homogeneous. This occurs in cases in which several physical interactions –spin, charge, lattice, and/or orbital– are simultaneously active. This phenomenon causes interesting effects, such as colossal magnetoresistance, and it also appears crucial to understand the high-temperature superconductors.

1.2 Mesoscopic superconductivity

The field of mesoscopic physics has started from the study of phase coherent effects at low temperatures. [42] In the last twenty years, remarkable technological improvements allowed to fabricate structures of mesoscopic size in a controllable way. At present, a variety of mesoscopic systems like single electron transistors, quantum wires, quantum dots, quantum Hall systems,

normal metal-superconductor-ferromagnet hybrid structures, magnetic multilayer systems, charge density waves, carbon nanotubes, graphene, small metallic nanoparticles and nanomechanical systems, are being intensively investigated both experimentally and theoretically. [43] In the past, experimental studies of quantum phenomena were limited to natural systems such as atoms and molecules. An important advantage of the artificial systems compared to the natural systems is that their transport properties can be measured in a more controllable way. The field of the mesoscopic physics has now been matured, profoundly overlapping with other fields, e.g., superconductivity, magnetism,[44, 45] random matrix theory[46] or quantum chaos. [47] The field of the mesoscopic physics in superconducting systems is called *mesoscopic superconductivity*. Mesoscopic effects show up in the transport properties of mesoscopic devices, e.g. current or noise. A marked example seen in superconducting systems is the Andreev reflection (AR).[48]

In normal metal / superconductor junctions, AR is one of the most important processes for low energy transport. The AR is a process that an injected electron is converted into a reflected hole at the interface. Therefore, the AR can double the conductance. We show a schematic illustration of the AR in Fig. 1.6. Taking the AR into account, Blonder, Tinkham and Klapwijk proposed the formula for the calculation of the tunneling conductance[49]. This method makes it possible to clarify the energy gap profile of superconductors.

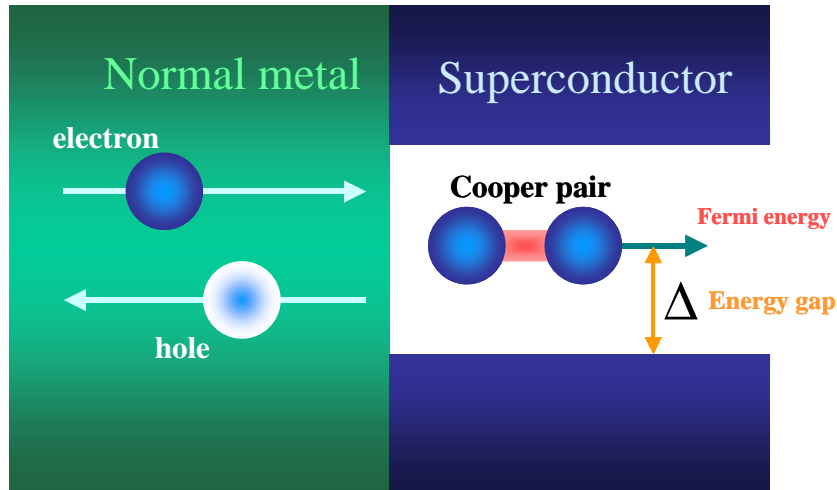


Figure 1.6: Schematic of Andreev reflection.

1.2.1 Proximity effect

Proximity effect in conventional superconductor junctions

Proximity effect is defined as a phenomenon that Cooper pairs penetrate into normal metal from superconductor (see Fig. 1.7). Here, the coherence length is given by $\sqrt{D/2\pi T}$ with diffusion constants D and temperature T . Proximity effect influences crucially junction properties, e.g. density of states in the normal metal or junction conductance. Due to the penetration of the Cooper pairs, the density of states in the normal metal is strongly modified and mimics that in the superconductor[50] as shown in Fig. 1.8. To elucidate how the proximity effect influences the charge transport, in 1991, Kastalsky et al. measured conductance in normal metal/superconductor (InGaAs/Nb) junctions[51]. As seen in Fig. 1.9, they found a zero bias conductance peak (ZBCP) due to the proximity effect in the junctions. This is understood, as illustrated in Fig. 1.10, by interference effect of electrons and holes. Consider at point a , where an electron is Andreev or normally reflected. Normally reflected electron is again Andreev or normally reflected at point b . Then, Andreev reflected electron can come back along the same path due to the retroreflectivity. In this way, two holes interfere with each other, which results in the enhancement of Andreev reflection probability. At zero bias voltage, retroreflectivity is complete and hence ZBCP appears.[52, 53] This was confirmed by quasiclassical Green's function method by Volkov et al. [54] Proximity effect is a basic concept widely used to interpret physical phenomena in superconducting junctions.

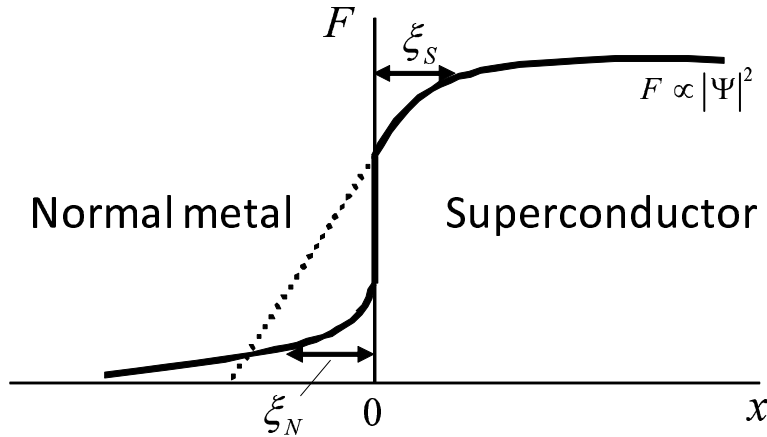


Figure 1.7: Schematic of proximity effect. F is anomalous Green's function.

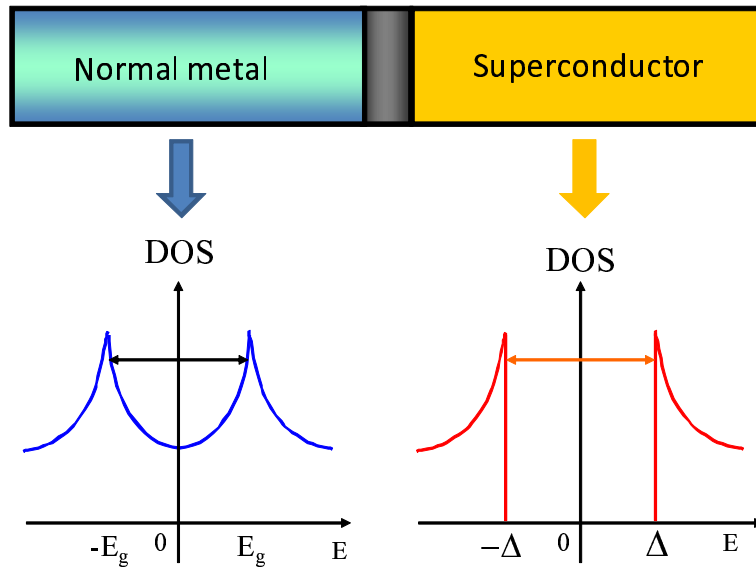


Figure 1.8: Schematic of the mini gap. The density of states (DOS) in the normal metal mimics that in the superconductor. The characteristic energy in the gap-like structure is called *minigap*(E_g).

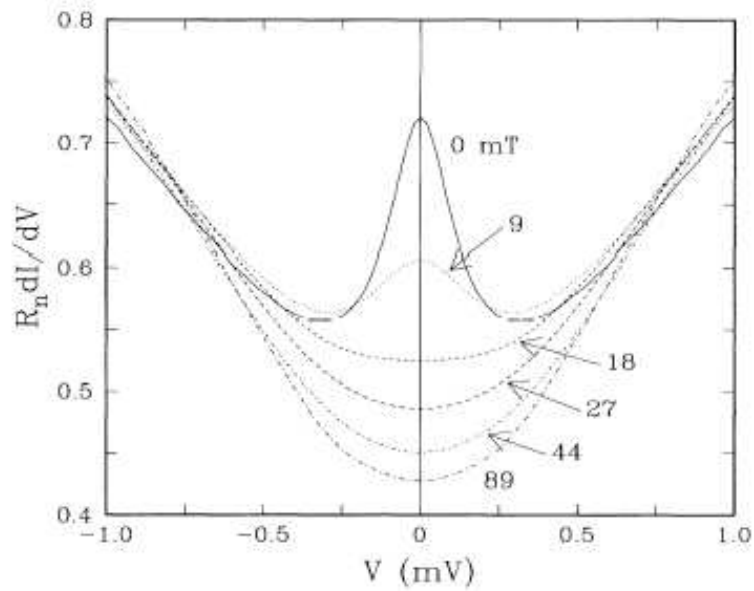


Figure 1.9: Conductance in InGaAs/Nb junction[51].

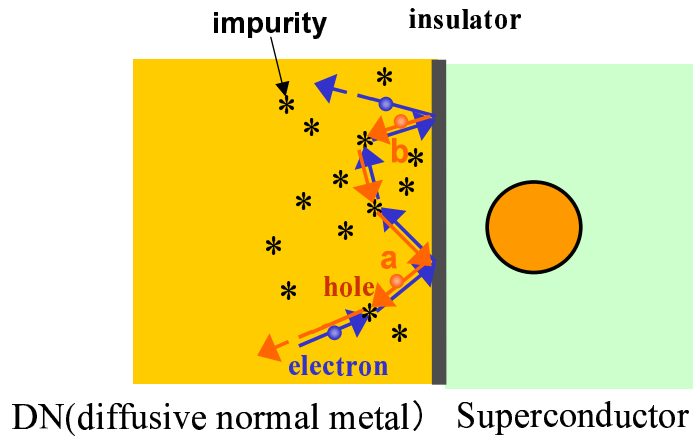


Figure 1.10: Schematic of the interference which leads to ZBCP.

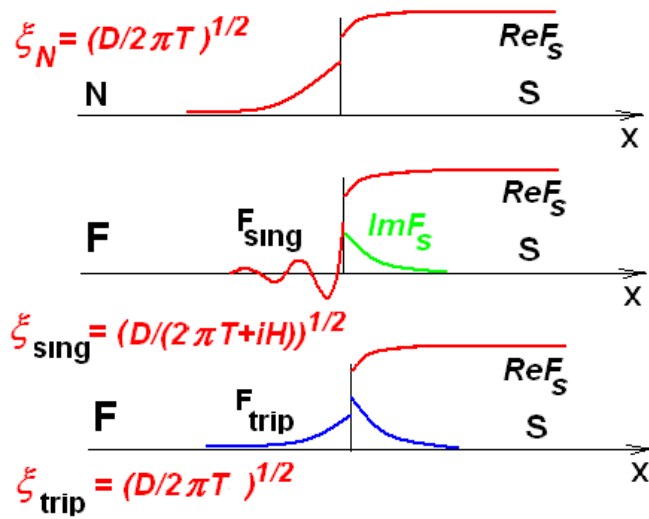


Figure 1.11: Sketch of the penetration of Cooper pairs. ξ , D , T and H denote the coherence length, diffusion constant, temperature, and exchange field, respectively. Also, N, F and S denote normal metal, ferromagnet and superconductor, respectively. The middle (lower) panel shows the penetration of single (triplet) Cooper pairs.

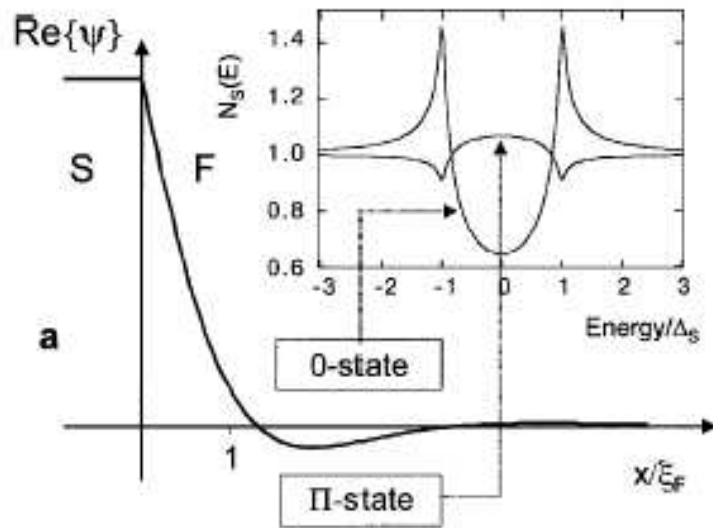


Figure 1.12: Exponentially damped oscillations of the real part of the superconducting order parameter induced into a ferromagnetic material by proximity effect. The space coordinate x denotes the distance from the superconductor/ferromagnet interface. The period of the oscillations is set by the coherence length ξ_F . 0 state and π state correspond to positive and negative signs of the real part of the order parameter, respectively. Inset: superconducting density of states at zero temperature in the 0 and π states for an exchange energy much larger than the energy gap. [57]

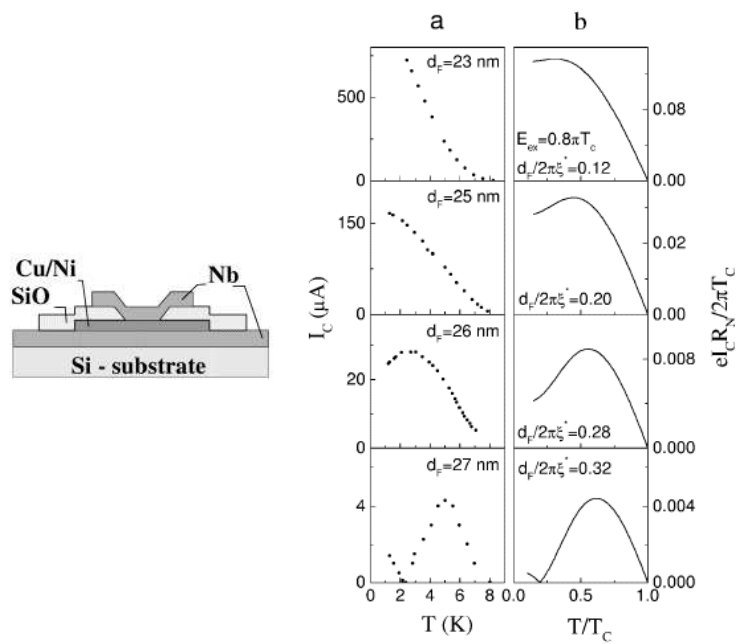


Figure 1.13: (a) Critical current I_c as a function of temperature for Nb/CuNi/Nb junctions with different ferromagnet-layer thicknesses between 23 and 27 nm as indicated. (b) Model calculations of the temperature dependence of the critical current in a superconductor/ferromagnet/superconductor junction.[58]

In ferromagnet/supereconductor junctions, the proximity effect is qualitatively changed. Due to the presence of the exchange field, the induced Cooper pairs in the ferromagnet have nonzero center of mass momentum, similar to the FFLO state. Also, since triplet pairings can survive the exchange field, they can penetrate deeply into the ferromagnet compared to the singlet pairings. This triggered the study of *long range proximity effect*. [21, 55, 56] See the sketch of the penetration of Cooper pairs in Fig. 1.11. The oscillations of the condensate function (anomalous Green's function) in the ferromagnet due to the nonzero center of mass momentum lead to interesting peculiarities. The sign-changed state of the condensate function due to the oscillations is found to make a qualitative change in the density of states in the ferromagnet, as confirmed experimentally in PdNi/Nb junctions (see Fig. 1.12). [57] The Josephson current in supereconductor/ferromagnet/supereconductor junctions also shows oscillatory behavior as a function of the temperature [58] as shown in Fig. 1.13.

Proximity effect in unconventional superconductor junctions

Proximity effect in unconventional superconductor junctions is quite different from that in conventional superconductor junctions. It is clarified that the mid gap Andreev resonant state (MARS) formed at the interface [59] competes with the proximity effect in d -wave junctions [60] while MARS enhances it in p -wave junctions [61]. This plays a pivotal role on the junction properties. Let us discuss this effect in more detail.

Figure 1.14 shows the local density of states $\rho(\varepsilon)$ in the diffusive normal metal (DN) of DN/ p_x -wave superconductor junctions. As is seen, a zero energy peak appears which is stronger near the DN/ p_x -wave superconductor interface.

On the other hand, in DN/ d -wave superconductor junctions, we will see different characteristics. We have chosen d -wave superconductor with $\Delta_{\pm} = \Delta_0 \cos[2(\theta \mp \alpha)]$. For $\alpha = 0$, MARS is absent and proximity effect becomes conventional one. In this case, $\rho(\varepsilon)$ at $x = -L/4$ has a gap like structure (curve a in the left panel of Fig. 1.15). Although $\rho(\varepsilon)$ at $x = -L/4$ has a broad peak like structure for $\alpha = \pi/8$, $\rho(0) \leq 1$ is satisfied contrary to the DN/ p_x -wave superconductor junction. For $\alpha = \pi/4$, due to the absence of the proximity effect, $\rho(\varepsilon) = 1$ for any case. Thus, we can conclude that line shapes of $\rho(\varepsilon)$ in DN region of DN/ p_x -wave superconductor junctions are significantly different from those of DN/ d -wave superconductor junctions.

Most striking feature is seen in the resistance R . The zero-voltage resistance as a function of R_d/R_b (R_d and R_b are resistances of the DN and the barrier at the DN/ p -wave interface, respectively) is depicted in Fig. 1.16 for

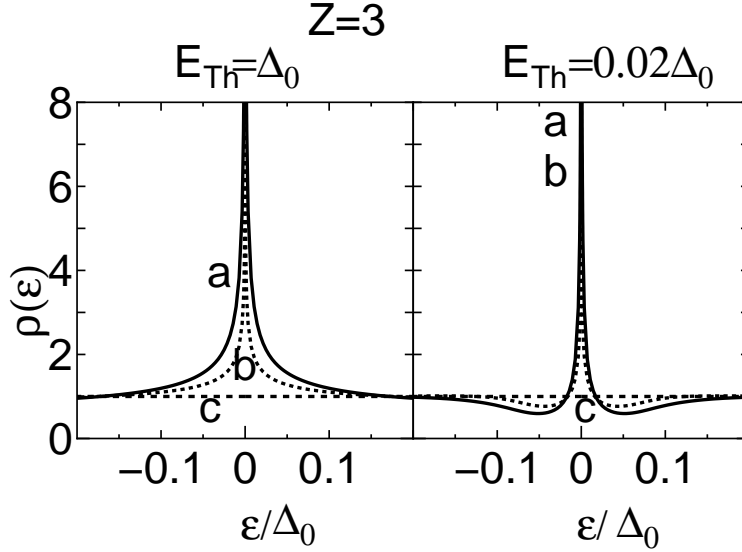


Figure 1.14: Normalized local density of states $\rho(\varepsilon)$ in the DN of DN/ p_x -wave superconductor junctions for (a) $x = -L/4$; (b) $x = -L/2$; and (c) $x = -L$. [61] DN/ p_x -wave superconductor interface is located at $x = 0$ while the other end of DN is located at $x = -L$.

the DN/ p -wave superconductor junctions with the p_y -wave and the p_x -wave cases (curves a and b of Fig. 1.16). For the p_y -wave case, R increases linearly as a function of R_d , where no proximity effect appears (curve a of Fig. 1.16). For the p_x -wave case, R is independent of R_d (curve b of Fig. 1.16). This anomalous R dependence is a most striking feature by the enhanced proximity effect by the MARS. The corresponding result for the DN/ s -wave superconductor junctions (curve c) and DN/ d_{xy} -wave superconductor junctions (curve d) is also plotted as a reference. For s -wave case, it is well known that R has a reentrant behavior $\partial R/\partial R_d|_{R_d=0} < 0$ as shown in curve c of Fig. 1.16. In p -wave cases, this reentrant behavior of R does not appear. For d_{xy} -wave case, due to the formation of the MARS as in the case of p_x -wave junction, R at $R_d = 0$ is identical to that for p_x -wave junction (curve b of Fig. 1.16). However, for nonzero R_d , R/R_b increases linearly with R_d/R_b due to the absence of the proximity effect.

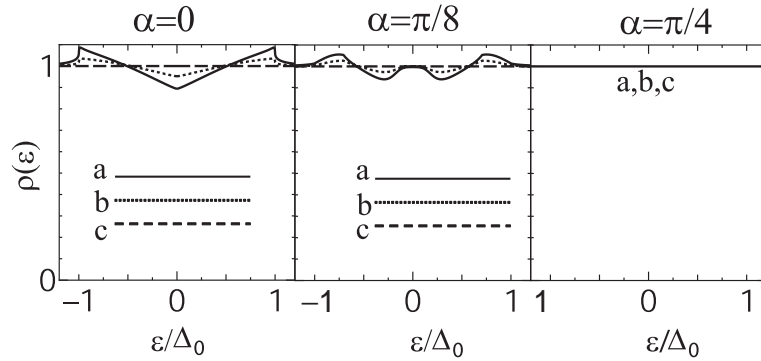


Figure 1.15: Normalized local density of states $\rho(\varepsilon)$ in DN for DN/ d -wave superconductor junction. We have chosen d -wave superconductor with $\Delta_{\pm} = \Delta_0 \cos[2(\theta \mp \alpha)]$. $\alpha = 0$ (left panel), $\alpha = \pi/8$ (middle panel), and $\alpha = \pi/4$ (right panel). a, $x = -L/4$; b, $x = -L/2$; and c, $x = -L$. [61] DN/ d -wave superconductor interface is located at $x = 0$ while the other end of DN is located at $x = -L$.

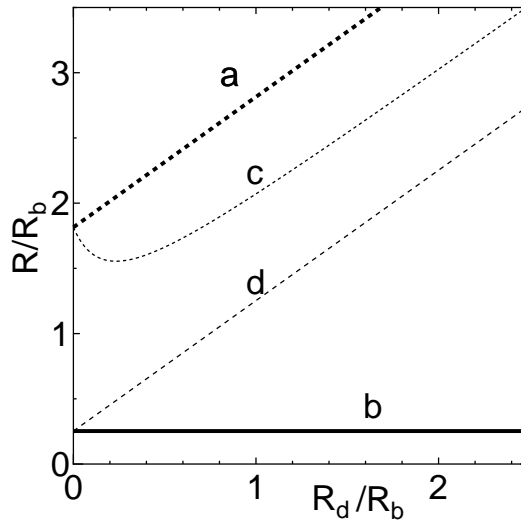


Figure 1.16: Total zero voltage resistance of the junctions R is plotted as a function of R_d/R_b with a, p_y -wave; and b, p_x -wave. The curves c and d represent the dependence for the DN/ s -wave superconductor junctions and DN/ d_{xy} -wave superconductor junctions, respectively. [61]

1.2.2 Josephson effect

The macroscopic phase coherence in superconducting state also manifests itself in Josephson effect. In 1962, Josephson published his celebrated paper and concluded the followings[62]

1. current flows between superconductors with different phases φ_L and φ_R at zero voltage, depending on the phase difference $\varphi_0 = \varphi_L - \varphi_R$ (dc Josephson effect).
2. when applying a bias voltage V , alternating current flows with frequency proportional to V (ac Josephson effect).

Fundamental equations for Josephson effect are

$$J = J_C \sin \varphi, \quad (1.3)$$

$$\varphi = \varphi_0 + \frac{2e}{\hbar} \int_0^t V dt. \quad (1.4)$$

Especially, when $V = \text{const.}$ we obtain

$$J = J_C \sin \left[\left(\frac{2eV}{\hbar} \right) t + \varphi_0 \right]. \quad (1.5)$$

After the discovery of the Josephson effect, it has been under intensive investigation. General properties of Josephson current clarified can be summarized as follows:[63]

(1) A change of phase of the order parameter of 2π in any of the electrodes is not accompanied by a change in their physical state. Consequently, this change must not influence the supercurrent across a junction, which should be a 2π periodic function, $J(\varphi) = J(\varphi + 2\pi)$.

(2) Changing the direction of a supercurrent flow across the junction must cause a change of the sign of the phase difference; therefore $J(\varphi) = -J(-\varphi)$. Note that this is violated in superconductors with broken time-reversal symmetry, leading to spontaneous currents.

(3) A dc supercurrent can flow only if there is a gradient of the order-parameter phase. Hence, in the absence of phase difference, $\varphi = 0$, there should be zero supercurrent, $J(2\pi n) = 0, n = 0, \pm 1, \pm 2, \dots$

(4) It follows from (1) and (2) that the supercurrent should also be zero at $\varphi = n\pi, J(\pi n) = 0, n = 0, \pm 1, \pm 2, \dots$

As follows from Eqs. (1)-(4), $J(\varphi)$ can in general be decomposed into a Fourier series

$$J(\varphi) = \sum_{n \geq 1} \{I_n \sin(n\varphi) + J_n \cos(n\varphi)\} \quad (1.6)$$

where I_n and J_n are coefficients to be determined. The J_n vanish if time-reversal symmetry is not broken.

1.3 Vortex

Superconductors under magnetic fields show the so-called Meissner effect, that is, the magnetic fields applied to superconducting material are expelled from the inside of the material. Some superconductors, called type I exhibit a perfect Meissner effect up to a critical field H_c , and at this critical field the transition to the normal state takes place. In the other superconductors, called type II, magnetic fields are excluded up to a lower critical field H_{c1} , and at an upper critical field H_{c2} the superconductivity is broken. In the intermediate field region $H_{c1} < H < H_{c2}$, the magnetic field partly penetrates into the material keeping the superconductivity. The magnetic fields penetrate into the superconductors in the form of quantized flux lines which have a topological nature, classified according to one dimensional homotopy group π_1 in the order parameter space. These two types of superconductors are characterized by the Ginzburg-Landau parameter κ which is defined by the ratio of the penetration depth and the coherence length. Namely, if $\kappa < (>)1/\sqrt{2}$, the superconductor is type-I(II). The quantized flux lines show characteristic phenomena in type-II superconductors, and a system constituted of such flux lines has a variety of physical aspects. Around the flux line, the supercurrent circularly flows and the order parameter of superconductivity varies by $2\pi n$ in its phase (n is an integer). The structure of such a flux line is called vortex, and the superconducting state at $H_{c1} < H < H_{c2}$ is called vortex state.

Because superconducting gap Δ has a spatial dependence in the vortex state, it is expected that some kind of the quantum well is formed and the quantized energy levels due to the well will appear in the well (see Fig. 1.17). Around a vortex, the phase of the order parameter Δ varies by 2π with a rotation about the vortex center when one quantum flux penetrates there. Taking the z -axis in the direction of the flux line with cylindrical coordinates $r = (r, \theta, z)$, the order parameter Δ around a vortex is expressed as $\Delta(r) = |\Delta(r)| \exp(i\theta)$. Because of the indeterminacy of the phase factor $\exp(i\theta)$ at the vortex center $r = 0$, the magnitude of the gap becomes zero inevitably. Thus, the gap $\Delta(r)$ is $\Delta(0) = 0$ at the vortex center, and far from the vortex it recovers to the uniform value Δ . This spatial structure of the energy gap gives rise to low-energy bound states below the gap around a vortex as in the quantum well systems.

The existence of the low-energy bound states around a vortex was first

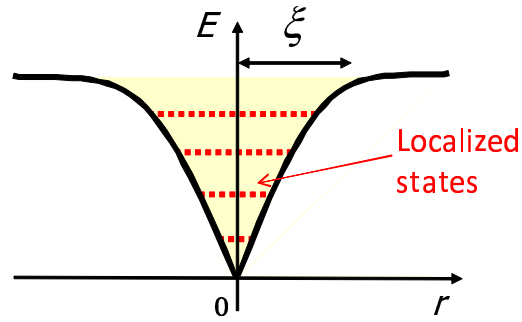


Figure 1.17: Schematic of Andreev bound states.

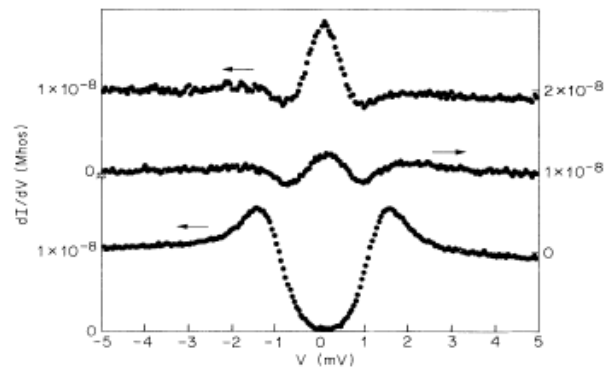


Figure 1.18: dI/dV vs V for NbSe_2 , taken at three positions: on a vortex (top curve), about 75 \AA from a vortex (middle), and 2000 \AA from a vortex (bottom). The zero of each successive curve is shifted up by one quarter of the vertical scale.[65]

discussed from a microscopic model in 1964 by Caroli, de Gennes, and Matricon[64]. Energy spectra in spatially inhomogeneous superconductors can be obtained as the eigenenergy spectra of the Bogoliubov-de Gennes (BdG) equation. The BdG equation corresponds to the Schrödinger equation for superconducting systems. Caroli et al. applied the BdG equation to a vortex system and found low-energy excited states bounded around the vortex.[64] These bound states due to vortices are dubbed *Andreev bound states*. The Andreev bound states can play a pivotal role on the thermodynamics and transport phenomena in superconductors under magnetic fields. Theoretically, several theorists have studied the electronic structure around vortices and its effects on physical phenomena. Experimentally, nevertheless, it had taken rather long time to study directly the electronic structure around vortices.

In 1989, however, Hess et al. first succeeded in experimentally observing the electronic structure around vortices[65]. They investigated the energy spectra around vortices by the scanning tunneling microscope (STM). The tunneling current I of the normal state/insulator/ superconductor junction is given as

$$I(V) \propto \int_{-\infty}^{\infty} dE N(E) (f(E) - f(E + eV)) \quad (1.7)$$

where $N(E)$ is the density of states in the superconductor, V is the bias voltage applied to the junction, and $f(E)$ is the Fermi distribution function. Differentiating this equation with respect to V , one obtains the differential conductance,

$$\frac{dI}{dV} \propto - \int_{-\infty}^{\infty} dE N(E) \frac{\partial}{\partial V} f(E + eV) \approx N(-eV). \quad (1.8)$$

The derivative of the Fermi function becomes very sharply peaked at $E = -eV$ at low temperatures. This equation means that we can obtain the density of states $N(E)$ of the superconductor by measuring the differential conductance dI/dV at sufficiently low temperatures. The spatial resolved probe, STM, enables us to measure dI/dV at each position on the surface of the superconductor, so that we can obtain the local density of states $N(r, E)$ of the superconductor. In absence of vortices, or sufficiently far from a vortex, the BCS energy gap should appear in the energy spectra. Near the vortex center, on the other hand, finite density of states was expected to exist inside the gap, due to the above-mentioned low-energy bound states around a vortex. Figure 1.18 displays the experimental results for the energy spectra at the vortex center and at some distance from it, observed first

with STM in 1989 by Hess et al. [65] The superconducting material used in the experiment was a clean type-II superconductor, the layered hexagonal compound $2H\text{-NbSe}_2$. It was remarkable that a large peak appeared in the experimentally observed data at the zero bias voltage at the vortex center. The BCS gap is certainly recovered far from the vortex center.

Stimulated by the STM experiments, theoretical studies also developed. By solving the BdG equations numerically, it was clarified that the zero-bias peak appeared at the vortex center and the peak split into two peaks at positive and negative energies at some distance from the vortex center. [66, 67]

Zero energy peak at the vortex core is known to be sensitive to impurity scattering.[68, 69, 70] Figure 1.19 shows a local density of states of a superconducting vortex core measured as a function of disorder in the alloy system $\text{Nb}_{1-x}\text{Ta}_x\text{Se}_2$ using a low-temperature STM.[68] The peak observed in the zero-bias conductance at a vortex center is found to be very sensitive to disorder. As the mean free path is decreased by substitutional alloying, the peak gradually disappears and for $x = 0.2$ the density of states in the vortex center is found to be equal to that in the normal state. The vortex-core spectra hence may provide a sensitive measure of the quasiparticle scattering time.

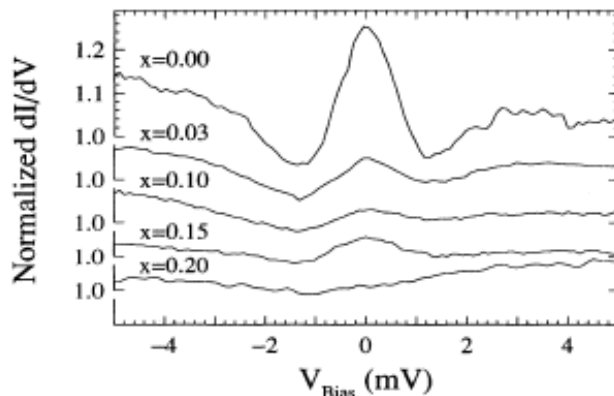


FIG. 3. Spectra taken at the center of a vortex core for various Ta substitutions at 1.3 K and 0.3 T. The spectra are normalized to the differential conductance at high bias.

Figure 1.19: Spectra of $\text{Nb}_{1-x}\text{Ta}_x\text{Se}_2$ taken at the core center for various Ta substitution.[68]

Furthermore, STM is now considered as a useful probe to detect the pairing symmetry of superconductors because the structure of local density of

states around the core reflects the pairing symmetry. [71, 72] In fact, it is found that local density of states in d -wave superconductor has a four fold symmetry. See Figs. 1.20 and 1.21. This is consistent with some experimental facts. Figure 1.22 depicts dI/dV of NbSe₂ measured by STM[73]. Clearly, the anisotropic structure is seen, which suggest that this material is an anisotropic superconductor.

However, a discrepancy arises in d -wave superconductors. The conventional theory for d -wave vortices based on Bogoliubov-de Gennes mean-field theory predicts a zero-energy peak in the local density of states at the vortex core[74]. However, spectrum obtained by STM in one of the high- T_c materials, Bi₂Sr₂CaCu₂O_{8+x}, giving directly the local density of states around the vortex core, shows only a small-double peak structure at energies ± 7 meV[75] (see Fig. 1.23). A similar situation was also observed in YBa₂Cu₃O_{7-x} compounds[76].

To resolve this discrepancy, several theoretical attempts have been made: $d_{x^2-y^2} + s$ state[77], $d_{x^2-y^2} + id_{xy}$ state[78, 79], antiferromagnetic vortex core[80, 81, 82], staggered flux state[83], vortex core with small $k_F\xi_0$ [84, 85], and vortex undergoing quantum zero-point motion in a d -wave superconductor[86]. Here, k_F is the Fermi wave number and ξ_0 is the coherence length. However, the reason of this discrepancy is still controversial.

1.4 Nonequilibrium Green's functions formalism

Studies of the transport equation for electrons interacting with phonons by means of diagrammatic techniques started in the early sixties by Konstantinov-Perel[87] and Kadanoff-Baym[88]. In 1964, Keldysh applied his Green's functions technique to derive the kinetic equations for electrons interacting with phonons in a rather elegant way[89]. Since then the so-called nonequilibrium Keldysh Green's functions method has been extensively used to describe electronic transport phenomena, e.g. weak localization, electron-electron interaction, and impurity scattering in metals[90, 91, 92], nonequilibrium superconductivity[93, 94, 95, 96], as well as for derivation of kinetic equations for ³He[97, 98], quasi-1D conductors with charge density waves[99, 100, 101], and Langevin equations for a particle in dissipative environment [102, 103]. In particular for the case of superconductors, the diagrammatic Keldysh technique is not enough to properly account for the nonequilibrium properties of the system and it must be supplemented by considering Green's functions not only as 2×2 matrices in time ordered space or Keldysh space, but also as

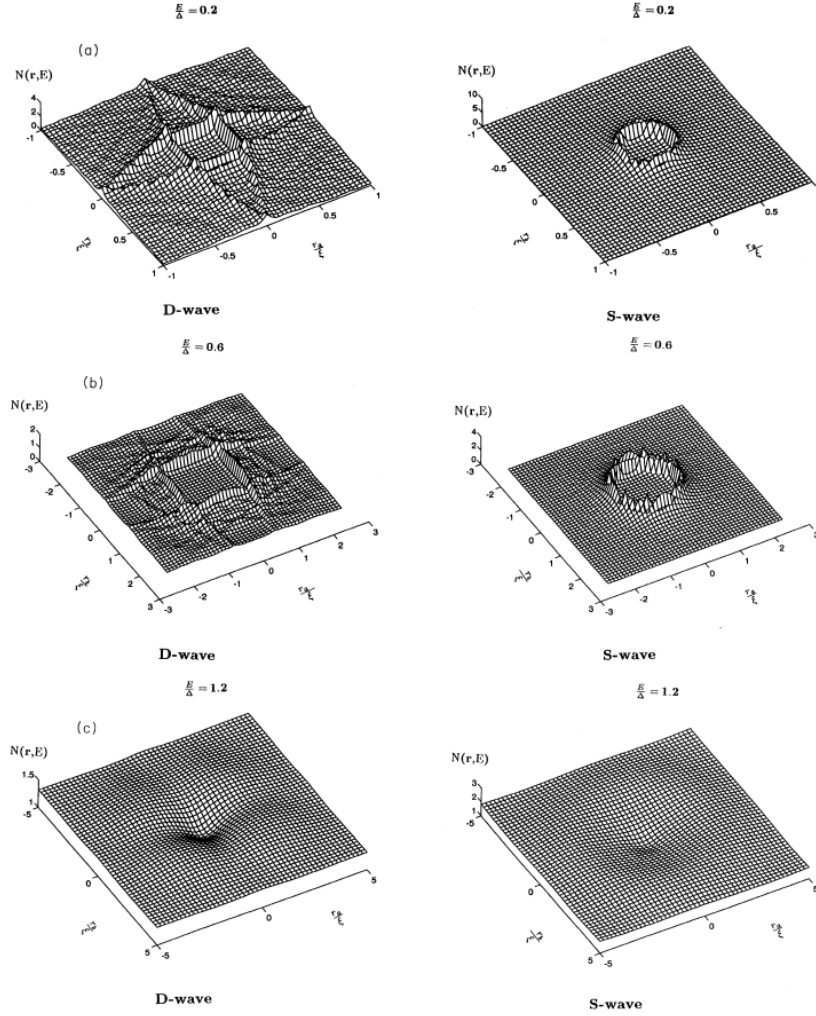


FIG. 1. (a) Local density of states $N(r,E)$ vs $r=r_x\hat{a}+r_y\hat{b}$ for $E/\Delta(T)=0.2$ for d - and s -wave pairing. (b) Local density of states $N(r,E)$ vs $r=r_x\hat{a}+r_y\hat{b}$ for $E/\Delta(T)=0.6$ for d - and s -wave pairing. (c) Local density of states $N(r,E)$ vs $r=r_x\hat{a}+r_y\hat{b}$ for $E/\Delta(T)=1.2$ for d - and s -wave pairing.

Figure 1.20: Local density of states at different energies[71] Left panels shows the results of d -wave superconductor. Right panels shows the results of s -wave superconductor.

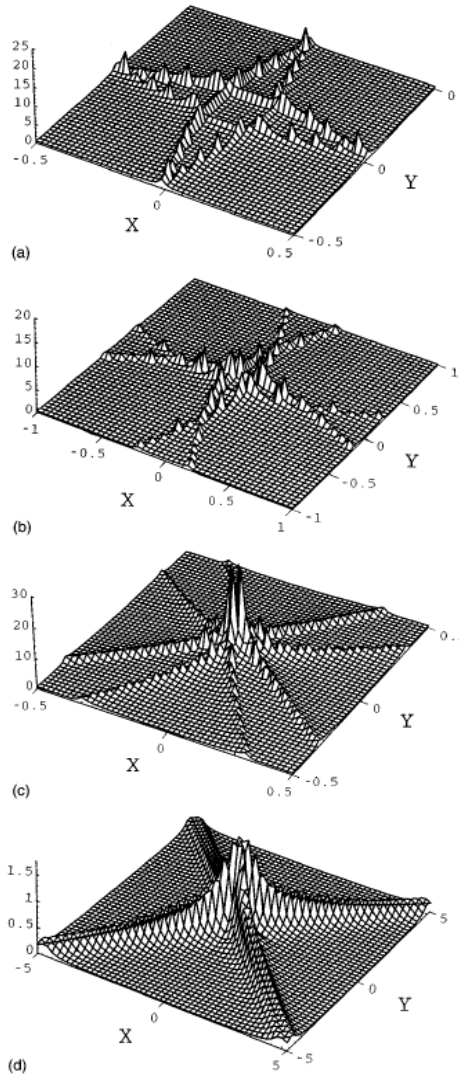


Figure 1.21: Local density of states in d -wave superconductor at different energies[72] Four fold symmetry is seen, which reflects d -wave symmetry.

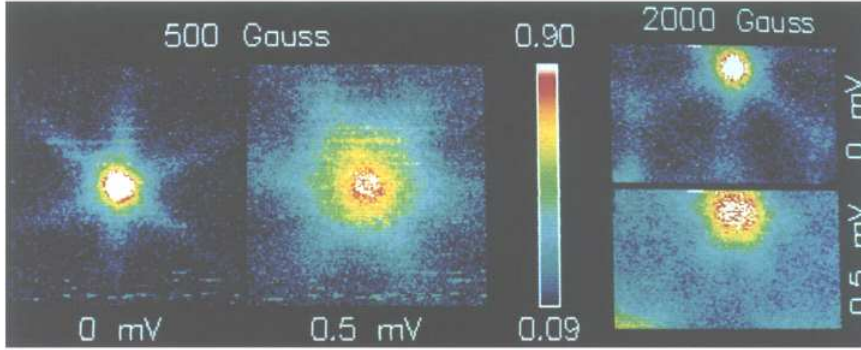


FIG. 4. Simultaneously taken XY images of $dI/dV(0 \text{ mV}, x, y)$ and $dI/dV(0.5 \text{ mV}, x, y)$ with $B = 500 \text{ G}$ and the same for 2000 G . The width of all images is 1500 \AA . Differential tunneling conductance of 0.9 and larger in normalized units is shown as white.

Figure 1.22: dI/dV of NbSe_2 measured by STM[73].

2×2 matrices in particle-hole space (also called Nambu space).[104, 105] The Nambu representation allows to incorporate in a compact way the pair potential, essential to describe superconductivity, into the standard diagrammatics used in the Keldysh technique.

1.4.1 Keldysh formalism

Keldysh method[89] is widely used to derive equation of motion in superconductors. In real time formalism, one can formulate nonequilibrium superconducting states. Now, we define

$$\psi(\mathbf{r}, t) = \exp(iHt) \psi(\mathbf{r}) \exp(-iHt), \quad (1.9)$$

$$\psi^\dagger(\mathbf{r}, t) = \exp(iHt) \psi^\dagger(\mathbf{r}) \exp(-iHt), \quad (1.10)$$

$$x = (\mathbf{r}, t), \psi(\mathbf{r}) = \frac{1}{\sqrt{V}} \sum_{\mathbf{k}} e^{i\mathbf{k}\mathbf{r}} c_{\mathbf{k}}, \psi^\dagger(\mathbf{r}) = \frac{1}{\sqrt{V}} \sum_{\mathbf{k}} e^{-i\mathbf{k}\mathbf{r}} c_{\mathbf{k}}^\dagger, \quad (1.11)$$

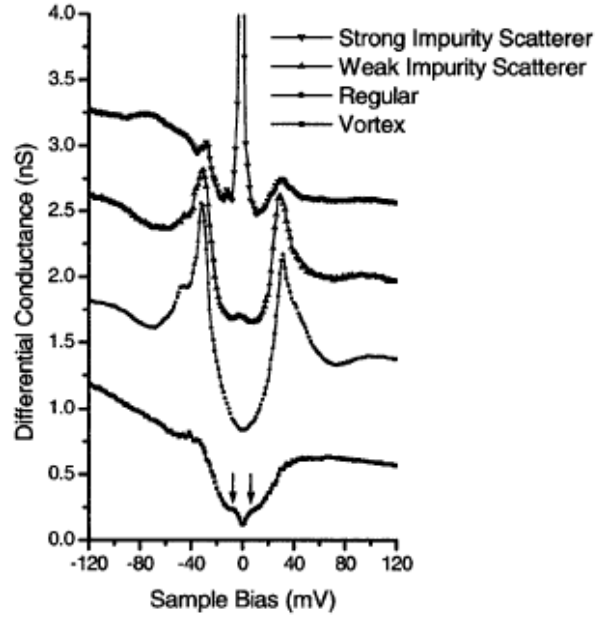


Figure 1.23: dI/dV of $\text{Bi}_2\text{Sr}_2\text{CaCu}_2\text{O}_{8+x}$ taken at different locations measured by STM[75]. The top two spectra, taken at the center of a Zn impurity resonance (strong) and an impurity resonance of unknown source (weak), respectively, show a peak in the DOS just below the Fermi energy ($\sim -1.5\text{mV}$). The third spectrum, taken on a ‘regular’ (free of impurity resonances and magnetic vortices) part of the surface, shows a superconducting energy gap with $\Delta = 32\text{ mV}$. The bottom spectrum, taken at the center of a vortex core, shows two local maxima at 67 mV , as indicated by the two solid arrows. In addition, both coherence peaks at the gap edge are completely suppressed.

and

$$\hat{G}_{11}(x1, x2) = -i \langle T (\psi(x1)\psi^\dagger(x2)) \rangle \quad (1.12)$$

$$= \begin{cases} -i\psi(x1)\psi^\dagger(x2)(t_1 > t_2) \\ i\psi^\dagger(x2)\psi(x1)(t_1 < t_2) \end{cases}, \quad (1.13)$$

$$\hat{G}_{12}(x1, x2) = i \langle \psi^\dagger(x2)\psi(x1) \rangle, \quad (1.14)$$

$$\hat{G}_{21}(x1, x2) = -i \langle \psi(x1)\psi^\dagger(x2) \rangle, \quad (1.15)$$

$$\hat{G}_{22}(x1, x2) = -i \langle \tilde{T} (\psi(x1)\psi^\dagger(x2)) \rangle \quad (1.16)$$

$$= \begin{cases} -i\psi(x1)\psi^\dagger(x2)(t_1 < t_2) \\ i\psi^\dagger(x2)\psi(x1)(t_1 > t_2) \end{cases}. \quad (1.17)$$

Therefore, we have

$$\hat{G}_{12} + \hat{G}_{21} = \hat{G}_{11} + \hat{G}_{22}. \quad (1.18)$$

By defining

$$\hat{G} = \begin{pmatrix} \hat{G}_{11} & \hat{G}_{12} \\ \hat{G}_{21} & \hat{G}_{22} \end{pmatrix}, L = \frac{1}{\sqrt{2}} \begin{pmatrix} 1 & -1 \\ 1 & 1 \end{pmatrix} \quad (1.19)$$

we transform \hat{G}

$$\hat{G} \rightarrow L\tau_3\hat{G}L^\dagger = \begin{pmatrix} G^R & G^K \\ 0 & G^A \end{pmatrix} \quad (1.20)$$

$$G^R = \hat{G}_{11} - \hat{G}_{12} \quad (1.21)$$

$$G^A = \hat{G}_{11} - \hat{G}_{21} \quad (1.22)$$

$$G^K = \hat{G}_{11} + \hat{G}_{22}. \quad (1.23)$$

This is called the Keldysh representaion[96].

1.4.2 Gor'kov equation

BCS Hamiltonian reads

$$\int \left[\psi_\alpha^\dagger \left(-\frac{\nabla^2}{2m} - \mu \right) \psi_\alpha + \frac{g}{2} \psi_\beta^\dagger \psi_\alpha^\dagger \psi_\alpha \psi_\beta \right] d^3\mathbf{r}. \quad (1.24)$$

Here,

$$\psi_\alpha(\mathbf{r}, \tau) = \exp(H\tau) \psi_\alpha(\mathbf{r}) \exp(-H\tau), \quad (1.25)$$

$$\psi_\alpha^\dagger(\mathbf{r}, \tau) = \exp(H\tau) \psi_\alpha^\dagger(\mathbf{r}) \exp(-H\tau), \quad (1.26)$$

$$\psi_\alpha(\mathbf{r}) = \frac{1}{\sqrt{V}} \sum_{\mathbf{k}} e^{i\mathbf{k}\mathbf{r}} c_{\mathbf{k}\alpha}, \psi_\alpha^\dagger(\mathbf{r}) = \frac{1}{\sqrt{V}} \sum_{\mathbf{k}} e^{-i\mathbf{k}\mathbf{r}} c_{\mathbf{k}\alpha}^\dagger. \quad (1.27)$$

We define $x = (\mathbf{r}, \tau)$ and

$$G_{\alpha\beta}(x1, x2) = \left\langle T_\tau \left(\psi_\alpha(x1) \psi_\beta^\dagger(x2) \right) \right\rangle \quad (1.28)$$

$$= \begin{cases} \psi_\alpha(x1) \psi_\beta^\dagger(x2), (\tau_1 > \tau_2) \\ -\psi_\beta^\dagger(x2) \psi_\alpha(x1), (\tau_1 < \tau_2) \end{cases} . \quad (1.29)$$

Using Heisenberg's equation of motion, we get

$$\frac{\partial G_{\alpha\beta}(x1, x2)}{\partial \tau_1} = \delta_{\alpha\beta} \delta(x1 - x2) + \left(\frac{\nabla_1^2}{2m} + \mu \right) G_{\alpha\beta}(x1, x2) \quad (1.30)$$

$$-g \left\langle T_\tau \left(\psi_\gamma^\dagger(x1) \psi_\gamma(x1) \psi_\alpha(x1) \psi_\beta^\dagger(x2) \right) \right\rangle . \quad (1.31)$$

Wick's theorem gives

$$\begin{aligned} & \left\langle T_\tau \left(\psi_\gamma^\dagger(x1) \psi_\gamma(x1) \psi_\alpha(x1) \psi_\beta^\dagger(x2) \right) \right\rangle \\ &= - \left\langle T_\tau \left(\psi_\gamma(x1) \psi_\gamma^\dagger(x1) \right) \right\rangle \left\langle T_\tau \psi_\alpha(x1) \psi_\beta^\dagger(x2) \right\rangle \\ &+ \left\langle T_\tau \left(\psi_\alpha(x1) \psi_\gamma^\dagger(x1) \right) \right\rangle \left\langle T_\tau \psi_\gamma(x1) \psi_\beta^\dagger(x2) \right\rangle \\ &- \left\langle T_\tau \left(\psi_\alpha(x1) \psi_\gamma(x1) \right) \right\rangle \left\langle T_\tau \psi_\gamma^\dagger(x1) \psi_\beta^\dagger(x2) \right\rangle . \end{aligned} \quad (1.32)$$

Also, we have

$$\begin{aligned} & - \left\langle T_\tau \left(\psi_\gamma(x1) \psi_\gamma^\dagger(x1) \right) \right\rangle \left\langle T_\tau \psi_\alpha(x1) \psi_\beta^\dagger(x2) \right\rangle \\ &+ \left\langle T_\tau \left(\psi_\alpha(x1) \psi_\gamma^\dagger(x1) \right) \right\rangle \left\langle T_\tau \psi_\gamma(x1) \psi_\beta^\dagger(x2) \right\rangle \\ &= - \sum_{\gamma\gamma} (x1) G_{\alpha\beta}(x1, x2) + \sum_{\alpha\gamma} (x1) G_{\gamma\beta}(x1, x2) \end{aligned} \quad (1.33)$$

$$\sum_{\alpha\beta} (x) = \left\langle T_\tau \left(\psi_\alpha(x) \psi_\beta^\dagger(x) \right) \right\rangle \quad (1.34)$$

Equation (1.34) is called self energy. Now, we define

$$F_{\alpha\beta}^\dagger(x1, x2) = \left\langle T_\tau \psi_\alpha^\dagger(x1) \psi_\beta^\dagger(x2) \right\rangle , \quad (1.35)$$

$$F_{\alpha\beta}(x1, x2) = \left\langle T_\tau \psi_\alpha(x1) \psi_\beta(x2) \right\rangle , \quad (1.36)$$

$$\overline{G}_{\alpha\beta}(x1, x2) = - \left\langle T_\tau \psi_\alpha^\dagger(x1) \psi_\beta(x2) \right\rangle = G_{\beta\alpha}(x2, x1), \quad (1.37)$$

$$\Delta_{\alpha\beta}(x) = |g| F_{\alpha\beta}(x, x) . \quad (1.38)$$

For singlet pairing, we have $\Delta_{\alpha\beta}(x) = -\Delta_{\beta\alpha}(x)$ and assume that electron electron interaction is independent of spin. Then, we get

$$\Delta_{\alpha\beta}(x) = i\tau_{\alpha\beta}^{(2)} \Delta(x) \quad (1.39)$$

$$G_{\alpha\beta}(x1, x2) = \delta_{\alpha\beta} G(x1, x2) \quad (1.40)$$

$$F_{\alpha\beta}(x1, x2) = i\tau_{\alpha\beta}^{(2)} F(x1, x2) . \quad (1.41)$$

By incorporating self energy into μ , we obtain

$$\left(\frac{\partial}{\partial \tau_1} - \frac{\nabla_1^2}{2m} - \mu \right) G_{\alpha\beta}(x1, x2) + \Delta(x1) F^\dagger(x1, x2) = \delta(x1 - x2) \quad (1.42)$$

and for \bar{G}, F, F^\dagger similarly

$$\check{G}^{-1}(x1) \check{G}(x1, x2) = \delta(x1 - x2), \quad (1.43)$$

$$\check{G}(x1, x2) \equiv \begin{pmatrix} G(x1, x2) & F(x1, x2) \\ -F^\dagger(x1, x2) & \bar{G}(x1, x2) \end{pmatrix}, \quad (1.44)$$

$$\check{G}^{-1} \equiv \tau_3 \frac{\partial}{\partial \tau} + \check{H}, \check{H} \equiv \begin{pmatrix} -\frac{\nabla^2}{2m} - \mu & -\Delta \\ \Delta^* & -\frac{\nabla^2}{2m} - \mu \end{pmatrix}. \quad (1.45)$$

This is called Gor'kov equation and widely used to study superconducting properties.[106]

1.4.3 Quasiclassical approximation

Quasiclassical approximation is a well-used method to study the Fermionic systems at low temperatures. [107] This method was first formulated by Eilenberger[93] to study the equilibrium state. Later, Eliashberg[94] generalized this theory to apply to the nonequilibrium states. Now, we define $\mathbf{p}_+ = \mathbf{p} + \frac{\mathbf{k}}{2}$ and $\mathbf{p}_- = \mathbf{p} - \frac{\mathbf{k}}{2}$. Consider stationary systems which satisfies $p_F \gg \xi^{-1}$. Here, ξ is coherence length and $\xi^{-1} \sim \frac{\Delta}{v_F}$. Quasiclassical Green's functions are defined as

$$g_{\omega_n}(\hat{\mathbf{p}}, \mathbf{k}) = \oint \frac{1}{\pi i} G_{\omega_n}(\mathbf{p}_+, \mathbf{p}_-) d\xi_p, \quad (1.46)$$

$$\bar{g}_{\omega_n}(\hat{\mathbf{p}}, \mathbf{k}) = \oint \frac{1}{\pi i} \bar{G}_{\omega_n}(\mathbf{p}_+, \mathbf{p}_-) d\xi_p, \quad (1.47)$$

$$f_{\omega_n}(\hat{\mathbf{p}}, \mathbf{k}) = \oint \frac{1}{\pi i} F_{\omega_n}(\mathbf{p}_+, \mathbf{p}_-) d\xi_p, \quad (1.48)$$

$$f_{\omega_n}^\dagger(\hat{\mathbf{p}}, \mathbf{k}) = \oint \frac{1}{\pi i} F_{\omega_n}^\dagger(\mathbf{p}_+, \mathbf{p}_-) d\xi_p \quad (1.49)$$

where the path of integration is chosen to take the contributions from poles near Fermi surface. By Fourier transforming Gor'kov equation, we obtain

$$[\check{G}^{-1}\check{G}] = 1, \quad (1.50)$$

$$[AB] = \int A(\mathbf{p}_+, \mathbf{p}) B(\mathbf{p}, \mathbf{p}_-) d^3\mathbf{p}, \check{G}^{-1} = \check{G}_0^{-1} + \check{H} - \check{\Sigma}, \quad (1.51)$$

$$\check{G}_0^{-1} = \begin{pmatrix} -i\omega + \xi_p + \frac{\mathbf{v}\mathbf{k}}{2} + \frac{k^2}{8m} & 0 \\ 0 & i\omega + \xi_p + \frac{\mathbf{v}\mathbf{k}}{2} + \frac{k^2}{8m} \end{pmatrix}, \quad (1.52)$$

$$\check{H} = \begin{pmatrix} -\frac{e}{c}\mathbf{v}\mathbf{A}(\mathbf{k}) + e\varphi & -\Delta(\mathbf{k}) \\ \Delta^*(\mathbf{k}) & \frac{e}{c}\mathbf{v}\mathbf{A}(\mathbf{k}) + e\varphi \end{pmatrix}, \check{\Sigma} = \begin{pmatrix} \check{\Sigma}_1 & \check{\Sigma}_2 \\ -\check{\Sigma}_2^\dagger & \check{\Sigma}_1 \end{pmatrix}. \quad (1.53)$$

Similarly, we have

$$[\check{G}\check{G}^{-1}] = 1, \quad (1.54)$$

$$\check{G}^{-1} = \check{G}_0^{-1} + \check{H} - \check{\Sigma}, \quad (1.55)$$

$$\check{G}_0^{-1} = \begin{pmatrix} i\omega + \xi_p - \frac{\mathbf{v}\mathbf{k}}{2} + \frac{k^2}{8m} & 0 \\ 0 & -i\omega + \xi_p - \frac{\mathbf{v}\mathbf{k}}{2} + \frac{k^2}{8m} \end{pmatrix}, \quad (1.56)$$

$$\check{H} = \begin{pmatrix} -\frac{e}{c}\mathbf{v}\mathbf{A}(\mathbf{k}) + e\varphi & -\Delta(\mathbf{k}) \\ \Delta^*(\mathbf{k}) & \frac{e}{c}\mathbf{v}\mathbf{A}(\mathbf{k}) + e\varphi \end{pmatrix}, \check{\Sigma} = \begin{pmatrix} \check{\Sigma}_1 & \check{\Sigma}_2 \\ -\check{\Sigma}_2^\dagger & \check{\Sigma}_1 \end{pmatrix}. \quad (1.57)$$

From eq. (1.50) and eq.(1.54), we have

$$\mathbf{v}_F\mathbf{k}\check{g} - i\omega_n(\check{\tau}_3\check{g} - \check{g}\check{\tau}_3) + [\check{H}\check{g} - \check{g}\check{H}] = \check{I}, \quad (1.58)$$

$$\check{I} = [\check{\Sigma}\check{g} - \check{g}\check{\Sigma}] = \begin{pmatrix} I_1 & I_2 \\ -I_2^\dagger & I_1 \end{pmatrix}, \check{g}_{\omega_n}(\hat{\mathbf{p}}, \mathbf{k}) = \begin{pmatrix} g_{\omega_n} & f_{\omega_n} \\ -f_{\omega_n}^\dagger & \bar{g}_{\omega_n} \end{pmatrix}. \quad (1.59)$$

Equation (1.58) is the Eilenberger equation. With the use of Fourier transformation, Eilenberger equation reads

$$\mathbf{v}_F\mathbf{k}\check{g} - i\omega_n(\check{\tau}_3\check{g} - \check{g}\check{\tau}_3) + \check{H}\check{g} - \check{g}\check{H} = \check{I}, \quad (1.60)$$

$$\check{g}_{\omega_n}(\hat{\mathbf{p}}, \mathbf{r}) = \int \frac{d^3\mathbf{k}}{(2\pi)^3} e^{i\mathbf{k}\mathbf{r}} \check{g}_{\omega_n}(\hat{\mathbf{p}}, \mathbf{k}). \quad (1.61)$$

In homogeneous systems, we have

$$g + \bar{g} = 0, g^2 - f f^\dagger = 1. \quad (1.62)$$

Hereafter, we assume that this relation holds. Then, we obtain the normalization condition $\check{g}^2 = 1$. Note that there is a problem with this normalization condition in the clean limit in finite size systems. In fact, quasiclassical

approximation does not work in restricted geometry due to quasiparticle interference between the interfaces.[108] However, the normalization condition should hold in finite systems in the dirty limit –it is obtained as a saddle point solution in nonlinear sigma model.[109]

Equation (1.60) can be rewritten as

$$-iv_F \hat{\nabla} \check{g} + \check{H}_0 \check{g} - \check{g} \check{H}_0 = \check{I}, \quad (1.63)$$

$$\hat{\nabla} \check{g} = \begin{pmatrix} \nabla g & (\nabla - \frac{2ie}{c} \mathbf{A}) f \\ -(\nabla + \frac{2ie}{c} \mathbf{A}) f^\dagger & -\nabla g \end{pmatrix}, \check{H}_0 = \begin{pmatrix} -i\omega_n & -\Delta \\ \Delta^* & i\omega_n \end{pmatrix}. \quad (1.64)$$

Here, we incorporate a vector potential A . Next, we consider dirty limit case,

$$\frac{1}{\tau} \gg T_c, \text{ i.e., } l \ll \xi_0. \quad (1.65)$$

Here, τ , T_c , l , and ξ_0 are relaxation time, transition temperature, mean free path and coherence length, respectively. When impurity scattering is strong, we can set

$$\check{g} = \check{g}_0 + \hat{\mathbf{v}}_F \check{\mathbf{g}}, |\mathbf{g}| \ll g_0 \quad (1.66)$$

Here, \check{g}_0 is independent of \mathbf{v}_F . $\hat{\mathbf{v}}_F$ is a unit vector parallel to the momentum. Then, with the Eilenberger equation and the normalization condition, we get

$$\check{\mathbf{g}} = -l_{tr} \hat{\nabla} \check{g}_0, l_{tr} = v_F \tau_{tr}. \quad (1.67)$$

Here, τ_{tr} is the scattering mean free time. Introducing dimension d and diffusion constant $D = \frac{1}{d} v_F l_{tr}$, we obtain

$$iD \hat{\nabla} \left(\check{g}_0 \hat{\nabla} \check{g}_0 \right) + (\check{H}_0 \check{g}_0 - \check{g}_0 \check{H}_0) = 0. \quad (1.68)$$

This is the Usadel equation which corresponds to the diffusion equation for the quasiclassical Green's functions and widely used to study proximity effect in superconducting junctions.[110] Recently, by applying the nonlinear sigma model[111, 112], the Usadel equation has been derived [109] and generalized to incorporate Coulomb interaction.[113]

For the actual calculation, it is convenient to use the parametrization of quasiclassical Green's functions. For the Eilenberger equation, the Riccati parametrization is known to give a stable and fast numerical method to solve the Eilenberger equations.[114] The Riccati parametrization is defined as

$$\check{g} = - \begin{pmatrix} (1+ab)^{-1} & 0 \\ 0 & (1+ba)^{-1} \end{pmatrix} \begin{pmatrix} 1-ab & 2ia \\ -2ib & -(1-ba) \end{pmatrix}. \quad (1.69)$$

Then, the Eilenberger equations becomes

$$v_F \nabla a + (2\omega + \Delta^* a) a - \Delta = 0, \quad (1.70)$$

$$v_F \nabla b - (2\omega + \Delta b) b + \Delta^* = 0 \quad (1.71)$$

with Matsubara frequency ω . From these equations, we see that the following relations hold with wave vector k and position r :

$$b(\omega, k, r) = a^*(\omega, -k, r) \quad (1.72)$$

for even parity pairing and

$$b(\omega, k, r) = -a^*(\omega, -k, r) \quad (1.73)$$

for odd parity pairing.

For the Usadel equation, the so-called θ -parametrization is often used. In this case, we express \check{g} as

$$\check{g} = \cos \psi \sin \theta \hat{\tau}_1 + \sin \psi \sin \theta \hat{\tau}_2 + \cos \theta \hat{\tau}_3, \quad (1.74)$$

with Pauli matrix in the electron hole space, $\hat{\tau}_1$, $\hat{\tau}_2$, and $\hat{\tau}_3$. Since \check{g} obeys Usadel equation, following equations are satisfied,

$$D \left[\frac{\partial^2}{\partial x^2} \theta - \left(\frac{\partial \psi}{\partial x} \right)^2 \cos \theta \sin \theta \right] + 2i\varepsilon \sin \theta = 0, \quad (1.75)$$

$$\frac{\partial}{\partial x} \left[\sin^2 \theta \left(\frac{\partial \psi}{\partial x} \right) \right] = 0. \quad (1.76)$$

The second equation represents the conservation of the supercurrent and $\partial \psi / \partial x = 0$ when there is no supercurrent. This representation gives a stable solution for the numerical calculation in real energy.

For the calculation of the thermodynamical quantities, we usually use Matsubara representation. As a numerically stable parametrization, the representation using function Φ is recommendable, namely

$$g = \frac{\omega}{\sqrt{\omega^2 + \Phi_\omega \Phi_{-\omega}^*}}, \quad (1.77)$$

$$f = \frac{\Phi_\omega}{\sqrt{\omega^2 + \Phi_\omega \Phi_{-\omega}^*}}, \quad (1.78)$$

$$-f^\dagger = \frac{\Phi_{-\omega}^*}{\sqrt{\omega^2 + \Phi_\omega \Phi_{-\omega}^*}}. \quad (1.79)$$

Then, Usadel equation reads

$$\xi^2 \frac{\pi T_C}{G_\omega} \frac{\partial}{\partial x} \left(G_\omega^2 \frac{\partial}{\partial x} \Phi_\omega \right) - \omega \Phi_\omega = 0 \quad (1.80)$$

with $\xi = \sqrt{D/2\pi T_C}$ and critical temperature T_C . θ and Φ -parametrizations are related to each other as follows:

$$\sin \theta \cos \psi = \frac{g}{2\omega} (\Phi_\omega + \Phi_{-\omega}^*), \quad (1.81)$$

$$\sin \theta \sin \psi = \frac{ig}{2\omega} (\Phi_\omega - \Phi_{-\omega}^*). \quad (1.82)$$

1.5 Purpose and outline of this thesis

Up to now, no bulk material has been identified as odd frequency superconductor, which has severely hampered the progress of the study of odd frequency superconductivity (note that a bulk odd-frequency state could be realized in the heavy-fermion compounds CeCu_2Si_2 and CeRhIn_5 [115, 116, 117], but this is still controversial). The study of odd frequency superconductivity now lies in the womb of time. To facilitate the development, it is desirable to clarify manifestations of odd frequency pairing in measurable quantities like density of states.

In view of this, we study superconducting systems with broken symmetry other than $U(1)$ in this thesis –the presence of ferromagnet, vortex and surface breaks symmetry in spin space and translational symmetry. These broken symmetry is an important ingredient of the appearance of odd frequency superconductivity which hardly appears in bulk materials. By considering these symmetry breaking systems, we will clarify how this exotic pairing arises and manifests itself in observable quantities, and also related phenomena, which will shed new light on the physics of the odd frequency superconductivity.

In chapter 2, we study the conditions for the appearance of the peak in the density of states in diffusive ferromagnet, in normal metal / diffusive ferromagnet / superconductor junctions. A detailed theoretical study of the tunneling conductance and the density of states in these junctions is presented.

In chapter 3, we investigate the proximity effect and pairing symmetry in diffusive ferromagnet / superconductor junctions. Various possible symmetry classes in a superconductor are considered which are consistent with the Pauli's principle: even-frequency spin-singlet even-parity state, even-frequency spin-triplet odd-parity state, odd-frequency spin-triplet even-parity state and odd-frequency spin-singlet odd-parity state. The relevance of the odd-frequency to the density of states is discussed.

In chapter 4, we study pairing symmetry inside the Abrikosov vortex core in superconductors. We show that only odd-frequency spin-singlet chiral p -wave pairing is allowed at the center of the core in s -wave superconductors as

a consequence of the broken translational symmetry. This makes it possible to provide a novel interpretation of the Andreev bound states inside the core as *the manifestation of the odd-frequency pairing*. We also unveil the sum rule behind this phenomenon. Based on these results, we propose the experimental setup to verify the existence of odd-frequency pairing in bulk materials by using superconducting scanning tunneling spectroscopy.

In chapter 5, we study the density of states in chiral p -wave superconductor in the presence of an Abrikosov vortex in front of a specular surface. We clarify that the density of states at the shadow region behind the vortex is sensitive to the chirality. When the chirality of the vortex is the same as (opposite to) that of the superconductor, the zero energy peak (gap) of the density of states at the shadow region emerges. This is because the density of states at the shadow region has a linear term of the vector potential. Based on the results, we propose chirality sensitive test on superconductors.

In chapter 6, a summary of this thesis and outlook are given.

Bibliography

- [1] J. Bardeen, L. N. Cooper and J. R. Schrieffer, Phys. Rev. **108**, 1175 (1957).
- [2] J. G. Bednorz, and K. A. Müller, Z. Phys B **64**, 189 (1986).
- [3] Y. Maeno, H. Hashimoto, K. Yoshida, S. Nishizaki, T. Fujita, J. G. Bednorz, and F. Lichtenberg, Nature **372**, 532 (1994).
- [4] K. Ishida, H. Mukuda, Y. Kitaoka, K. Asayama, Z. Q. Mao, Y. Mori and Y. Maeno, Nature **396**, 658 (1998).
- [5] G. M. Luke, Y. Fudamoto, K. M. Kojima, M. I. Larkin, J. Merrin, B. Nachumi, Y. J. Uemura, Y. Maeno, Z. Q. Mao, Y. Mori, H. Nakamura and M. Sgrist, Nature **394**, 558 (1998).
- [6] A. P. Mackenzie and Y. Maeno, Rev. Mod. Phys. **75**, 657 (2003).
- [7] A. Altland and M. R. Zirnbauer, Phys. Rev. B **55**, 1142 (1997).
- [8] E. P. Wigner, Proc. Cambridge Philos. Soc. **47**, 790 (1951); Ann. Math. **67**, 325 (1958).
- [9] F. J. Dyson, J. Math. Phys. **3**, 140 (1962).
- [10] P. W. Anderson, J. Phys. Chem. Solids **11**, 26 (1959).
- [11] A. M. Goldman and N. Markovic, Phys. Today **51**, 39 (1998).
- [12] Y. Dubi, Y. Meir and Y. Avishai, Nature **449**, 876, (2007).
- [13] P. Fulde and A. Ferrel, Phys. Rev. **135**, A550 (1964).
- [14] A. Larkin and Y. Ovchinnikov, Sov. Phys. JETP **20**, 762 (1965).
- [15] Y. Matsuda and H. Shimahara, J. Phys. Soc. Jpn. **76**, 051005 (2007).

- [16] R. Casalbuoni and G. Narduli, *Rev. Mod. Phys.* **76**, 263 (2004).
- [17] Subir Sachdev, *Quantum Phase Transitions*, (Cambridge University Press, 1999).
- [18] P. W. Anderson and H. Suhl, *Phys. Rev.* **116**, 898 (1959).
- [19] M. B. Maple, and O. Fisher, Eds., *in Superconductivity in Ternary Compounds II, Topics in Current Physics* (Springer-Verlag, Berlin, 1982).
- [20] A. I. Buzdin, *Rev. Mod. Phys.* **77**, 935 (2005).
- [21] F. S. Bergeret, A. F. Volkov, and K. B. Efetov, *Phys. Rev. Lett.* **86**, 4096 (2001); F. S. Bergeret, A. F. Volkov, and K. B. Efetov, *Rev. Mod. Phys.* **77**, 1321 (2005).
- [22] S. S. Saxena, P. Agarwal, K. Ahilan, F. M. Grosche, R. K. W. Haselwimmer, M. J. Steiner, E. Pugh, I. R. Walker, S. R. Julian, P. Monthoux, G. G. Lonzarich, A. Huxley, I. Shelkin, D. Braithwaite, and J. Flouquet, *Nature (London)* **406**, 587 (2000).
- [23] C. Pfleiderer, M. Uhlarz, S. M. Hayden, R. Vollmer, H. v. Lohneysen, N. R. Bernhoeft, and G. G. Lonzarich, *Nature (London)* **412**, 58 (2001).
- [24] D. Aoki, A. Huxley, E. Ressouche, D. Braithwaite, J. Flouquet, J. Brison, E. Lhotel, and C. Paulsen, *Nature (London)* **413**, 613 (2001).
- [25] E. Bauer, G. Hilscher, H. Michor, Ch. Paul, E. W. Scheidt, A. Griboanov, Yu. Seropegin, H. Noël, M. Sigrist, and P. Rogl, *Phys. Rev. Lett.* **92**, 027003 (2004).
- [26] T. Akazawa, H. Hidaka, H. Kotegawa, T. Kobayashi, T. Fujiwara, E. Yamamoto, Y. Haga, R. Settai, and Y. Ōnuki, *J. Phys. Soc. Jpn.* **73**, 3129 (2004).
- [27] N. Kimura, K. Ito, K. Saitoh, Y. Umeda, H. Aoki, and T. Terashima, *Phys. Rev. Lett.* **95**, 247004 (2005).
- [28] I. Sugitani, Y. Okuda, H. Shishido, T. Yamada, A. Thamizhavel, E. Yamamoto, T. D. Matsuda, Y. Haga, T. Takeuchi, R. Settai, and Y. Ōnuki, *J. Phys. Soc. Jpn.* **75**, 043703 (2006).
- [29] M. Hanawa, J. Yamaura, Y. Muraoka, F. Sakai, and Z. Hiroi, *J. Phys. Chem. Solids* **63**, 1027 (2002).

- [30] K. Togano, P. Badica, Y. Nakamori, S. Orimo, H. Takeya, and K. Hirata, Phys. Rev. Lett. **93**, 247004 (2004).
- [31] P. Badica, T. Kondo, and K. Togano, J. Phys. Soc. Jpn **74**, 1014 (2005).
- [32] H. Q. Yuan, D. F. Agterberg, N. Hayashi, P. Badica, D. Vandervelde, K. Togano, M. Sigrist, and M. B. Salamon, Phys. Rev. Lett. **97**, 017006 (2006).
- [33] E. I. Rashba, Fiz. Tverd. Tela (Leningrad) **2** 1224 (1960) [Sov. Phys. Solid State **2** 1109 (1960)].
- [34] V. M. Edelstein, Sov. Phys. JETP **68**, 1244 (1989); Phys. Rev. Lett. **75**, 2004 (1995); J. Phys. Condens. Matter **8**, 339 (1996).
- [35] L. P. Gor'kov and E. I. Rashba, Phys. Rev. Lett. **87** 037004 (2001).
- [36] S. Fujimoto, Phys. Rev. B **72**, 024515 (2005); J. Phys. Soc. Jpn. **75**, 083704 (2006); J. Phys. Soc. Jpn. **76**, 034712 (2007).
- [37] V. L. Berezinskii, JETP Lett. **20**, 287 (1974).
- [38] R.S. Keizer, S.T.B. Goennenwein, T.M. Klapwijk, G. Miao, G. Xiao, and A. Gupta, Nature **439**, 825 (2006).
- [39] I. Sosnin, H. Cho, V. T. Petrashov, and A. F. Volkov, Phys. Rev. Lett. **96**, 157002 (2006).
- [40] Y. Tanaka, A. A. Golubov, S. Kashiwaya, and M. Ueda, Phys. Rev. Lett. **99**, 037005 (2007).
- [41] E. Dagotto, Science **309**, 257 (2005).
- [42] B. L. Al'tshuler and P. Lee, Physics Today **41**, 36 (1988).
- [43] *Coulomb and Interference effects in Small Electronic Structures*, ed. C. Glattli, M. Sanquer, J. Tran Than Van (Series Moriond Condensed Matter Physics, Editions Frontieres, 1994); *Mesoscopic Electron Transport*, ed. L. L. Sohn, L. Kouwenhoven and G. Schön (NATO ASI Series E 345, Kluwer Academic Publishers, 1997); *Quantum Physics at Mesoscopic Scales*, ed. C. Glattli, M. Sanquer, J. Tran Than Van (Series Moriond Condensed Matter Physics, Editions Frontieres, 1999); *Spin Dependent Transport in Magnetic Nanostructures*, edited by S. Maekawa and T. Shinjo (Taylor and Francis, London, 2002); *Semiconductor Spintronics and Quantum Computation*, edited by D. D.

- Awschalom, D. Loss, and N. Samarth (Springer, Berlin, 2002); *Quantum Noise in Mesoscopic Physics*, edited by Yu. V. Nazarov (NATO ASI Series II, Kluwer, Dordrecht, 2003).
- [44] I. Zutic, J. Fabian, and S. Das Sarma, *Rev. Mod. Phys.* **76**, 323 (2004).
 - [45] Y. Tserkovnyak, A. Brataas, G. E. W. Bauer, and B. I. Halperin, *Rev. Mod. Phys.* **77**, 1375 (2005).
 - [46] M. L Mehta, *Random Matrices*, (Academic Pr, 2004).
 - [47] K. Nakamura and T. Harayama, *Quantum Chaos and Quantum Dots*, (Oxford Univ Pr (Sd), 2004).
 - [48] A. F. Andreev, *Sov. Phys. JETP* **19** 1228 (1964).
 - [49] G. E. Blonder, M. Tinkham, and T. M. Klapwijk, *Phys. Rev. B* **25** 4515 (1982).
 - [50] A. A. Golubov and M. Yu. Kupriyanov, *J. Low Temp. Phys.* **70**, 83 (1988); W. Belzig, C. Bruder, and G. Schön, *Phys. Rev. B* **54**, 9443 (1996).
 - [51] A. Kastalsky, A. W. Kleinsasser, L. H. Greene, R. Bhat, F. P. Milliken, and J. P. Harbison, *Phys. Rev. Lett.* **67**, 3026 (1991).
 - [52] B. J. van Wees, P. de Vries, P. Magnee, and T. M. Klapwijk, *Phys. Rev. Lett.* **69**, 510 (1992).
 - [53] C. W. J. Beenakker, *Rev. Mod. Phys.* **69**, 731 (1997); *Phys. Rev. B* **46**, 12 841 (1992).
 - [54] A. F. Volkov, A. V. Zaitsev, and T. M. Klapwijk, *Physica C1* **210**, 21 (1993).
 - [55] M. Giroud, H. Courtois, K. Hasselbach, D. Mailly, and B. Pannetier, *Phys. Rev. B* **58**, R11872 (1998).
 - [56] V. T. Petrashov, I. A. Sosnin, I. Cox, A. Parsons, and C. Troadec, *Phys. Rev. Lett.* **83**, 3281 (1999).
 - [57] T. Kontos, M. Aprili, J. Lesueur, and X. Grison, *Phys. Rev. Lett.* **86**, 304 (2001).
 - [58] V. V. Ryazanov, V. A. Oboznov, A. Yu. Rusanov, A. V. Veretennikov, A. A. Golubov, and J. Aarts, *Phys. Rev. Lett.* **86**, 2427 (2001).

- [59] C. R. Hu, Phys. Rev. Lett. **72**, 1526 (1994) ; J. Yang, and C. R. Hu, Phys. Rev. B **50**, 16766 (1994).
- [60] Y. Tanaka, Y.V. Nazarov and S. Kashiwaya, Phys. Rev. Lett. **90**, 167003 (2003); Y. Tanaka, Y.V. Nazarov, A. A. Golubov and S. Kashiwaya, Phys. Rev. B **69** 144519 (2004).
- [61] Y. Tanaka and S. Kashiwaya, Phys. Rev. B **70**, 012507 (2004); Y. Tanaka, S. Kashiwaya and T. Yokoyama, Phys. Rev. B **71**, 094513 (2005).
- [62] D. B. Josephson, Phys. Lett. **12**, 251 (1962).
- [63] A. A. Golubov, M. Yu. Kupriyanov, and E. Il'ichev Rev. Mod. Phys. **76**, 411 (2004).
- [64] C. Caroli, P. G. de Gennes and J. Matricon, Phys. Lett. **9**, 307 (1964)
- [65] H. F. Hess, R. B. Robinson, R. C. Dynes, J. M. Valles, Jr., and J. V. Waszczak, Phys. Rev. Lett. **62**, 214 (1989).
- [66] D. Shore, M. Huang, A. T. Dorsey and J. P. Sethna, Phys. Rev. Lett. **62**, 3089 (1989).
- [67] F. Gygi and M. Schlüter, Phys. Rev. B **43**, 7609 (1991).
- [68] C. Renner, A. D. Kent, P. Niedermann, Ø. Fischer, and F. Lévy, Phys. Rev. Lett. **67**, 1650 (1991).
- [69] A. A. Golubov and U. Hartmann, Phys. Rev. Lett. **72**, 3602 (1994).
- [70] A. P. Volodin, A. A. Golubov, J. Aarts, Z. Physik, B **102**, 317 (1997).
- [71] N. Schopohl and K. Maki, Phys. Rev. B **52**, 490 (1995).
- [72] M. Ichioka, N. Hayashi, N. Enomoto, and K. Machida Phys. Rev. B **53**, 15316 (1996).
- [73] H. F. Hess, R. B. Robinson and J. V. Waszczak, Phys. Rev. Lett. **64** 2711 (1990).
- [74] Y. Wang and A. H. MacDonald, Phys. Rev. B **52**, 3876 (1995).
- [75] S. H. Pan, E. W. Hudson, A. K. Gupta, K.-W. Ng, H. Eisaki, S. Uchida, and J. C. Davis, Phys. Rev. Lett. **85**, 1536 (2000).

- [76] I. Maggio-Aprile, Ch. Renner, A. Erb, E. Walker, and Ø. Fischer, Phys. Rev. Lett. **75**, 2754 (1995).
- [77] A. Himeda, M. Ogata, Y. Tanaka and S. Kashiwaya, J. Phys. Soc. Jpn. **66**, 3367 (1997).
- [78] M. Franz and Z. Tesanovic, Phys. Rev. Lett. **80**, 4763 (1998).
- [79] J. H. Han and D.-H. Lee, Phys. Rev. Lett. **85**, 1100 (2000).
- [80] D. P. Arovas, A. J. Berlinsky, C. Kallin, and Shou-Cheng Zhang, Phys. Rev. Lett. **79**, 2871 (1997).
- [81] M. Ogata, Int. J. Mod. Phys. **13**, 3560 (1999).
- [82] B. M. Andersen, H. Bruus, and P. Hedegård, Phys. Rev. **B61**, 6298 (2000).
- [83] J. Kishine, P. A. Lee, and Xiao-Gang Wen, Phys. Rev. Lett. **86**, 5365 (2001); Q.-H. Wang, J. H. Han and D.-H. Lee, Phys. Rev. Lett. **87**, 167004 (2001).
- [84] Y. Morita, M. Kohmoto, and K. Maki, Phys. Rev. Lett. **78**, 4841 (1997).
- [85] K. Yasui and T. Kita, Phys. Rev. Lett. **83**, 4168 (1999).
- [86] P. Nikolić, S. Sachdev, and L. Bartosch, Phys. Rev. B **74**, 144516 (2006).
- [87] O. V. Konstantinov and V. I. Perel, Zh. Eksp. Teor. Fiz. **39**, 197 (1960); [Sov. Phys. JETP **12**, 142 (1961)].
- [88] L. P. Kadanoff and G. Baym, *Quantum Statistical Mechanics* (Benjamin, New York, 1962).
- [89] L. V. Keldysh, Sov. Phys. JETP **20**, 1018 (1965).
- [90] B. L. Altshuler and A. G. Aronov, Pis'ma Zh. Eksp. Teor. Fiz. **27**, 700 (1978); [JETP Lett. **27**, 662 (1978)].
- [91] B. L. Altshuler and A. G. Aronov, Zh. Eksp. Teor. Fiz. **75**, 1610 (1978); [Sov. Phys. JETP **48**, 812 (1978)].
- [92] B. L. Altshuler and A. G. Aronov, Pis'ma, Zh. Eksp. Teor. Fiz. **30**, 514, (1979); [JETP Lett. **30**, 482 (1979)].

- [93] G. Eilenberger, Z. Phys. **214**, 195 (1968).
- [94] G. M. Eliashberg, Sov. Phys. JETP **34**, 668 (1971).
- [95] A. I. Larkin and Yu. V. Ovchinnikov, Sov. Phys. JETP **28**, 1200 (1969).
- [96] A. I. Larkin and Yu. V. Ovchinnikov, Sov. Phys. JETP **41**, 960 (1975);
Sov. Phys. JETP **46** 155 (1977).
- [97] P. Wölfle, Prog. Low Temp. Phys. **7**, 191 (1978).
- [98] J. W. Serene and D. Rainer, Phys. Rep. **101**, 221 (1983).
- [99] S. N. Artemenko and A. F. Volkov, Zh. Eksp. Teor. Fiz. **80**, 2018
(1981); [Sov. Phys. JETP **53**, 1050 (1981)].
- [100] S. N. Artemenko and A. F. Volkov, Zh. Eksp. Teor. Fiz. **81**, 1872
(1981); [Sov. Phys. JETP **54**, 992 (1981)].
- [101] U. Eckern, J. Low Temp. Phys. **62**, 525 (1986).
- [102] Guang-Zhao Zhou, Zhao-bin Su, Bai-lin Hao, and Lu Yu, Phys. Rev.
B **22**, 338 (1980).
- [103] A. Schmid, J. Low Temp. Phys. **49**, 609 (1982).
- [104] Y. Nambu, Phys. Rev. **117**, 648 (1960).
- [105] J. R. Schrieffer, *The Theory of Superconductivity*, (Benjamin, New
York, 1964).
- [106] L. P. Gor'kov, Sov. Phys. JETP **9**, 1364 (1959); Sov. Phys. JETP **10**,
998 (1960)
- [107] A. I. Larkin and Yu. N. Ovchinnikov, in *Nonequilibrium Superconductivity*,
edited by D. N. Langenberg and A. I. Larkin (North Holland,
Amsterdam, 1986), p. 493; J. Rammer and H. Smith Rev. Mod. Phys.
58, 323 (1986); C. J. Lambert and R. Raimondi, J. Phys.: Condens.
Matter **10**, 901 (1998); N. B. Kopnin, *Theory of Nonequilibrium Superconductivity*,
Clarendon Press, Oxford, (2001); Venkat Chandrasekhar,
cond-mat/0312507, Chapter published in, " *The Physics of Superconductors*,"
Vol II, edited by Bennemann and Ketterson, Springer-Verlag,
2004.
- [108] A. Shelankov and M. Ozana, Phys. Rev. B **61**, 7077 (2000).

- [109] M. V. Feigelman, A. I. Larkin, and M. A. Skvortsov, Phys. Rev. B **61**, 12361 (2000).
- [110] K.D. Usadel, Phys. Rev. Lett. **25** 507 (1970).
- [111] K. B. Efetov, A. I. Larkin, and D. E. Khmel'nitsky, Zh. Eksp. Teor. Fiz. **79**, 1120 (1980) [Sov. Phys. JETP **52**, 568 (1980)].
- [112] K. B. Efetov, Adv. Phys. **32**, 53 (1983); *Supersymmetry in Disorder and Chaos* (Cambridge University Press, New York, 1997).
- [113] P. Schwab and R. Raimondi, Ann. Phys. (Leipzig) **12**, 471 (2003).
- [114] N. Schopohl, cond-mat/9804064 (unpublished).
- [115] Y. Fuseya, H. Kohno and K. Miyake, J. Phys. Soc. Jpn. **72**, 2914 (2003).
- [116] S. Kawasaki, T. Mito, Y. Kawasaki, G.-q. Zheng, Y. Kitaoka, D. Aoki, Y. Haga, and Y. Onuki, Phys. Rev. Lett. **91**, 137001 (2003).
- [117] Guo-qing Zheng, N. Yamaguchi, H. Kan, Y. Kitaoka, J. L. Sarrao, P. G. Pagliuso, N. O. Moreno, and J. D. Thompson, Phys. Rev. B **70**, 014511 (2004).

Chapter 2

Resonant proximity effect in normal metal / diffusive ferromagnet / superconductor junctions

2.1 Introduction

There is a continuously growing interest in the physics of charge and spin transport in ferromagnet / superconductor (F/S) junctions. One of the applications of F/S junctions is determination of the spin polarization of the F layer. Analyzing signatures of Andreev reflection [1] in differential conductance by a modified Blonder, Tinkham and Klapwijk (BTK) theory[2], one can estimate the spin polarization of the F layer [3, 4, 5, 6, 7, 8]. This method was generalized and applied to ferromagnet / unconventional superconductor junctions[9] . Most of these works are applicable to ballistic ferromagnets while understanding of physics in contacts between diffusive ferromagnets (DF) and (both conventional and unconventional) superconductors (S) is not complete yet. The model should also properly take into account the proximity effect in the DF/S system.

In DF/S junctions Cooper pairs penetrating into the DF layer from the S layer have nonzero momentum due to the exchange field[10, 11, 12, 13, 14, 15]. This property results in many interesting phenomena[16, 17, 18, 19, 20, 21, 22, 23, 24, 25, 26, 28, 27, 29, 30]. One interesting consequence of the oscillations of the pair amplitude is the spatially damped oscillating behavior of the density of states (DOS) in a ferromagnet predicted theoretically [31, 33, 32, 34] in various regimes. The energy dependent DOS calculated in the clean [32]

and the dirty [35] limits exhibits rich structures. Experimentally DOS in F/S bilayers was measured by Kontos *et al.* who found a broad DOS peak around zero energy when the π -phase shift occurs[37]. In diffusive ferromagnet/superconductor (DF/S) junctions the zero-energy DOS may have a sharp peak [35]. However the conditions for the appearance of such anomaly have not been studied systematically so far.

The purpose of the present chapter is to calculate DOS in N/DF/S junctions and to formulate the conditions for the zero-energy DOS peak in two regimes corresponding to the weak proximity effect (large DF/S interface resistance) and strong proximity effect (small DF/S interface resistance). We will show that in the former case the condition is equivalent to the one of Ref. [35], while in the latter case the new condition is found. The calculation will be performed in the zero-temperature regime by varying the interface resistances as well as the resistance, the exchange field and the Thouless energy of the DF layer. Since DOS is a fundamental quantity, this *resonant proximity effect* can influence various physical quantities like transport phenomena.

It is known that in contacts involving unconventional superconductors the so-called zero-bias conductance peak (ZBCP) takes place due to the formation of the midgap Andreev resonant states (MARS) [38, 39, 40, 41]. An interplay of the resonant proximity effect with MARS in DF/*d*-wave superconductor (DF/D) junctions is an interesting subject which deserves theoretical study.

Therefore, we will formulate theoretical model for the charge transport in the normal metal/DF/*s*- and *d*-wave superconductor (N/DF/S) junctions and to study the influence of the resonant proximity effect due to the exchange field on the tunneling conductance and the DOS. A number of physical phenomena may coexist in these structures such as impurity scattering, oscillating pair amplitude, phase coherence and MARS. We will employ the quasiclassical Usadel equations [42] with the Kupriyanov-Lukichev boundary conditions [43] generalized by Nazarov within the circuit theory [44]. The generalized boundary conditions are relevant for the actual junctions when the barrier transparency is not small. New physical phenomena regarding zero-bias conductance are properly described within this approach, e.g., the crossover from a ZBCP to a zero bias conductance dip (ZBCD). The generalized boundary conditions were recently applied to the study of contacts of diffusive normal metals (DN) with conventional [45] and unconventional superconductors [46, 47, 48]. Here we consider the case of N/DF/S junctions with a weak ferromagnet having small exchange field comparable with the superconducting gap. SF contacts with weak ferromagnets were realized in recent experiments with, e.g., CuNi alloys [16], Ni doped Pd[37] or magnetic semiconductors. Therefore, our results are applicable to these materials and

may be observed experimentally.

The normalized conductance of the N/DF/S junction $\sigma_T(eV) = \sigma_S(eV)/\sigma_N(eV)$ will be studied as a function of the bias voltage V , where $\sigma_{S(N)}(eV)$ is the tunneling conductance in the superconducting (normal) state. We will consider the influence of various parameters on $\sigma_T(eV)$, such as the height of the interface insulating barriers, the resistance R_d , the exchange field h and the Thouless energy E_{Th} in the DF layer. In the case of d -wave superconductor, important parameter is the angle between the normal to the interface and the crystal axis of d -wave superconductor α . Throughout the chapter we confine ourselves to zero temperature and put $k_B = \hbar = 1$.

The organization of this chapter is as follows. In section 2, we will provide the detailed derivation of the expression for the normalized tunneling conductance. In section 3, the results of calculations are presented for various types of junctions. In section 4, the summary of the obtained results is given.

2.2 Formulation

In this section we introduce the model and the formalism. We consider a junction consisting of normal and superconducting reservoirs connected by a quasi-one-dimensional diffusive ferromagnet (DF) conductor with a length L much larger than the mean free path. The interface between the DF conductor and the S electrode has a resistance R_b while the DF/N interface has a resistance R'_b . The positions of the DF/N interface and the DF/S interface are denoted as $x = 0$ and $x = L$, respectively. We model infinitely narrow insulating barriers by the delta function $U(x) = H\delta(x - L) + H'\delta(x)$. The resulting transparency of the junctions T_m and T'_m are given by $T_m = 4 \cos^2 \phi / (4 \cos^2 \phi + Z^2)$ and $T'_m = 4 \cos^2 \phi / (4 \cos^2 \phi + Z'^2)$, where $Z = 2H/v_F$ and $Z' = 2H'/v_F$ are dimensionless constants and ϕ is the injection angle measured from the interface normal to the junction and v_F is Fermi velocity.

We apply the quasiclassical Keldysh formalism in the following calculation of the tunneling conductance. The 4×4 Green's functions in N, DF and S are denoted by $\check{G}_0(x)$, $\check{G}_1(x)$ and $\check{G}_2(x)$ respectively where the Keldysh component $\hat{K}_{0,1,2}(x)$ is given by $\hat{K}_i(x) = \hat{R}_i(x)\hat{f}_i(x) - \hat{f}_i(x)\hat{A}_i(x)$ with retarded component $\hat{R}_i(x)$, advanced component $\hat{A}_i(x) = -\hat{R}_i^*(x)$ using distribution function $\hat{f}_i(x)$ ($i = 0, 1, 2$). In the above, $\hat{R}_0(x)$ is expressed by $\hat{R}_0(x) = \hat{\tau}_3$ and $\hat{f}_0(x) = f_{l0} + \hat{\tau}_3 f_{t0}$. $\hat{R}_2(x)$ is expressed by $\hat{R}_2(x) = g\hat{\tau}_3 + f\hat{\tau}_2$ with $g = \epsilon/\sqrt{\epsilon^2 - \Delta^2}$ and $f = \Delta/\sqrt{\Delta^2 - \epsilon^2}$, where $\hat{\tau}_2$ and $\hat{\tau}_3$ are the Pauli matrices, and ϵ denotes the quasiparticle energy measured from the Fermi energy and $\hat{f}_2(x) = \tanh(\epsilon/2T)$ in thermal equilibrium with temperature T .

We put the electrical potential zero in the S-electrode. In this case the spatial dependence of $\check{G}_1(x)$ in DF is determined by the static Usadel equation [42],

$$D \frac{\partial}{\partial x} [\check{G}_1(x) \frac{\partial \check{G}_1(x)}{\partial x}] + i[\check{H}, \check{G}_1(x)] = 0 \quad (2.1)$$

with the diffusion constant D in DF. Here \check{H} is given by

$$\check{H} = \begin{pmatrix} \hat{H}_0 & 0 \\ 0 & \hat{H}_0 \end{pmatrix},$$

with $\hat{H}_0 = (\epsilon - (+)h)\hat{\tau}_3$ for majority(minority) spin where h denotes the exchange field. Note that we assume a weak ferromagnet and neglect the difference of Fermi velocity between majority spin and minority spin. The Nazarov's generalized boundary condition for $\check{G}_1(x)$ at the DF/S interface is given in Refs.[45, 47]. The generalized boundary condition for $\check{G}_1(x)$ at the DF/N interface has the form:

$$\frac{L}{R_d} (\check{G}_1 \frac{\partial \check{G}_1}{\partial x})|_{x=0+} = -R_b'^{-1} \langle B \rangle', \quad (2.2)$$

$$B = \frac{2T'_m[\check{G}_0(0_-), \check{G}_1(0_+)]}{4 + T'_m([\check{G}_0(0_-), \check{G}_1(0_+)]_+ - 2)}.$$

The average over the various angles of injected particles at the interface is defined as

$$\langle B(\phi) \rangle^{(l)} = \frac{\int_{-\pi/2}^{\pi/2} d\phi \cos \phi B(\phi)}{\int_{-\pi/2}^{\pi/2} d\phi T^{(l)}(\phi) \cos \phi}$$

with $B(\phi) = B$ and $T^{(l)}(\phi) = T_m^{(l)}$. The resistance of the interface R_b is given by

$$R_b^{(l)} = R_0^{(l)} \frac{2}{\int_{-\pi/2}^{\pi/2} d\phi T^{(l)}(\phi) \cos \phi}.$$

Here $R_0^{(l)}$ is Sharvin resistance given by $R_0^{(l)-1} = e^2 k_F^2 S_c^{(l)} / (4\pi^2)$ in the three-dimensional case.

The electric current per spin direction is expressed using $\check{G}_1(x)$ as

$$I_{el} = \frac{-L}{8eR_d} \int_0^\infty d\epsilon \text{Tr}[\hat{\tau}_3 (\check{G}_1(x) \frac{\partial \check{G}_1(x)}{\partial x})^K], \quad (2.3)$$

where $(\check{G}_1(x) \frac{\partial \check{G}_1(x)}{\partial x})^K$ denotes the Keldysh component of $(\check{G}_1(x) \frac{\partial \check{G}_1(x)}{\partial x})$. In the actual calculation it is convenient to use the standard θ -parameterization where function $\hat{R}_1(x)$ is expressed as $\hat{R}_1(x) = \hat{\tau}_3 \cos \theta(x) + \hat{\tau}_2 \sin \theta(x)$. The parameter $\theta(x)$ is a measure of the proximity effect in DF.

The distribution function $\hat{f}_1(x)$ is given by $\hat{f}_1(x) = f_l(x) + \hat{\tau}_3 f_t(x)$ where the component $f_t(x)$ determines the conductance of the junction we are now concentrating on. From the retarded or advanced component of the Usadel equation, the spatial dependence of $\theta(x)$ is determined by the following equation

$$D \frac{\partial^2}{\partial x^2} \theta(x) + 2i(\epsilon - (+)h) \sin[\theta(x)] = 0 \quad (2.4)$$

for majority(minority) spin, while for the Keldysh component we obtain

$$D \frac{\partial}{\partial x} \left[\frac{\partial f_t(x)}{\partial x} \cosh^2 \theta_{im}(x) \right] = 0. \quad (2.5)$$

At $x = 0$, since f_{t0} is the distribution function in the normal electrode, it is given by

$$f_{t0} = \frac{1}{2} \{ \tanh[(\epsilon + eV)/(2T)] - \tanh[(\epsilon - eV)/(2T)] \}. \quad (2.6)$$

Next we focus on the boundary condition at the DF/N interface. Taking the retarded part of Eq. (2.2), we obtain

$$\frac{L}{R_d} \frac{\partial \theta(x)}{\partial x} \Big|_{x=0_+} = \frac{\langle F \rangle'}{R'_b},$$

$$F = \frac{2T'_m \sin \theta_0}{(2 - T'_m) + T'_m \cos \theta_0}, \quad (2.7)$$

with $\theta_0 = \theta(0_+)$.

On the other hand, from the Keldysh part of Eq. (2.2), we obtain

$$\frac{L}{R_d} \left(\frac{\partial f_t}{\partial x} \right) \cosh^2 \theta_{im}(x) \Big|_{x=0_+} = - \frac{\langle I_{b1} \rangle' (f_{t0} - f_t(0_+))}{R'_b}, \quad (2.8)$$

with

$$I_{b1} = \frac{T_m'^2 \Lambda'_1 + 2T'_m (2 - T'_m) \text{Real}\{\cos \theta_0\}}{|(2 - T'_m) + T'_m \cos \theta_0|^2}$$

$$\Lambda'_1 = (1 + |\cos \theta_0|^2 + |\sin \theta_0|^2).$$

Finally, we obtain the following result for the electric current through the contact

$$I_{el} = \frac{1}{2e} \int_0^\infty d\epsilon \frac{f_{t0}}{\frac{R_b}{\langle I_{b0} \rangle} + \frac{R_d}{L} \int_0^L \frac{dx}{\cosh^2 \theta_{im}(x)} + \frac{R'_b}{\langle I_{b1} \rangle'}}. \quad (2.9)$$

Then the differential resistance R per one spin projection at zero temperature is given by

$$R = \frac{2R_b}{\langle I_{b0} \rangle} + \frac{2R_d}{L} \int_0^L \frac{dx}{\cosh^2 \theta_{im}(x)} + \frac{2R'_b}{\langle I_{b1} \rangle'}. \quad (2.10)$$

with

$$I_{b0} = \frac{T_m^2 \Lambda_1 + 2T_m(2 - T_m)\Lambda_2}{2 | (2 - T_m) + T_m[g \cos \theta_L + f \sin \theta_L] |^2},$$

$$\begin{aligned} \Lambda_1 &= (1 + |\cos \theta_L|^2 + |\sin \theta_L|^2)(|g|^2 + |f|^2 + 1) \\ &\quad + 4\text{Imag}[fg^*]\text{Imag}[\cos \theta_L \sin \theta_L^*], \end{aligned} \quad (2.11)$$

$$\Lambda_2 = \text{Real}\{g(\cos \theta_L + \cos \theta_L^*) + f(\sin \theta_L + \sin \theta_L^*)\}. \quad (2.12)$$

This is an extended version of the Volkov-Zaitsev-Klapwijk formula [49]. For a d -wave junction, the function I_{b0} is given by the following expression[47]

$$I_{b0} = \frac{T_m}{2} \frac{C_0}{|(2 - T_m)(1 + g_+g_- + f_+f_-) + T_m[\cos \theta_L(g_+ + g_-) + \sin \theta_L(f_+ + f_-)]|^2}$$

$$\begin{aligned} C_0 &= T_m(1 + |\cos \theta_L|^2 + |\sin \theta_L|^2)[|g_+ + g_-|^2 + |f_+ + f_-|^2 \\ &\quad + |1 + f_+f_- + g_+g_-|^2 + |f_+g_- - g_+f_-|^2] \end{aligned}$$

$$\begin{aligned}
& +2(2 - T_m)\text{Real}\{(1 + g_+^*g_-^* + f_+^*f_-^*)((\cos\theta_L + \cos\theta_L^*)(g_+ + g_-) + (\sin\theta_L + \sin\theta_L^*)(f_+ + f_-))\} \\
& +4T_m\text{Imag}(\cos\theta_L \sin\theta_L^*)\text{Imag}[(f_+ + f_-)(g_+^* + g_-^*)], \tag{2.13}
\end{aligned}$$

$g_{\pm} = \varepsilon/\sqrt{\varepsilon^2 - \Delta_{\pm}^2}$, $f_{\pm} = \Delta_{\pm}/\sqrt{\Delta_{\pm}^2 - \varepsilon^2}$ and $\Delta_{\pm} = \Delta \cos 2(\phi \mp \alpha)$. In the above α , $\theta_{im}(x)$ and θ_L denote the angle between the normal to the interface and the crystal axis of d -wave superconductors, the imaginary part of $\theta(x)$ and $\theta(L_-)$ respectively. Then the total tunneling conductance in the superconducting state $\sigma_S(eV)$ is given by $\sigma_S(eV) = \sum_{\uparrow,\downarrow} 1/R$. The local normalized DOS $N(\varepsilon, x)$ in the DF layer is given by

$$N(\varepsilon, x) = \frac{1}{2} \sum_{\uparrow,\downarrow} \text{Re} \cos \theta(x).$$

It is important to note that in the present approach, according to the circuit theory, $R_d/R_b^{(\prime)}$ can be varied independently of $T_m^{(\prime)}$, *i.e.*, independently of $Z^{(\prime)}$. Based on this fact, we can choose $R_d/R_b^{(\prime)}$ and $Z^{(\prime)}$ as independent parameters.

In the following section, we will discuss the DOS and the normalized tunneling conductance $\sigma_T(eV) = \sigma_S(eV)/\sigma_N(eV)$ where $\sigma_N(eV)$ is the tunneling conductance in the normal state given by $\sigma_N(eV) = \sigma_N = 1/(R_d + R_b + R_b')$.

2.3 Results

In this section, we first formulate the conditions for the formation of zero-energy peak in DOS. Next, we study the influence of the resonant proximity effect on tunneling conductance as well as the DOS in the DF region. The resonant proximity effect are shown to be characterized as follows. When the proximity effect is weak ($R_d/R_b \ll 1$), the resonant condition is given by $R_d/R_b \sim 2h/E_{Th}$ due to the exchange splitting of DOS in different spin subbands. When the proximity effect is strong ($R_d/R_b \gg 1$), the condition is given by $E_{Th} \sim h$ and is realized when the length of a ferromagnet is equal to the coherence length $\xi_F = \sqrt{D/h}$.

In subsections 2.3.2 and 2.3.3, we choose $R_d/R_b = 1$ and $R_d/R_b = 5$ as typical values representing the weak and strong proximity regime, respectively. We fix $Z' = 3$ because this parameter doesn't change the results qualitatively and consider the case of high barrier at the N/DF interface, $R_d/R_b' = 0.1$, when the proximity effect is strong.

2.3.1 Conditions for the formation of zero-energy peak in DOS

Below we will concentrate on the DOS at $x = 0$ (N/DF interface) in the regime of large resistance of the N/DF interface, $R_d/R'_b \ll 1$ and will also fix the barrier transparency parameters $Z = 3$, $Z' = 3$.

In order to study the condition for the appearance of the zero energy DOS peak, we plot the normalized zero energy DOS at $x = 0$ as a function of $E_{Th} = D/L^2$. Figure 2.1 shows the DOS for $R_d/R'_b = 0.1$ and various h/Δ . In Fig. 2.1 (a) the zero-energy peak appears at $E_{Th} \sim 2hR_b/R_d$, while in Fig. 2.1 (b) and (c) the peak appears at $E_{Th} \sim h$. Thus we can conclude that the condition for the DOS peak for large R_d/R_b is essentially different from the one for small R_d/R_b .

Figure 2.2 shows the DOS as a function of ε for the parameters corresponding to the peaks in Fig. 2.1 for various h/Δ . In all these cases the DOS peak appears around zero energy. For small h/Δ the DOS peak is narrow but it becomes broader with the increase of h/Δ . It's important to note that this peak does *not* always require the sign change of pair amplitude. This is also clear from the fact that the peak occurs for large Thouless energy (short DF) when there is no sign change. For other set of parameters the DOS peak is smeared as they break the condition $E_{Th} \sim 2hR_b/R_d$ or $E_{Th} \sim h$.

Let us first discuss the case of strong proximity effect in detail. Fig. 2.3 shows the zero energy DOS at $x = 0$ as a function of E_{Th} for $h/\Delta = 1$ and various R_d/R'_b with (a) $R_d/R_b = 5$ and (b) $R_d/R_b = 10$. In this case the peak at $E_{Th} \sim h$ is suppressed with increasing R_d/R'_b . Therefore this condition is valid for small R_d/R'_b .

Figure 2.4 shows the spatial dependence of $\text{Im}\theta$ for majority spin for $R_d/R'_b = 0.1$, $E_{Th}/\Delta = 1$ and various h/Δ with (a) $R_d/R_b = 5$ and (b) $R_d/R_b = 10$. For the appearance of the DOS peak, large value of $\text{Im}\theta$ is needed because the normalized DOS is given by $\text{Re}\cos(\theta) = \cos(\text{Re}(\theta)) \cosh(\text{Im}(\theta))$. As seen from Fig. 2.4, the magnitude of $\text{Im}\theta$ increases with the increase of the distance from the DF/S interface and achieves a maximum when $E_{Th} = h$.

Note that the zero-energy DOS at $x = 0$ does not depend on E_{Th} if the condition $E_{Th} = h$ holds. To explain that, let's write Eqs. 2.4 and 2.7 at $\varepsilon = 0$:

$$\frac{\partial^2}{\partial y^2}\theta(y) - (+)2i \sin[\theta(y)] = 0 \quad (2.14)$$

$$\frac{1}{R_d} \frac{\partial \theta(y)}{\partial y} \Big|_{y=0+} = \frac{\langle F \rangle'}{R'_b} \quad (2.15)$$

where $y \equiv x/\sqrt{D/h}$. Since for $E_{Th} = h$ we have $D/h \equiv E_{Th}L^2/h = L^2$, the above equations don't contain E_{Th} as a parameter. Similar arguments can be applied to another boundary condition at DF/S interface. This proves the above statement about independence of the zero-energy DOS at $x = 0$ on E_{Th} .

Now let us discuss the weak proximity effect and derive the condition $R_d/R_b \sim 2h/E_{Th}$, following Ref. [35]. When spatial variation of θ is small, i.e., $L \ll \sqrt{D/|\varepsilon \mp h|}$ (for the spin-up or spin-down subband respectively) and both R_d/R_b and R_d/R'_b are small (weak proximity effect), θ can be expanded as $\theta = \theta_0 + \theta_1 x + \theta_2 x^2$ where $\theta_1, \theta_2 \ll \theta_0$. Note that the derivatives of θ are proportional to these quantities at the interfaces (see Eq. (2.7) and Ref. [45]).

In this case the solution of the Usadel equation in the spin-up subband satisfying boundary conditions has the form:

$$\cos \theta_{0\uparrow} = \frac{\frac{R_d}{R'_b} + \frac{R_d}{R_b}g - \frac{2i(\varepsilon-h)}{E_{Th}}}{\sqrt{\left(\frac{R_d}{R_b}f\right)^2 + \left(\frac{R_d}{R'_b} + \frac{R_d}{R_b}g - \frac{2i(\varepsilon-h)}{E_{Th}}\right)^2}}. \quad (2.16)$$

For $R_d/R'_b = 0$ and $\varepsilon = 0$, the DOS has the form

$$\cos \theta_{0\uparrow} = \frac{\frac{2ih}{E_{Th}}}{\sqrt{\left(\frac{R_d}{R_b}\right)^2 - \left(\frac{2h}{E_{Th}}\right)^2}}, \quad (2.17)$$

which provides the resonant condition $R_d/R_b \sim 2h/E_{Th}$. Similar result follows for the spin-down subband by replacing h by $-h$.

Another resonant condition for the strong proximity effect, $E_{Th} \sim h$, is equivalent to the condition $L \sim \sqrt{D/h}$. Thus, zero-energy DOS peak appears when the proximity effect is strong and the length of ferromagnet is of the order of the coherence length in a ferromagnet $\xi_F = \sqrt{D/h}$.

Let us discuss the physical meaning of two conditions. In DN/S junctions there is a minigap E_g , where $E_g \sim E_{Th}R_d/R_b$ for weak proximity effect, or $E_g \sim E_{Th}$ for strong proximity effect[47]. In DF/S junctions this minigap is shifted by h , then the DOS peak appears when $h \sim E_g$.

Note that in the calculations we have fixed $Z = Z' = 3$, but the specific parameter choice does not change the results qualitatively.

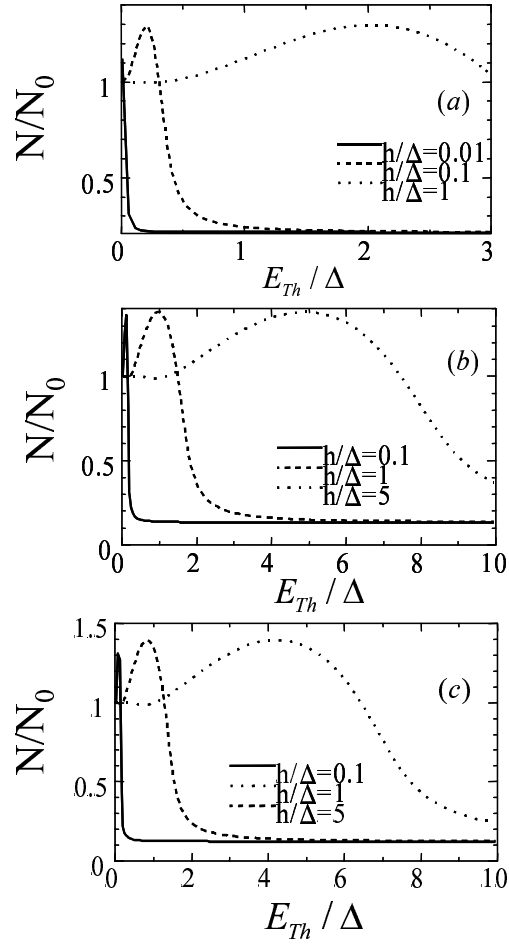


Figure 2.1: Normalized zero energy DOS as a function of E_{Th} for large resistance of the N/DF interface $R_d/R'_b = 0.1$ and various h/Δ with resistance ratios at the DF/S interface (a) $R_d/R_b = 1$, (b) $R_d/R_b = 5$ and (c) $R_d/R_b = 10$.

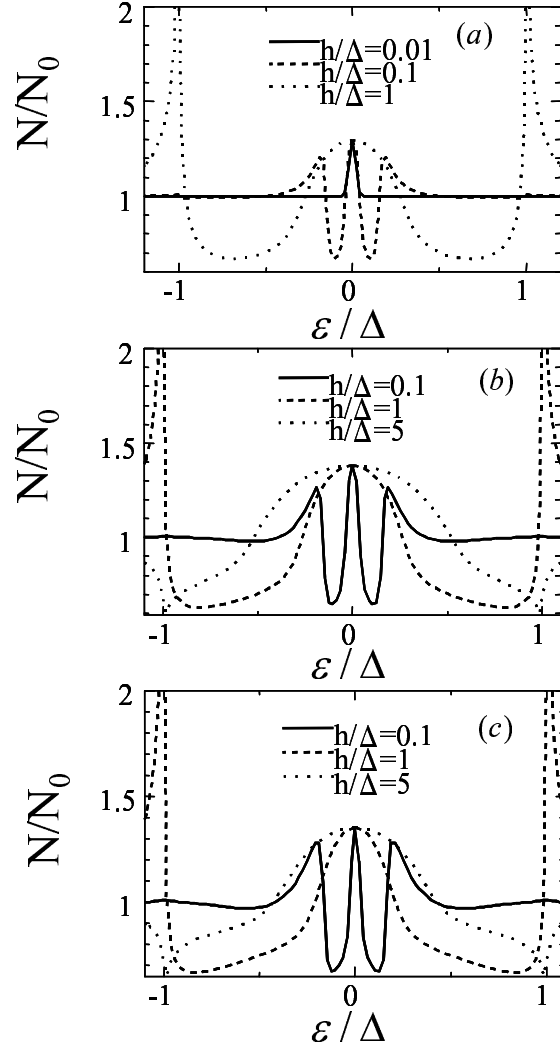


Figure 2.2: Normalized DOS as a function of ε for $R_d/R'_b = 0.1$ and various h/Δ with (a) $R_d/R_b = 1$ and $E_{Th} = 2hR_b/R_d = 2h$, (b) $R_d/R_b = 5$ and $E_{Th} = h$, and (c) $R_d/R_b = 10$ and $E_{Th} = h$.

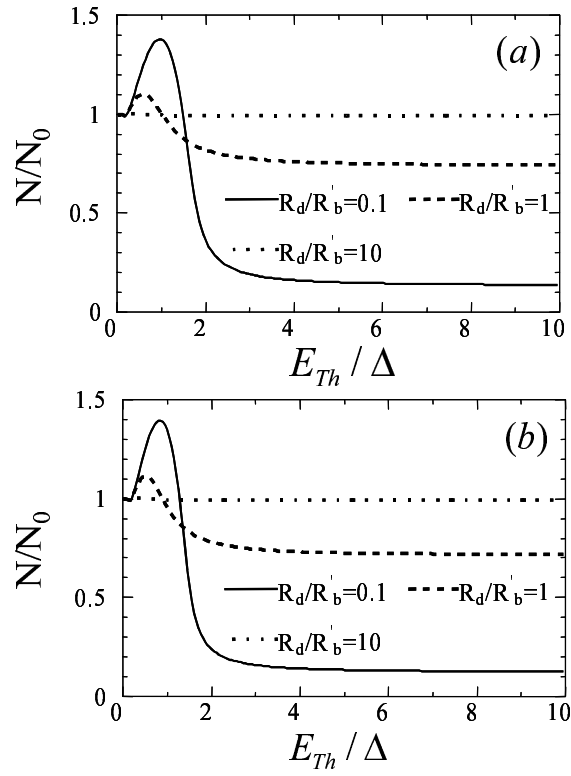


Figure 2.3: Normalized DOS at zero energy as a function of E_{Th} for $h/\Delta = 1$ and various R_d/R'_b with (a) $R_d/R_b = 5$ and (b) $R_d/R_b = 10$.

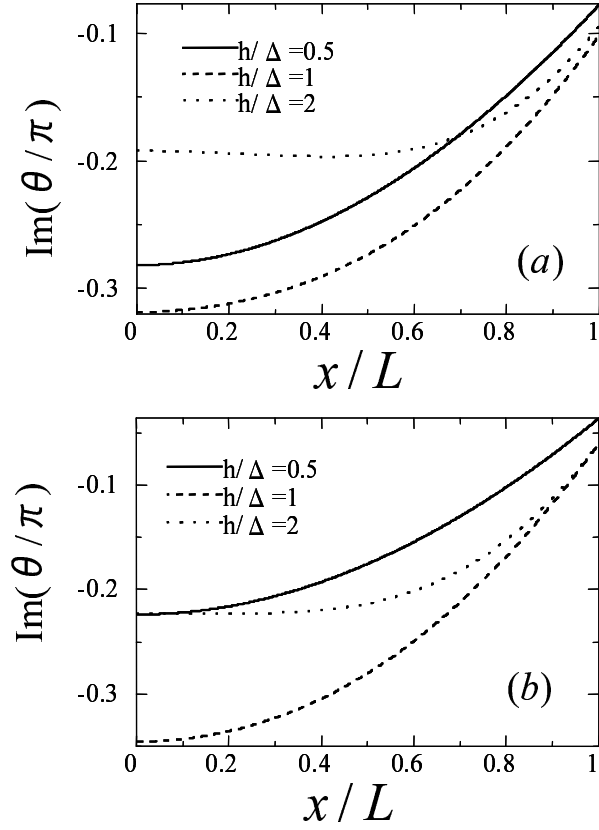


Figure 2.4: Spatial dependence of $\text{Im}\theta$ for majority spin for $R_d/R'_b = 0.1$, $E_{Th}/\Delta = 1$ and various h/Δ with (a) $R_d/R_b = 5$ and (b) $R_d/R_b = 10$. The DF/N interface and the DF/S interface are located at $x = 0$ and $x = L$ respectively.

2.3.2 Junctions with s -wave superconductors

Here, we first choose the weak proximity regime and relatively small Thouless energy, $E_{Th}/\Delta = 0.01$. In this case the resonant condition is satisfied for $h/\Delta = 0.005$. In Fig. 2.5 the tunneling conductance is plotted for $R_d/R_b = 1$, $E_{Th}/\Delta = 0.01$ and various h/Δ with (a) $Z = 3$ and (b) $Z = 0$. The ZBCP and ZBCD occur due to the proximity effect for $h = 0$. For $h/\Delta = 0.005$, the resonant ZBCP appears and split into two peaks or dips at $eV \sim \pm h$ with increasing h/Δ . The value of the resonant ZBCP exceeds unity. Note that ZBCP due to the conventional proximity effect in DN/S junctions is always less than unity [50, 49, 45] and therefore is qualitatively different from the resonant ZBCP in the DF/S junctions.

The corresponding normalized DOS of the DF is shown in Fig. 2.6. Note that in the DN/S junctions, the proximity effect is almost independent on Z parameter[45]. We have checked numerically that this also holds for the proximity effect in DF/S junctions. Figure 2.6 displays the DOS for $Z = 3$, $R_d/R_b = 1$ and $E_{Th}/\Delta = 0.01$ with (a) $h/\Delta = 0$ and (b) $h/\Delta = 0.005$ corresponding to the resonant condition. For $h = 0$, a sharp dip appears at zero energy over the whole DF region. For nonzero energy, the DOS is almost unity and spatially independent. For $h/\Delta = 0.005$ a zero energy peak appears in the region of DF near the DF/N interface. This peak is responsible for the large ZBCP shown in Fig. 2.5. Therefore ZBCP in DF/S junctions has different physical origin compared to the one in DN/S junctions.

Next we choose the strong proximity regime and relatively small Thouless energy, $E_{Th}/\Delta = 0.01$. In the present case, the resonant ZBCP is expected for $h/\Delta = 0.01$. Figure 2.7 displays the tunneling conductance for $R_d/R_b = 5$ and $E_{Th}/\Delta = 0.01$ and various h/Δ with (a) $Z = 3$ and (b) $Z = 0$. In this case we also find resonant ZBCP and splitting of the peak as in Fig. 2.5. The corresponding DOS of Fig. 2.7(a) is shown in Fig. 2.8 for (a) $h/\Delta = 0$ and (b) $h/\Delta = 0.01$. For $h = 0$, a sharp dip appears at zero energy. For finite energy the DOS is almost unity and spatially independent. For $h/\Delta = 0.01$ a peak occurs at zero energy in the range of x near the DF/N interface. We can find similar structures in the corresponding conductance as shown in Fig. 2.7. The DOS around zero energy is strongly suppressed at the DF/S interface ($x = L$) compared to the one in Fig. 2.6.

Let us study the junctions with relatively large Thouless energy. In this case, tunneling conductance is insensitive to the change of Z . In Fig. 2.9 we show the tunneling conductance and corresponding DOS for $Z = 3$, $R_d/R_b = 1$, $E_{Th}/\Delta = 10$ and various h/Δ . We find the broad peak of the conductance by the resonant proximity effect for $h/\Delta = 5$ in Fig. 2.9 (a). For $h/\Delta = 0$, the DOS has a gap-like structure as shown in Fig. 2.9 (b) while for $h/\Delta = 5$

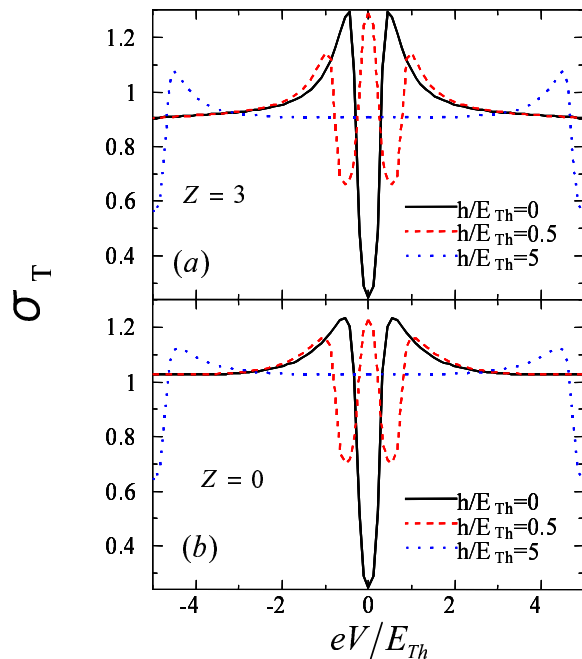
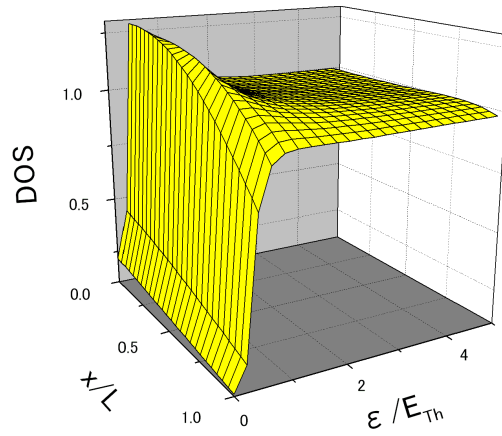


Figure 2.5: Normalized tunneling conductance for s -wave superconductors with $R_d/R_b = 1$ and $E_{Th}/\Delta = 0.01$.

it has a zero-energy peak as shown in Fig. 2.9 (c). Similar plots are shown in Fig. 2.10 for $Z = 3$, $R_d/R_b = 5$, $E_{Th}/\Delta = 10$ and various h/Δ . We find the broad ZBCP by the resonant proximity effect for $h/\Delta = 10$ in Fig. 2.10 (a). The DOS for $h/\Delta = 0$ has a gap-like structure as shown in Fig. 2.10 (b). For $h/\Delta = 10$ a zero-energy peak appears as shown in Fig. 2.10 (c).

Before ending this subsection we will look at the spatial dependence of the proximity parameter, θ . Figure 2.11 displays the spatial dependence of $\text{Re}\theta$ and $\text{Im}\theta$ for majority spin at zero energy. We choose the same parameters as those in Fig 2.5 (a) and Fig 2.7 (a) for (a) and (b), and (c) and (d) in Fig. 2.11 respectively. For the appearance of the DOS peak, large value of $\text{Im}\theta$ is needed because the normalized DOS is given by $\text{Re}\cos(\theta) = \cos(\text{Re}(\theta))\cosh(\text{Im}(\theta))$. When the resonant conditions are satisfied, $\text{Im}\theta$ has an actually large value as shown in Fig. 2.11 (b) and (d). Otherwise we can see the damped oscillating behavior of the proximity parameter. In contrast to $\text{Im}\theta$, $\text{Re}\theta$ becomes suppressed with increasing h/Δ independently of the resonant proximity effect (Fig. 2.11 (a) and (c)).

(a) $h/E_{Th} = 0$



(b) $h/E_{Th} = 0.5$

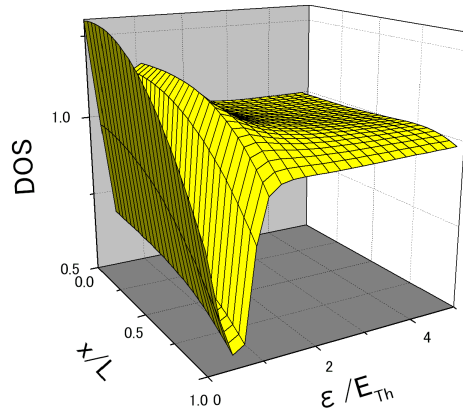


Figure 2.6: Normalized DOS for s -wave superconductors with $Z = 3$, $R_d/R_b = 1$ and $E_{Th}/\Delta = 0.01$.

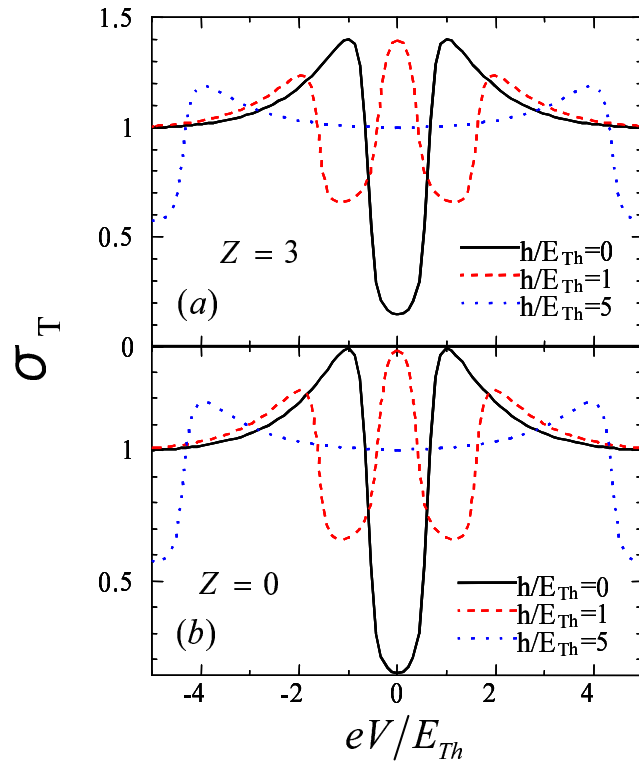
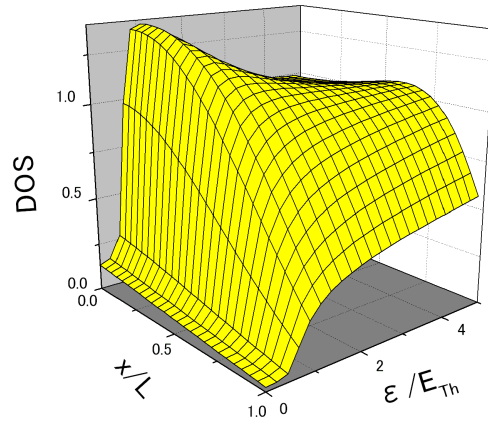


Figure 2.7: Normalized tunneling conductance for s -wave superconductors with $R_d/R_b = 5$ and $E_{Th}/\Delta = 0.01$.

(a) $h/E_{Th} = 0$



(b) $h/E_{Th} = 1$

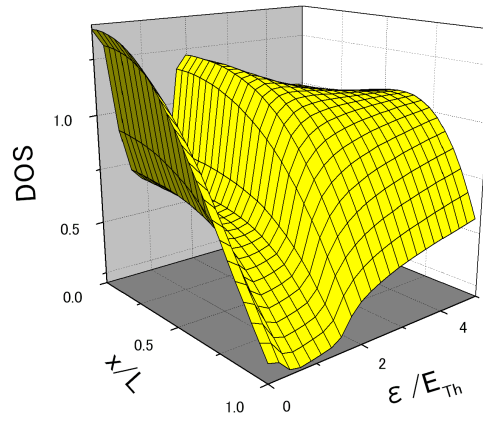


Figure 2.8: Normalized DOS for s -wave superconductors with $Z = 3$, $R_d/R_b = 5$ and $E_{Th}/\Delta = 0.01$.

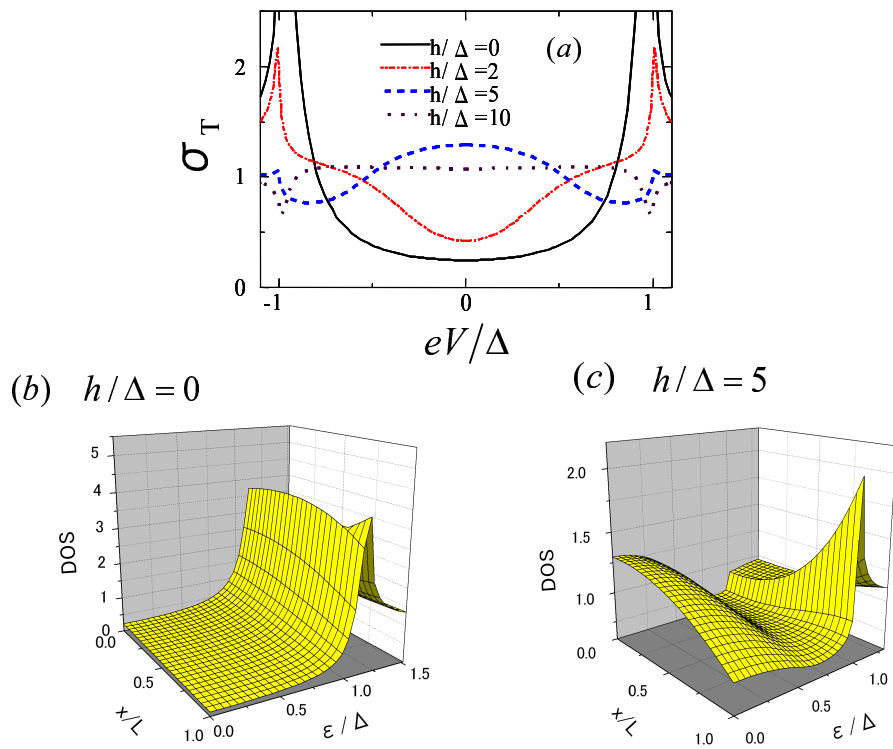


Figure 2.9: Normalized tunneling conductance and corresponding DOS for s -wave superconductors with $Z = 3$, $R_d/R_b = 1$ and $E_{Th}/\Delta = 10$.

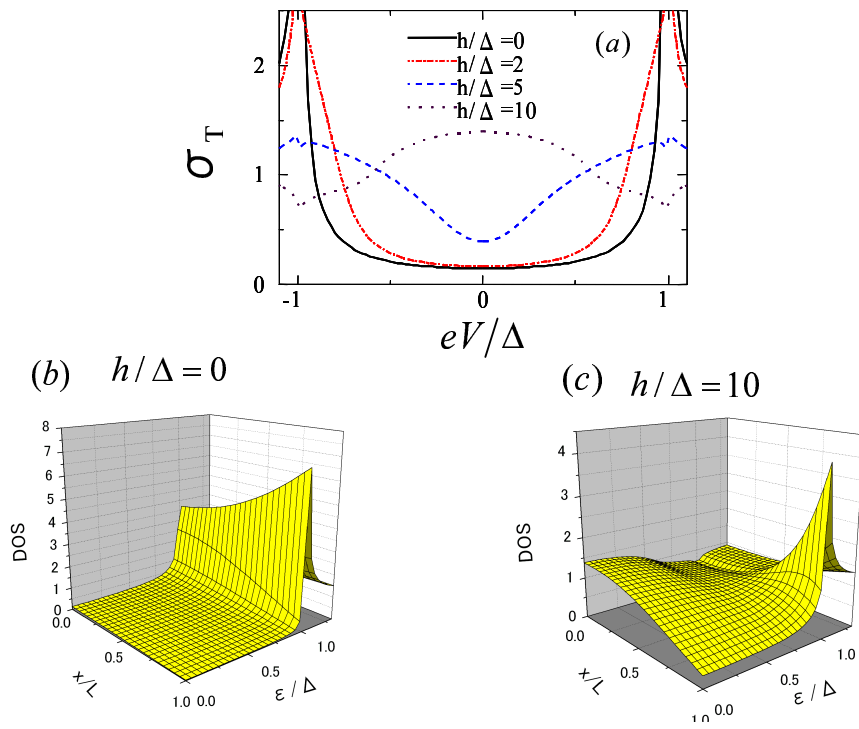


Figure 2.10: Normalized tunneling conductance and corresponding DOS for s -wave superconductors with $Z = 3$, $R_d/R_b = 5$ and $E_{Th}/\Delta = 10$.

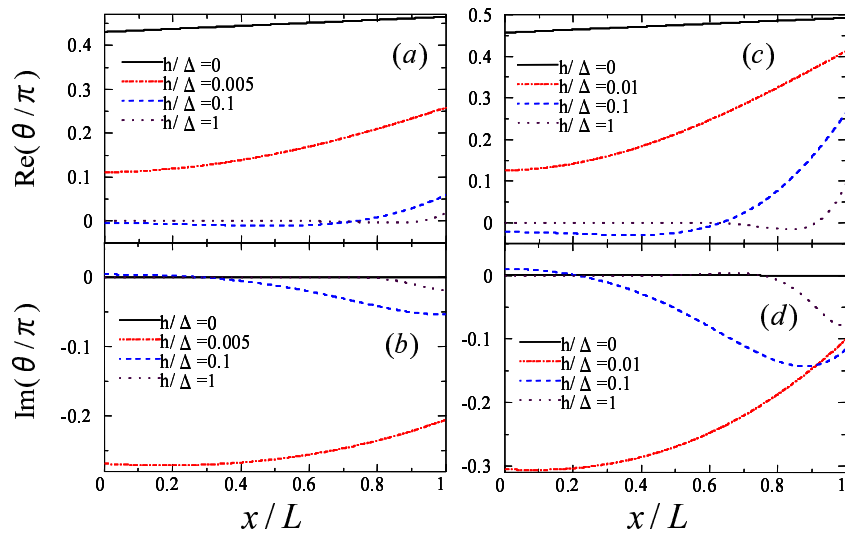


Figure 2.11: Spatial dependence of $\text{Re}\theta$ and $\text{Im}\theta$ for s -wave superconductors with $Z = 3$, $E_{Th}/\Delta = 0.01$. $R_d/R_b = 1$ (left panels) and $R_d/R_b = 5$ (right panels).

2.3.3 Junctions with d -wave superconductors

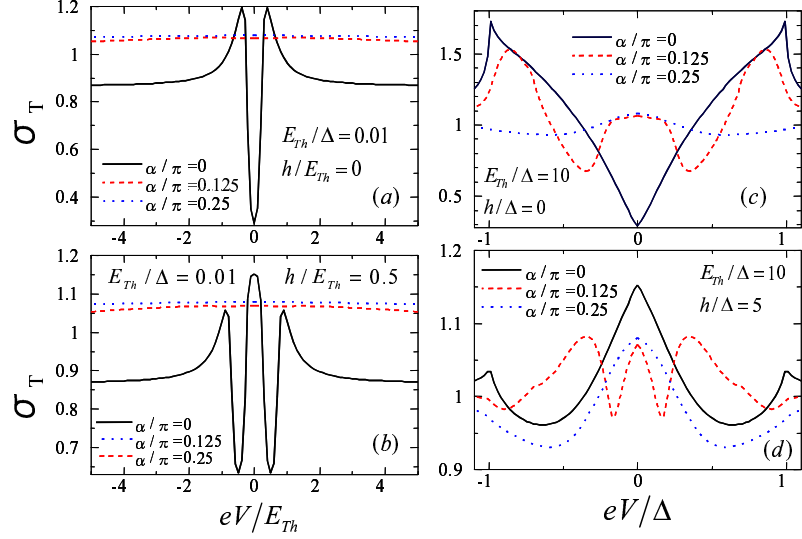


Figure 2.12: Normalized tunneling conductance for d -wave superconductors with $Z = 3$ and $R_d/R_b = 1$.

In this subsection, we focus on the d -wave junctions both for weak and strong proximity regimes. In this case, depending on the orientation angle α , the proximity effect is drastically changed: as α increases the proximity effect is suppressed[46, 47]. For $\alpha = 0$ we can expect similar results to the s -wave junctions since proximity effect exists while the MARS is absent. On the other hand, the tunneling conductance for large α is almost independent of h/Δ . Especially, the conductance is independent of h for $\alpha/\pi = 0.25$ due to the complete absence of the proximity effect. Two different mechanisms of formation of ZBCP exist in DF/D junctions: the ZBCP caused by the resonant proximity effect peculiar to a ferromagnet and the ZBCP caused by the MARS located at DF/D interface. When α increases, MARS are formed and at the same time the proximity effect becomes weakened. Therefore the MARS provide the dominant contribution to the ZBCP compared to the resonant proximity effect, as will be discussed below.

First we choose the weak proximity regime where the resonant condition is $h/\Delta = 0.005$. Figure 2.12 displays the tunneling conductance for $Z = 3$, $R_d/R_b = 1$ and various α with (a) $E_{Th}/\Delta = 0.01$ and $h/\Delta = 0$, (b) $E_{Th}/\Delta = 0.01$ and $h/\Delta = 0.005$, (c) $E_{Th}/\Delta = 10$ and $h/\Delta = 0$, and (d) $E_{Th}/\Delta = 10$ and $h/\Delta = 5$. For $E_{Th}/\Delta = 0.01$ and $h = 0$ ZBCD appears for $\alpha/\pi = 0$ due to the proximity effect as in the case of the s -wave junctions while ZBCP

appears for $\alpha/\pi = 0.25$ due to the formation of the MARS (Fig. 2.12 (a)). For $E_{Th}/\Delta = 0.01$ and $h/\Delta = 0.005$, the height of the ZBCP by the resonant proximity effect exceeds the one by MARS for $\alpha/\pi = 0.25$ (Fig. 2.12 (b)). Since in the ballistic junctions, the ZBCP for $\alpha/\pi = 0.25$ is most strongly enhanced[39, 40, 41], this ZBCP by the resonant proximity effect in DF is a remarkable feature. Such a feature is also expected for a larger magnitude of E_{Th} . For $E_{Th}/\Delta = 10$ and $h = 0$, a V-like shape of the conductance appears for $\alpha/\pi = 0$ while ZBCP appears for $\alpha/\pi = 0.25$ (Fig. 2.12 (c)). In this case, by choosing $h/\Delta = 5$, a broad peak by the resonant proximity effect appears for $\alpha/\pi = 0$ and its height exceeds the one for $\alpha/\pi = 0.25$ (Fig. 2.12 (d)).

We also study the DOS of the DF for the same parameters as those in Fig. 2.12 (d) with (a) $\alpha/\pi = 0$ and (b) $\alpha/\pi = 0.125$ in Fig. 2.13. For $\alpha/\pi = 0$ a zero-energy peak appears as in the case of s -wave junctions. With increasing α the DOS around zero energy becomes suppressed due to the reduction of the proximity effect. The extreme case is $\alpha/\pi = 0.25$, where the DOS is always unity since the proximity effect is completely absent.

Next we consider the junctions in the strong proximity regime. Figure 2.14 shows the tunneling conductance for $Z = 3$, $R_a/R_b = 5$ and various α with (a) $E_{Th}/\Delta = 0.01$ and $h/\Delta = 0$, (b) $E_{Th}/\Delta = 0.01$ and $h/\Delta = 0.01$, (c) $E_{Th}/\Delta = 10$ and $h/\Delta = 0$ and (d) $E_{Th}/\Delta = 10$ and $h/\Delta = 10$. In this case we also find the ZBCP for $\alpha = 0$ caused by the resonant proximity effect. This ZBCP becomes suppressed as α increases, as shown in Figs. 2.14(b) and (d).

The corresponding DOS of the DF for Fig. 2.14(d) is shown in Fig. 2.15. The line shapes of the LDOS at $x = 0$ are qualitatively similar to the tunneling conductance. The DOS at the DF/S interface ($x = L$) is drastically suppressed as compared to the one in Fig. 2.13.

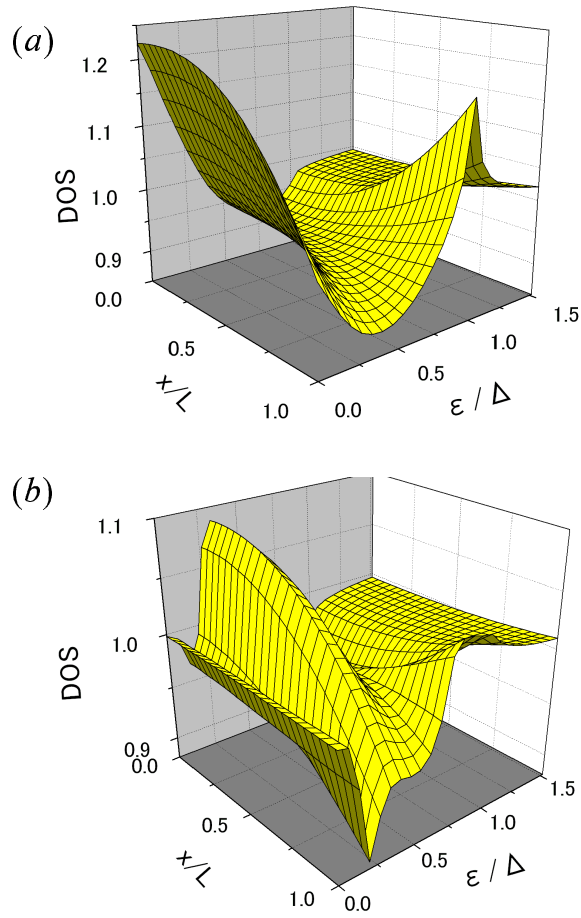


Figure 2.13: Normalized DOS for d -wave superconductors with $Z = 3$, $R_d/R_b = 1$, $E_{Th}/\Delta = 10$ and $h/\Delta = 5$. (a) $\alpha/\pi = 0$ and (b) $\alpha/\pi = 0.125$.

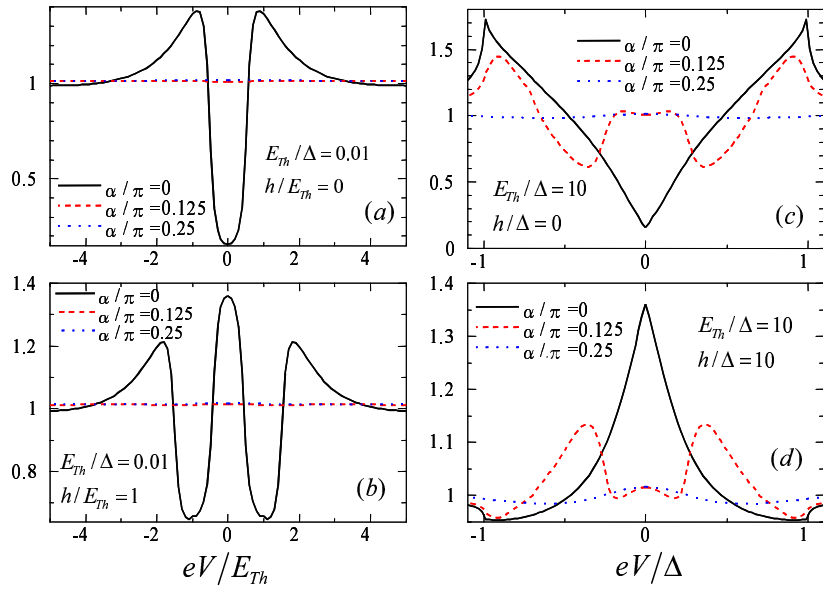


Figure 2.14: Normalized tunneling conductance for d -wave superconductors with $Z = 3$ and $R_d/R_b = 5$.

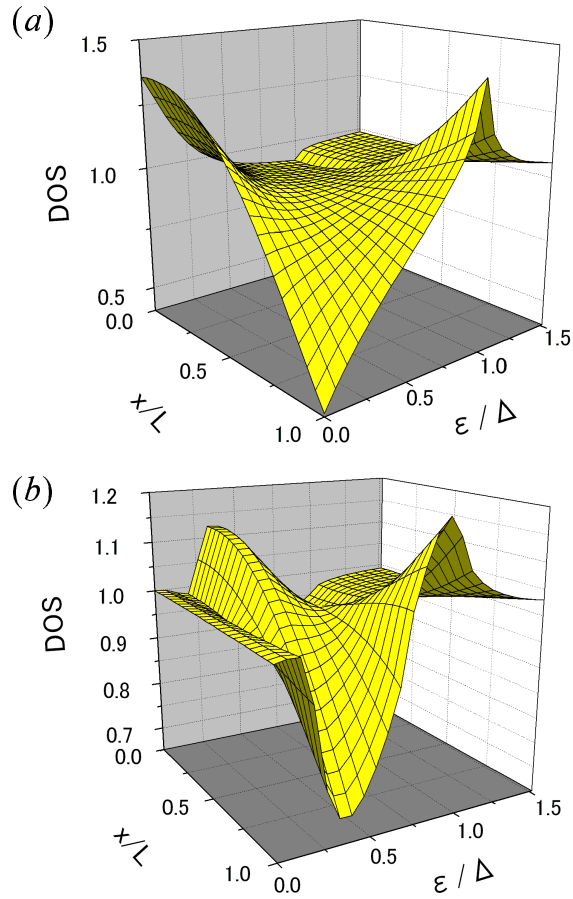


Figure 2.15: Normalized DOS for d -wave superconductors with $Z = 3$, $R_d/R_b = 5$, $E_{Th}/\Delta = 10$ and $h/\Delta = 10$. (a) $\alpha/\pi = 0$ and (b) $\alpha/\pi = 0.125$.

2.4 Conclusions

We have studied the conditions for the appearance of the DOS peak in diffusive ferromagnet, in normal metal / diffusive ferromagnet / s -wave superconductor junctions. We have discussed two regimes of weak and strong proximity effect depending on the ratio R_d/R_b . The results in the regime of weak proximity effect are essentially the same as found in Ref. [35]. However, in the regime of strong proximity effect the results are qualitatively different. Let us summarize the two conditions:

1. When the proximity effect is weak ($R_d/R_b \ll 1$), the condition for the DOS peak is $R_d/R_b \sim 2h/E_{Th}$.

2. When the proximity effect is strong ($R_d/R_b \gg 1$), the DOS peak appears when $E_{Th} \sim h$, i.e. when the length of ferromagnet is of the order of the coherence length $\sqrt{D/h}$.

Note that the above two conditions cross over into each other when $R_d/R_b \sim 2$. Since the DOS is a fundamental quantity affecting various physical properties, our results may have many applications like charge transport which we discussed.

We presented a detailed theoretical study of the tunneling conductance and the density of states in normal metal / diffusive ferromagnet / s - and d -wave superconductor junctions. We have clarified that the resonant proximity effect strongly influences the tunneling conductance and the density of states. There are several points which have been clarified in this chapter.

1. For s -wave junctions, due to the resonant proximity effect, a sharp ZBCP appears for small E_{Th} while a broad ZBCP appears for large E_{Th} . We have shown that the mechanism of the ZBCP in DF/S junctions is essentially different from that in DN/S junctions and is due to the strong enhancement of DOS at a certain value of the exchange field. As a result, the magnitude of ZBCP in DF/S can exceed its normal state value in contrast to the case of DN/S junctions.

2. For d -wave junctions at $\alpha = 0$, similar to the s -wave case, a sharp ZBCP is formed when the resonant condition is satisfied. At finite misorientation angle α , the MARS contribute to the conductance when $R_d/R_b \ll 1$ and $Z \gg 1$. With the increase of α the contribution of the resonant proximity effect becomes smaller while the MARS dominate the conductance. As a result, for sufficiently large α ZBCP exists independently of whether the resonant condition is satisfied or not. In the opposite case of the weak barrier, $R_d/R_b \gg 1$, the contribution of MARS is negligible and ZBCP appears only when the resonant condition is satisfied.

Bibliography

- [1] A.F. Andreev, Sov. Phys. JETP **19**, 1228 (1964).
- [2] G.E. Blonder, M. Tinkham, and T.M. Klapwijk, Phys. Rev. B **25**, 4515 (1982).
- [3] P. M. Tedrow and R. Meservey, Phys. Rev. Lett. **26**, 192 (1971); Phys. Rev. B **7**, 318 (1973); R. Meservey and P. M. Tedrow, Phys. Rep. **238**, 173 (1994).
- [4] S. K. Upadhyay, A. Palanisami, R. N. Louie, and R. A. Buhrman Phys. Rev. Lett. **81**, 3247 (1998).
- [5] R. J. Soulen Jr., J. M. Byers, M. S. Osofsky, B. Nadgorny, T. Ambrose, S. F. Cheng, P. R. Broussard, C. T. Tanaka, J. Nowak, J. S. Moodera, A. Barry, J. M. D. Coey Science **282**, 85 (1998)
- [6] I.I.Mazin, A.A.Golubov, and B.Nadgorny J.Appl.Phys. **89**, 7576 (2001).
- [7] G.T. Woods, R. J. Soulen, I. I. Mazin, B. Nadgorny, M. S. Osofsky, J. Sanders, H. Srikanth, W. F. Egelhoff, and R. Datla, Phys. Rev. B **70**, 054416 (2004).
- [8] W. Belzig, A. Brataas, Yu. V. Nazarov, G. E. W. Bauer, Phys. Rev. B **62**, 9726 (2000).
- [9] T. Hirai, Y. Tanaka, N. Yoshida, Y. Asano, J. Inoue, and S. Kashiwaya Phys. Rev. B **67**, 174501 (2003); N. Yoshida, Y. Tanaka, J. Inoue, and S. Kashiwaya, J. Phys. Soc. Jpn. **68**, 1071 (1999); S. Kashiwaya, Y. Tanaka, N. Yoshida, and M.R. Beasley, Phys. Rev. B **60**, 3572 (1999); I. Zutic and O.T. Valls, Phys. Rev. B **60**, 6320 (1999); **61**, 1555 (2000); N. Stefanakis, Phys. Rev. B **64**, 224502 (2001); J. Phys. Condens. Matter **13**, 3643 (2001).
- [10] A.I. Buzdin, L.N. Bulaevskii, and S.V. Panyukov, Pis'ma Zh. Eksp. Teor. Phys. 35, 147, (1982) [JETP Lett. 35, 178 (1982)].

- [11] A.I. Buzdin and M.Yu. Kupriyanov, *Pis'ma Zh. Eksp. Teor. Phys.* **53**, 308 (1991) [*JETP Lett.* **53**, 321 (1991)].
- [12] E. A. Demler, G. B. Arnold, and M. R. Beasley, *Phys. Rev. B* **55**, 15 174 (1997).
- [13] A. I. Buzdin, *Rev. Mod. Phys.* **77**, 935 (2005).
- [14] A. A. Golubov, M. Yu. Kupriyanov, and E. Il'ichev, *Rev. Mod. Phys.* **76**, 411 (2004).
- [15] F. S. Bergeret, A. F. Volkov, and K. B. Efetov, *Rev. Mod. Phys.* **77**, 1321 (2005).
- [16] V. V. Ryazanov, V. A. Oboznov, A. Yu. Rusanov, A. V. Veretennikov, A. A. Golubov, and J. Aarts, *Phys. Rev. Lett.* **86**, 2427 (2001); V. V. Ryazanov, V. A. Oboznov, A. V. Veretennikov, and A. Yu. Rusanov, *Phys. Rev. B* **65**, 020501(R) (2001); S. M. Frolov, D. J. Van Harlingen, V. A. Oboznov, V. V. Bolginov, and V. V. Ryazanov, *Phys. Rev. B* **70**, 144505.
- [17] T. Kontos, M. Aprili, J. Lesueur, F. Genet, B. Stephanidis, and R. Boursier, *Phys. Rev. Lett.* **89**, 137007 (2002).
- [18] Y. Blum, A. Tsukernik, M. Karpovski, and A. Palevski, *Phys. Rev. Lett.* **89**, 187004 (2002).
- [19] H. Sellier, C. Baraduc, F. Lefloch, and R. Calemczuk, *Phys. Rev. B* **68**, 054531 (2003).
- [20] A. Bauer, J. Bentner, M. Aprili, M. L. Della-Rocca, M. Reinwald, W. Wegscheider, and C. Strunk, *Phys. Rev. Lett.* **92**, 217001 (2004).
- [21] Z. Radovic, M. Ledvij, Lj. Dobrosavljevic-Grujic, A. I. Buzdin, and J. R. Clem, *Phys. Rev. B* **44**, 759 (1991).
- [22] L. R. Tagirov, *Phys. Rev. Lett.* **83**, 2058 (1999).
- [23] Ya. V. Fominov, N. M. Chtchelkatchev, and A. A. Golubov, *Pis'ma Zh. Eksp. Teor. Fiz.* **74**, 101 (2001) [*JETP Lett.* **74**, 96 (2001)]; Ya. V. Fominov, N. M. Chtchelkatchev, and A. A. Golubov, *Phys. Rev. B* **66**, 014507 (2002).
- [24] A. Rusanov, R. Boogaard, M. Hesselberth, H. Sellier, and J. Aarts, *Physica C* **369**, 300 (2002).

- [25] V.V.Ryazanov, V.A.Oboznov, A.S.Prokofiev, S.V.Dubonos, JETP Lett. **77**, 39 (2003).
- [26] A. Kadigrobov, R. I. Shekhter, M. Jonson and Z. G. Ivanov, Phys. Rev. B **60**, 14593 (1999).
- [27] R. Seviour, C. J. Lambert, and A. F. Volkov , Phys. Rev. B **59**, 6031 (1999).
- [28] M. Leadbeater, C. J. Lambert, K. E. Nagaev, R. Raimondi and A. F. Volkov, Phys. Rev. B **59**, 12264 (1999).
- [29] F. S. Bergeret, K. B. Efetov, and A. I. Larkin, Phys. Rev. B **62**, 11872 (2000); F. S. Bergeret, A. F. Volkov, and K. B. Efetov, Phys. Rev. Lett. **86**, 4096 (2001).
- [30] A. Kadigrobov, R. I. Shekhter, and M. Jonson, Europhys. Lett. **54**, 394 (2001).
- [31] A. Buzdin, Phys. Rev. B **62**, 11 377 (2000).
- [32] M. Zareyan, W. Belzig, and Yu. V. Nazarov, Phys. Rev. Lett. **86**, 308 (2001); Phys. Rev. B **65**, 184505 (2002).
- [33] I. Baladie and A. Buzdin, Phys. Rev. B **64**, 224514 (2001).
- [34] F. S. Bergeret, A. F. Volkov, and K. B. Efetov, Phys. Rev. B **65**, 134505 (2002).
- [35] A. A. Golubov, M. Yu. Kupriyanov, and Ya. V. Fominov, JETP Lett. **75**, 223 (2002).
- [36] V. N. Krivoruchko and E. A. Koshina, Phys. Rev. B **66**, 014521 (2002).
- [37] T. Kontos, M. Aprili, J. Lesueur, and X. Grison, Phys. Rev. Lett. **86**, 304 (2001); T. Kontos, M. Aprili, J. Lesueur, X. Grison, and L. Dumoulin, Phys. Rev. Lett. **93**, 137001 (2004).
- [38] L.J. Buchholtz and G. Zwicknagl, Phys. Rev. B **23** 5788 (1981); C. Bruder, Phys. Rev. B **41**, 4017 (1990); C.R. Hu, Phys. Rev. Lett. **72**, 1526 (1994).
- [39] Y. Tanaka and S. Kashiwaya, Phys. Rev. Lett. **74**, 3451 (1995); S. Kashiwaya, Y. Tanaka, M. Koyanagi and K. Kajimura, Phys. Rev. B **53**, 2667 (1996); Y. Tanuma, Y. Tanaka, and S. Kashiwaya Phys. Rev. B **64**, 214519 (2001).

- [40] S. Kashiwaya and Y. Tanaka, Rep. Prog. Phys. **63**, 1641 (2000) and references therein.
- [41] J. Geerk, X.X. Xi, and G. Linker: Z. Phys. B. **73**, (1988) 329; S. Kashiwaya, Y. Tanaka, M. Koyanagi, H. Takashima, and K. Kajimura, Phys. Rev. B **51** 1350 (1995); L. Alff, H. Takashima, S. Kashiwaya, N. Terada, H. Ihara, Y. Tanaka, M. Koyanagi, and K. Kajimura, Phys. Rev. B **55**, 14757 (1997); M. Covington, M. Aprili, E. Paraoanu, L.H. Greene, F. Xu, J. Zhu, and C.A. Mirkin, Phys. Rev. Lett. **79**, 277 (1997); J. Y. T. Wei, N.-C. Yeh, D. F. Garrigus and M. Strasik: Phys. Rev. Lett. **81**, (1998) 2542; I. Iguchi, W. Wang, M. Yamazaki, Y. Tanaka, and S. Kashiwaya: Phys. Rev. B **62**, (2000) R6131; F. Laube, G. Goll, H.v. Löhneysen, M. Fogelström, and F. Lichtenberg, Phys. Rev. Lett. **84**, 1595 (2000); Z.Q. Mao, K.D. Nelson, R. Jin, Y. Liu, and Y. Maeno, Phys. Rev. Lett. **87**, 037003 (2001); Ch. Wälti, H.R. Ott, Z. Fisk, and J.L. Smith, Phys. Rev. Lett. **84**, 5616 (2000); H. Aubin, L. H. Greene, Sha Jian and D. G. Hinks, Phys. Rev. Lett. **89**, 177001 (2002); Z. Q. Mao, M. M. Rosario, K. D. Nelson, K. Wu, I. G. Deac, P. Schiffer, Y. Liu, T. He, K. A. Regan, and R. J. Cava Phys. Rev. B **67**, 094502 (2003); A. Sharoni, O. Millo, A. Kohen, Y. Dagan, R. Beck, G. Deutscher, and G. Koren Phys. Rev. B **65**, 134526 (2002); A. Kohen, G. Leibovitch, and G. Deutscher Phys. Rev. Lett. **90**, 207005 (2003).
- [42] K.D. Usadel Phys. Rev. Lett. **25**, 507 (1970).
- [43] M.Yu. Kupriyanov and V. F. Lukichev, Zh. Exp. Teor. Fiz. **94** (1988) 139 [Sov. Phys. JETP **67**, (1988) 1163].
- [44] Yu. V. Nazarov, Superlattices and Microstructures **25**, 1221 (1999), cond-mat/9811155.
- [45] Y. Tanaka, A. A. Golubov and S. Kashiwaya, Phys. Rev. B **68** 054513 (2003).
- [46] Y. Tanaka, Y.V. Nazarov and S. Kashiwaya, Phys. Rev. Lett. **90** 167003 (2003).
- [47] Y. Tanaka, Y. V. Nazarov, A. A. Golubov and S. Kashiwaya, Phys. Rev. B **69** 144519 (2004).
- [48] Y. Tanaka and S. Kashiwaya, Phys. Rev. B **70** 012507 (2004); Y. Tanaka, S. Kashiwaya, and T. Yokoyama, Phys. Rev. B **71**, 094513 (2005); Y. Tanaka, Y. Asano, A. A. Golubov, and S. Kashiwaya, Phys. Rev. B, in press (2005).

- [49] A.F. Volkov, A.V. Zaitsev and T.M. Klapwijk, *Physica C* 210, **21** (1993).
- [50] A. Kastalsky, A.W. Kleinsasser, L.H. Greene, R. Bhat, F.P. Milliken, J.P. Harbison, *Phys. Rev. Lett.* **67**, 3026 (1991).

Chapter 3

Manifestation of the odd-frequency spin-triplet pairing state in diffusive ferromagnet/superconductor junctions

3.1 Introduction

Ferromagnet/superconductor structures with conventional spin-singlet s -wave superconductors have been the subject of extensive work during the past decade [1, 2, 3]. An exciting manifestation of anomalous proximity effect in these structures is the existence of the so-called π -junctions in SFS Josephson junctions confirmed experimentally in [4, 5, 6, 7, 8, 9, 10, 11, 12]. Recently, diffusive ferromagnet/superconductor (DF/S) junctions have received much attention due to the possibility of generation of the odd-frequency pairing in these structures [13, 2]. In DF, due to the isotropization by the impurity scattering, only even-parity s -wave pairing is allowed. Besides this, the exchange field breaks the time reversal symmetry and both spin-singlet and spin-triplet Cooper pairs can coexist. In accordance with the Pauli's principle, this spin-triplet state belongs to the odd-frequency spin-triplet even-parity (OTE) pairing [13, 2]. Various aspects of this state have been addressed in recent theoretical work [2, 14, 18, 15, 16, 17] and first experimental observation of the long-range proximity effect due to the odd-frequency pairing was reported in [19, 20].

Odd-frequency pairing is an unique state which was first proposed by

Berezinskii [21] as a hypothetical state of ^3He . The odd-frequency superconductivity was then discussed in the context of various pairing mechanisms involving strong correlations [22, 23, 24]. However, proximity effect in the presence of odd-frequency superconducting state has not been studied up to very recently.

A general theory of the proximity effect in junctions composed of diffusive normal metal (DN) and unconventional superconductor in the framework of the quasiclassical Green's function formalism was recently presented [25]. Various possible symmetry classes in a superconductor were considered in Ref.[25] which are consistent with the Pauli's principle: even-frequency spin-singlet even-parity (ESE) state, even-frequency spin-triplet odd-parity (ETO) state, odd-frequency spin-triplet even-parity (OTE) state and odd-frequency spin-singlet odd-parity (OSO) state. For each of the above four cases, symmetry and spectral properties of the induced pair amplitude in the DN were determined. It was shown that the pair amplitude in a DN belongs respectively to ESE, OTE, OTE and ESE pairing states. It is remarkable that OTE state is realized without assuming magnetic ordering in DN/ETO superconductor junctions, where the mid gap Andreev resonant state [26] formed at the interface penetrates into the DN and the resulting local density of states (LDOS) has a zero energy peak (ZEP) [27].

On the other hand, the existence of ZEP in LDOS in the DF/ ESE s -wave superconductor junctions has been established [29, 5, 30, 31, 32, 28]. Although the conditions of the formation of ZEP in DF regions were formulated in the previous chapter, possible relation between the ZEP and the formation of OTE pairing in DF has not been yet clarified. The present chapter addresses this issue. We also study the proximity effect in DF/ETO p -wave superconductor junctions. It was shown in Ref. [25] that only the OTE pairing state is generated without exchange field h . It is an interesting question how this unusual proximity effect is influenced by the exchange field.

The organization of this chapter is as follows. In section 2, we formulate the proximity effect model in DF / S junctions within the theory applicable to unconventional superconductor junctions where the MARS are naturally taken into account in the boundary condition for the quasiclassical Green's function [27]. We discuss the general properties of the proximity effect by choosing ESE, ETO, OTE, and OSO superconductor junctions. It is clarified that the OTE, ESE, ESE and OTE states are, respectively, generated in the DF in the presence of exchange field h . In section 3 we calculate the pair amplitude in DF for spin-singlet s -wave and spin-triplet p -wave superconductor junctions as an example of ESE and ETO superconductor junctions. For s -wave junctions, it is revealed that a generation of the OTE pairing state by

the exchange field h causes an enhancement of the zero energy LDOS in the DF. On the other hand, for p -wave superconductor junctions, a generation of ESE pairing state by h results in a splitting of ZEP of LDOS. We clarify the relation between the ZEP in LDOS and the generation of the OTE state in the DF. The summary of the results is given in section 4.

3.2 Formulation

Let us start with the formulation of the general symmetry properties of the quasiclassical Green's functions in the considered system following the discussion in the Ref. [25]. The elements of retarded and advanced Nambu matrices $\widehat{g}^{R,A}$

$$\widehat{g}^{R,A} = \begin{pmatrix} g^{R,A} & f^{R,A} \\ \tilde{f}^{R,A} & \tilde{g}^{R,A} \end{pmatrix} \quad (3.1)$$

are composed of the normal $g_{\alpha,\beta}^R(\mathbf{r}, \varepsilon, \mathbf{p})$ and anomalous $f_{\alpha,\beta}^R(\mathbf{r}, \varepsilon, \mathbf{p})$ components with spin indices α and β . Here $\mathbf{p} = \mathbf{p}_F / |\mathbf{p}_F|$, \mathbf{p}_F is the Fermi momentum, \mathbf{r} and ε denote coordinate and energy of a quasiparticle measured from the Fermi level respectively. The function f^R and the conjugated function \tilde{f}^R satisfy the following relation [34, 35]

$$\tilde{f}_{\alpha,\beta}^R(\mathbf{r}, \varepsilon, \mathbf{p}) = -[f_{\alpha,\beta}^R(\mathbf{r}, -\varepsilon, -\mathbf{p})]^*. \quad (3.2)$$

The Pauli's principle is formulated in terms of the retarded and the advanced Green's functions in the following way [34]

$$f_{\alpha,\beta}^A(\mathbf{r}, \varepsilon, \mathbf{p}) = -f_{\beta,\alpha}^R(\mathbf{r}, -\varepsilon, -\mathbf{p}). \quad (3.3)$$

By combining the above two equations, we obtain $\tilde{f}_{\beta,\alpha}^R(\mathbf{r}, \varepsilon, \mathbf{p}) = [f_{\alpha,\beta}^A(\mathbf{r}, \varepsilon, \mathbf{p})]^*$. Further, the definitions of the even-frequency and the odd-frequency pairing are $f_{\alpha,\beta}^A(\mathbf{r}, \varepsilon, \mathbf{p}) = f_{\alpha,\beta}^R(\mathbf{r}, -\varepsilon, \mathbf{p})$ and $f_{\alpha,\beta}^A(\mathbf{r}, \varepsilon, \mathbf{p}) = -f_{\alpha,\beta}^R(\mathbf{r}, -\varepsilon, \mathbf{p})$, respectively. Finally we get

$$\tilde{f}_{\beta,\alpha}^R(\mathbf{r}, \varepsilon, \mathbf{p}) = [f_{\alpha,\beta}^R(\mathbf{r}, -\varepsilon, \mathbf{p})]^* \quad (3.4)$$

for the even-frequency pairing and

$$\tilde{f}_{\beta,\alpha}^R(\mathbf{r}, \varepsilon, \mathbf{p}) = -[f_{\alpha,\beta}^R(\mathbf{r}, -\varepsilon, \mathbf{p})]^* \quad (3.5)$$

for the odd-frequency pairing. In the following, we consider a homogeneous ferromagnet/superconductor junctions with the exchange field h in a ferromagnet and focus on the Cooper pairs with $S_z = 0$. In this case, it is possible

to remove the external phase of the pair potential in the superconductor. We will concentrate on the retarded part of the Green's function.

We consider a junction consisting of a normal (N) and a superconducting reservoirs connected by a quasi-one-dimensional diffusive ferromagnet (DF) with a length L much larger than the mean free path as shown in Fig. 1.

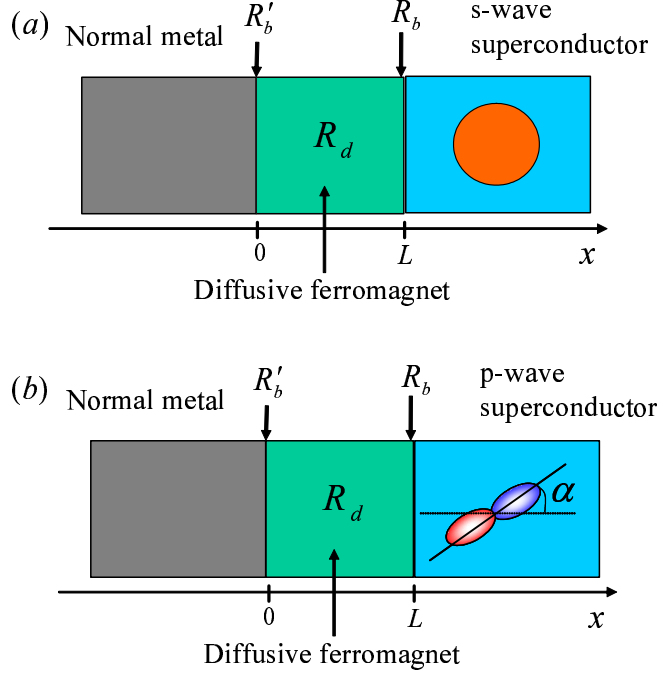


Figure 3.1: Schematic illustration of DF /S junctions where DF is connected to normal and superconducting reservoirs. (a)conventional spin-singlet s -wave superconductor and (b)spin-triplet p -wave superconductor junctions.

The interface between the DF and the superconductor (S) at $x = L$ has a resistance R_b and the N/DF interface at $x = 0$ has a resistance R'_b . The Green's function in the superconductor can be parameterized as $g_{\pm}(\varepsilon)\hat{\tau}_3 + f_{\pm}(\varepsilon)\hat{\tau}_2$ using Pauli's matrices, where the subscript $+$ ($-$) denotes the right (left) going quasiparticles. $g_{\pm}(\varepsilon)$ and $f_{\pm}(\varepsilon)$ are given by $g_{+}(\varepsilon) \equiv g_{\uparrow,\uparrow}^R(\mathbf{r}, \varepsilon, \mathbf{p}) = g_{\downarrow,\downarrow}^R(\mathbf{r}, \varepsilon, \mathbf{p})$, $g_{-}(\varepsilon) \equiv g_{\uparrow,\uparrow}^R(\mathbf{r}, \varepsilon, \bar{\mathbf{p}}) = g_{\downarrow,\downarrow}^R(\mathbf{r}, \varepsilon, \bar{\mathbf{p}})$, $f_{+}(\varepsilon) \equiv f_{\uparrow,\downarrow}^R(\mathbf{r}, \varepsilon, \mathbf{p})$, and $f_{-}(\varepsilon) \equiv f_{\uparrow,\downarrow}^R(\mathbf{r}, \varepsilon, \bar{\mathbf{p}})$, respectively, with $\bar{\mathbf{p}} = \bar{\mathbf{p}}_F / |\mathbf{p}_F|$ and $\bar{\mathbf{p}}_F = (-p_{Fx}, p_{Fy})$. Using the relations (3.4) and (3.5), we obtain that $f_{\pm}(\varepsilon) = [f_{\pm}(-\varepsilon)]^*$ for the even-frequency pairing and $f_{\pm}(\varepsilon) = -[f_{\pm}(-\varepsilon)]^*$ for the odd-frequency pairing, respectively, while $g_{\pm}(\varepsilon) = [g_{\pm}(-\varepsilon)]^*$ in both cases.

In the DF region, only the s -wave even-parity pairing state is allowed due to isotropization by impurity scattering. The resulting Green's function with majority and minority spin in the DF can be parameterized by $\cos\theta\hat{\tau}_3 + \sin\theta\hat{\tau}_2$ and $\cos\bar{\theta}\hat{\tau}_3 + \sin\bar{\theta}\hat{\tau}_2$ in a junction with an even-parity superconductor respectively. On the other hand, for odd-parity superconductor, the corresponding quantities for majority spin and minority spin are expressed by $\cos\theta\hat{\tau}_3 + \sin\theta\hat{\tau}_1$ and $\cos\bar{\theta}\hat{\tau}_3 + \sin\bar{\theta}\hat{\tau}_1$ respectively.

The function θ satisfies the Usadel equation [36]

$$D\frac{\partial^2\theta}{\partial x^2} + 2i(\varepsilon + h)\sin\theta = 0 \quad (3.6)$$

with the boundary conditions at the DF/S interface [27, 37]

$$\frac{L}{R_d}\left(\frac{\partial\theta}{\partial x}\right)\Big|_{x=L} = \frac{\langle F_1 \rangle}{R_b}, \quad (3.7)$$

$$F_1 = \frac{2T_1(f_S \cos\theta_L - g_S \sin\theta_L)}{2 - T_1 + T_1(\cos\theta_L g_S + \sin\theta_L f_S)} \quad (3.8)$$

and at the N/DF interface

$$\frac{L}{R_d}\left(\frac{\partial\theta}{\partial x}\right)\Big|_{x=0} = -\frac{\langle F_2 \rangle}{R'_b}, F_2 = \frac{2T_2 \sin\theta_0}{2 - T_2 + T_2 \cos\theta_0}, \quad (3.9)$$

respectively, with $\theta_L = \theta|_{x=L}$ and $\theta_0 = \theta|_{x=0}$. Here, R_d and D are the resistance and the diffusion constant in the DF, respectively. Function g_S is given by $g_S = (g_+ + g_-)/(1 + g_+g_- + f_+f_-)$ and $f_S = (f_+ + f_-)/(1 + g_+g_- + f_+f_-)$ for the even-parity pairing and $f_S = i(f_+g_- - f_-g_+)/(1 + g_+g_- + f_+f_-)$ for the odd-parity pairing, respectively, with $g_{\pm} = \varepsilon/\sqrt{\varepsilon^2 - \Delta_{\pm}^2}$, $f_{\pm} = \Delta_{\pm}/\sqrt{\Delta_{\pm}^2 - \varepsilon^2}$ and $\Delta_{\pm} = \Delta\Psi(\phi_{\pm})$ where $\Psi(\phi_{\pm})$ is the form factor with $\phi_+ = \phi$ and $\phi_- = \pi - \phi$. The brackets $\langle \dots \rangle$ denote averaging over the injection angle ϕ :

$$\langle F_{1(2)}(\phi) \rangle = \int_{-\pi/2}^{\pi/2} d\phi \cos\phi F_{1(2)}(\phi) / \int_{-\pi/2}^{\pi/2} d\phi T_{1(2)} \cos\phi, \quad (3.10)$$

$$T_1 = \frac{4 \cos^2 \phi}{Z^2 + 4 \cos^2 \phi}, \quad T_2 = \frac{4 \cos^2 \phi}{Z'^2 + 4 \cos^2 \phi}, \quad (3.11)$$

where $T_{1,2}$ are the transmission probabilities, Z and Z' are the barrier parameters for two interfaces.

The resistance at the interface $R_b^{(\prime)}$ is given by

$$R_b^{(\prime)} = \frac{2R_0^{(\prime)}}{\int_{-\pi/2}^{\pi/2} d\phi T_{1(2)}(\phi) \cos \phi}.$$

Here, $R_b^{(\prime)}$ denotes R_b or R_b' , and $R_0^{(\prime)}$ is Sharvin resistance, which in three-dimensional case is given by $R_0^{(\prime)} = 4\pi^2/(e^2 k_F^2 S_c^{(\prime)})$, where k_F is the Fermi wave-vector and $S_c^{(\prime)}$ is the constriction area.

Next, we focus on the Green's function of minority spin. The function $\bar{\theta}$ satisfies the following equation [36]:

$$D \frac{\partial^2 \bar{\theta}}{\partial x^2} + 2i(\varepsilon - h) \sin \bar{\theta} = 0 \quad (3.12)$$

with the boundary condition at the DF/S interface [27, 37]

$$\frac{L}{R_d} \left(\frac{\partial \bar{\theta}}{\partial x} \right) \Big|_{x=L} = \frac{\langle \bar{F}_1 \rangle}{R_b}. \quad (3.13)$$

Here, \bar{F}_1 is given by

$$\bar{F}_1 = \frac{2T_1(f_S \cos \bar{\theta}_L - g_S \sin \bar{\theta}_L)}{2 - T_1 + T_1(\cos \bar{\theta}_L g_S + \sin \bar{\theta}_L f_S)} \quad (3.14)$$

for spin-triplet superconductor and

$$\bar{F}_1 = \frac{2T_1(-f_S \cos \bar{\theta}_L - g_S \sin \bar{\theta}_L)}{2 - T_1 + T_1(\cos \bar{\theta}_L g_S - \sin \bar{\theta}_L f_S)} \quad (3.15)$$

for spin-singlet superconductor respectively. At the N/DF interface, the boundary condition reads

$$\frac{L}{R_d} \left(\frac{\partial \bar{\theta}}{\partial x} \right) \Big|_{x=0} = -\frac{\langle \bar{F}_2 \rangle}{R_b'}, \quad \bar{F}_2 = \frac{2T_2 \sin \bar{\theta}_0}{2 - T_2 + T_2 \cos \bar{\theta}_0}. \quad (3.16)$$

Here $\bar{\theta}_L = \bar{\theta} |_{x=L}$ and $\bar{\theta}_0 = \bar{\theta} |_{x=0}$.

Equations (3.12) and (3.13) can be transformed to

$$D \frac{\partial^2 \bar{\theta}^*(-\varepsilon)}{\partial x^2} + 2i(\varepsilon + h) \sin \bar{\theta}^*(-\varepsilon) = 0 \quad (3.17)$$

$$\frac{L}{R_d} \left(\frac{\partial \bar{\theta}^*(-\varepsilon)}{\partial x} \right) \Big|_{x=L} = \frac{\langle \bar{F}_1^*(-\varepsilon) \rangle}{R_b}, \quad (3.18)$$

$$\frac{L}{R_d} \left(\frac{\partial \bar{\theta}^*(-\varepsilon)}{\partial x} \right) \Big|_{x=0} = - \frac{\langle \bar{F}_2^*(-\varepsilon) \rangle}{R'_b}. \quad (3.19)$$

The pair amplitude is defined as

$$f_3(\varepsilon) = (\sin \theta - \sin \bar{\theta})/2 \quad (3.20)$$

in the spin-singlet case and as

$$f_0(\varepsilon) = (\sin \theta + \sin \bar{\theta})/2 \quad (3.21)$$

in the spin-triplet case.

Since only an even-parity s -wave pairing can exist in the DF due to the impurity scattering, f_3 and f_0 belong to the ESE and OTE state, respectively.

In the following, we will consider four possible symmetry classes of superconductivity in the junction, consistent with the Pauli's principle: ESE, ETO, OTE and OSO pairing states.

(1) Junction with ESE superconductor

In this case, $f_{\pm}(\varepsilon) = f_{\pm}^*(-\varepsilon)$ and $g_{\pm}(\varepsilon) = g_{\pm}^*(-\varepsilon)$ are satisfied. Then, $f_S(-\varepsilon) = f_S^*(\varepsilon) = f_S^*$ and $g_S(-\varepsilon) = g_S^*(\varepsilon) = g_S^*$ and we obtain for $\bar{F}_1^*(-\varepsilon)$

$$\bar{F}_1^*(-\varepsilon) = \frac{2T_1[-f_S \cos \bar{\theta}_L^*(-\varepsilon) - g_S \sin \bar{\theta}_L^*(-\varepsilon)]}{2 - T_1 + T_1[\cos \bar{\theta}_L^*(-\varepsilon)g_S - \sin \bar{\theta}_L^*(-\varepsilon)f_S]}.$$

It follows from a comparison of Eqs. 3.6-3.9 with Eqs. 3.17-3.19 that these equations are consistent with each other only when $\sin \bar{\theta}^*(-\varepsilon) = -\sin \theta(\varepsilon)$ and $\cos \bar{\theta}^*(-\varepsilon) = \cos \theta(\varepsilon)$. After simple calculation, we can show $f_3(\varepsilon) = f_3^*(-\varepsilon)$ and $f_0(\varepsilon) = -f_0^*(-\varepsilon)$. This relation is consistent with the fact [25] that f_3 and f_0 are the even-frequency and odd-frequency pairing state, respectively. When $h=0$, since $\sin \theta(\varepsilon) = -\sin \bar{\theta}(\varepsilon)$ is satisfied, the resulting f_0 is vanishing and only the ESE state exist. For $h \neq 0$, f_0 becomes nonzero and the OTE state is generated in DF.

(2) Junction with ETO superconductor

Now we have $f_{\pm}(\varepsilon) = f_{\pm}^*(-\varepsilon)$ and $g_{\pm}(\varepsilon) = g_{\pm}^*(-\varepsilon)$. Then, $f_S(-\varepsilon) = -f_S^*(\varepsilon) = -f_S^*$ and $g_S(-\varepsilon) = g_S^*(\varepsilon) = g_S^*$. As a result, $\bar{F}_1^*(-\varepsilon)$ is given by

$$\bar{F}_1^*(-\varepsilon) = - \frac{2T_1[f_S \cos \bar{\theta}_L^*(-\varepsilon) + g_S \sin \bar{\theta}_L^*(-\varepsilon)]}{2 - T_1 + T_1[\cos \bar{\theta}_L^*(-\varepsilon)g_S - \sin \bar{\theta}_L^*(-\varepsilon)f_S]}.$$

Eqs. 3.6-3.9 and Eqs. 3.17-3.19 are consistent if $\sin \theta^*(-\varepsilon) = -\sin \bar{\theta}(\varepsilon)$ and $\cos \theta^*(-\varepsilon) = \cos \bar{\theta}(\varepsilon)$. As in the case of ESE pairing, we can show $f_3(\varepsilon) = f_3^*(-\varepsilon)$ and $f_0(\varepsilon) = -f_0^*(-\varepsilon)$. For $h = 0$, OTE state is generated in

the DF as shown in Ref. [25]. The ESE state is generated by h , in contrast to the case of DF/ESE superconductor junctions.

(3) Junction with OTE superconductor

In this case $f_{\pm}(\varepsilon) = -f_{\pm}^*(-\varepsilon)$ and $g_{\pm}(\varepsilon) = g_{\pm}^*(-\varepsilon)$. Then $f_S(-\varepsilon) = -f_S^*(\varepsilon)$ and $g_S(-\varepsilon) = g_S^*(\varepsilon)$ and one can show that $\bar{F}_1^*(-\varepsilon)$ has the same form as in the case of ESE and ETO superconductor junctions. Then, we obtain $\sin \bar{\theta}^*(-\varepsilon) = -\sin \theta(\varepsilon)$ and $\cos \bar{\theta}^*(-\varepsilon) = \cos \theta(\varepsilon)$. Also $f_3(\varepsilon) = f_3^*(-\varepsilon)$ and $f_0(\varepsilon) = -f_0^*(-\varepsilon)$ are satisfied. For $h = 0$, only the OTE pairing state is generated in DF. Similar to the case of ETO junctions, ESE pairing is induced in the presence of h .

(4) Junction with OSO superconductor

We have $f_{\pm}(\varepsilon) = -f_{\pm}^*(-\varepsilon)$, $g_{\pm}(\varepsilon) = g_{\pm}^*(-\varepsilon)$, $f_S(-\varepsilon) = f_S^*(\varepsilon)$, and $g_S(-\varepsilon) = g_S^*(\varepsilon)$. One can show that $\bar{F}_1^*(-\varepsilon)$ takes the same form as in the cases of ESE, ETO, OTE superconductor junctions. Then, we obtain $\sin \bar{\theta}^*(-\varepsilon) = -\sin \theta(\varepsilon)$ and $\cos \bar{\theta}^*(-\varepsilon) = \cos \theta(\varepsilon)$. Also $f_3(\varepsilon) = f_3^*(-\varepsilon)$ and $f_0(\varepsilon) = -f_0^*(-\varepsilon)$ are satisfied. For $h = 0$, only the ESE pairing state is generated in DF. Similar to the case of ETO junctions, OTE pairing is induced in the presence of h .

We can now summarize the above results in the table below. As seen from the above discussion, $\sin \bar{\theta}^*(-\varepsilon) = -\sin \theta(\varepsilon)$, $\cos \bar{\theta}^*(-\varepsilon) = \cos \theta(\varepsilon)$, $f_3(\varepsilon) = f_3^*(-\varepsilon)$ and $f_0(\varepsilon) = -f_0^*(-\varepsilon)$ are satisfied for all cases. The real part of f_3 is an even function of ε while the imaginary part of it is an odd function of ε consistent with even-frequency pairing. On the other hand, the real part of f_0 is an odd function of ε while its imaginary part is an even function of ε consistent with odd-frequency pairing.

	Symmetry of the pairing in superconductors	Symmetry of the pairing in DF without exchange field	Symmetry of the pairing in DF
(1)	Even-frequency spin-singlet even-parity (ESE)	ESE	ESE + O TE
(2)	Even-frequency spin-triplet odd-parity (ETO)	OTE	OTE + E SE
(3)	Odd-frequency spin-triplet even-parity (OTE)	OTE	OTE + E SE
(4)	Odd-frequency spin-singlet odd-parity (OSO)	ESE	ESE + O TE

Within this formulation, the LDOS in the DF layer is given by

$$N/N_0 = \frac{1}{2}(\text{Re} \cos \theta + \text{Re} \cos \bar{\theta}) \quad (3.22)$$

where N_0 denotes the LDOS in the normal state. Below we will calculate f_3 , f_0 and LDOS at zero temperature. For this purpose, we will use the following parameter set $Z = 3$, $Z' = 3$, $E_{Th} \equiv D/L^2 = 0.1\Delta$ and $R_d/R'_b = 0.1$, which represents a typical DF/S junction. Our qualitative conclusions are not sensitive to the parameter choice.

3.3 Results

In the following, we will study two typical cases. As an example of ESE superconductor, the conventional spin-singlet s -wave pairing will be considered. We will clarify the generation of OTE pairing in DF by the exchange field

h consistent with preexisting results [13, 2]. We will also study spin-triplet p -wave superconductor as a typical example of ETO superconductor. In this case, ESE pairing state is induced by h . It should be remarked again that f_3 and f_0 denote the ESE and OTE pairing amplitudes, respectively.

3.3.1 Spin singlet s -wave superconductor junctions

Let us first study DF/spin-singlet s -wave superconductor junctions where we choose $R_d/R_b = 1$ and the form factor Ψ_{\pm} is given by $\Psi_{\pm} = 1$. Real and imaginary parts of f_3 and f_0 at $x = 0$ for various h/Δ are shown in Fig. 3.2. Without exchange field, *i.e.*, $h = 0$, only the f_3 is nonzero, consistent with conventional theory of proximity effect [38, 39, 37]. By introducing

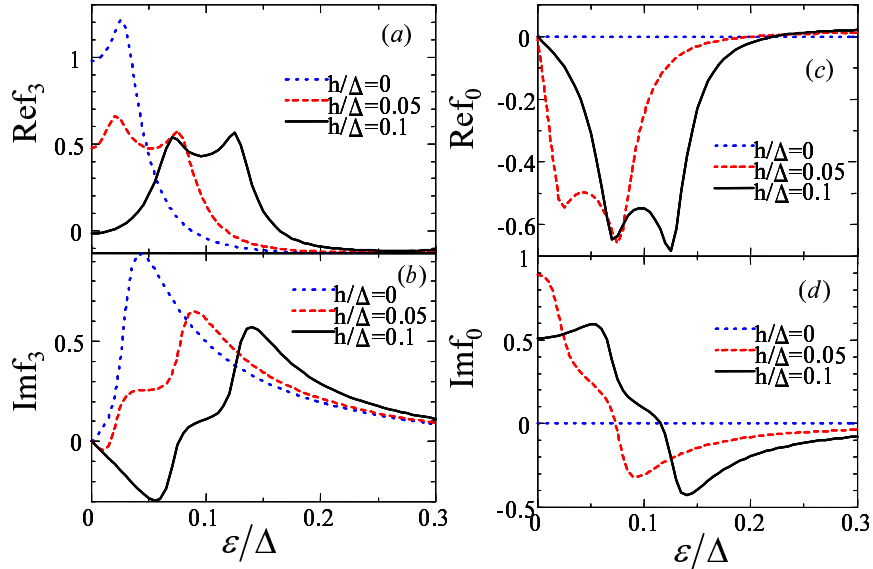


Figure 3.2: Real (a) and imaginary (b) parts of f_3 , and real (c) and imaginary (d) parts of f_0 in spin-singlet s -wave superconductor junctions. We choose $R_d/R_b = 1$.

the exchange field h , the magnitude of f_3 is suppressed for small ε while it is enhanced for large ε as shown in Figs. 3.2(a) and 3.2(b). On the other hand, the imaginary part of f_0 is enhanced for small magnitude of ε . The corresponding LDOS at N/DF interface normalized by its value in the normal state is plotted as a function of ε in Fig. 3.3. The LDOS has a minigap at $h = 0$ [38, 39]. As shown in Fig. 3.3, the LDOS is influenced crucially by h . A peak appears at zero energy with $h/\Delta = 0.05$. In this case $\text{Im}f_0$ has a

large value at zero energy as shown in Fig. 3.2(d). Thus large magnitude of $\text{Im}f_0$ at $\varepsilon = 0$ is responsible for the peak of the LDOS.

It was shown in the previous chapter that the condition for the formation of ZEP in the LDOS is given by $E_{Th} \sim 2hR_b/R_d$. This condition is consistent with the results shown in Fig. 3. As shown in Fig. 3.2, when this condition

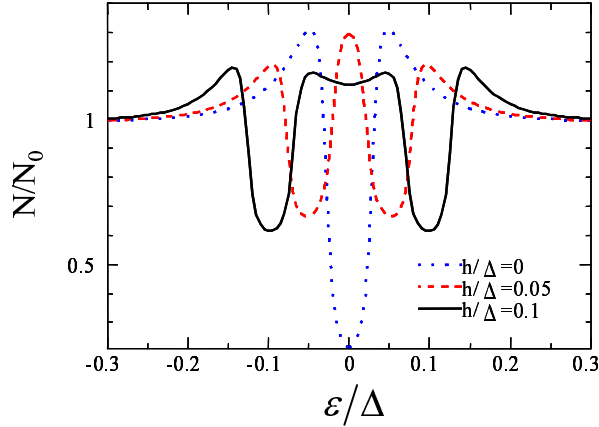


Figure 3.3: Normalized LDOS as a function of ε for $R_d/R_b = 1$ with various h/Δ in spin-singlet s -wave superconductor junctions.

is satisfied, $\text{Im}f_0$ has a large value at the zero energy. Thus it corresponds to the generation of the odd-frequency pairing amplitude f_0 at low energy. The spatial dependences of the pair amplitudes f_3 and f_0 at $\varepsilon = 0$ are shown in Fig. 3.4. The amplitude of f_3 is dominant near the DF/S interface while the magnitude of f_0 is enhanced at the N/DF interface.

Let us study the crossover between spin-singlet and spin-triplet pairing states. We show f_3 and f_0 as a function of h for $\varepsilon = 0$ at (a) $x = 0$, (b) $x = L/2$ and (c) $x = L$ in Fig. 3.5. f_0 increases from zero with h . At a certain value of h , f_0 has a maximum. If the value of h is larger than this value, the triplet component becomes dominant as shown in Fig. 3.5(a) and Fig. 3.5(b). The value of h at the crossover regime is given by the minigap in DN/S junctions. Let us discuss this regime in more detail. As shown in section II, $\sin\bar{\theta}(\varepsilon) = -\sin\theta^*(-\varepsilon)$ and $\cos\bar{\theta}(\varepsilon) = \cos\theta^*(-\varepsilon)$ are satisfied for any case. Then the ESE and OTE pair wave functions in the DF are given by

$$f_3(\varepsilon) = [\sin\theta(\varepsilon) + \sin\theta^*(-\varepsilon)]/2, \quad (3.23)$$

$$f_0(\varepsilon) = [\sin\theta(\varepsilon) - \sin\theta^*(-\varepsilon)]/2. \quad (3.24)$$

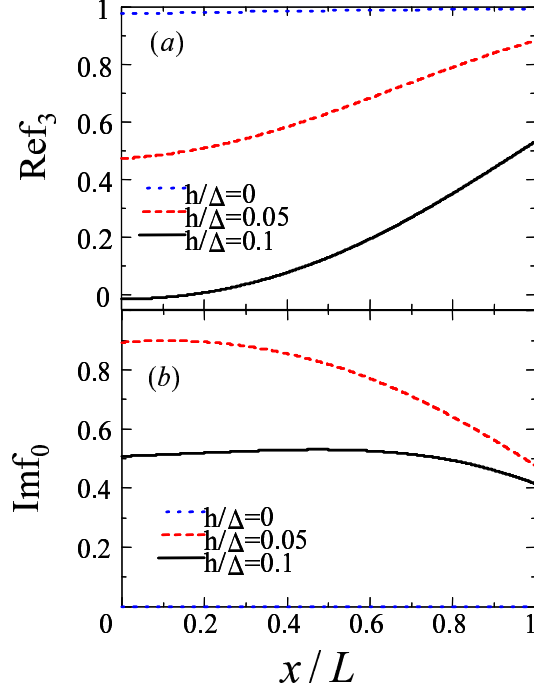


Figure 3.4: Spatial dependence of the pair amplitudes f_3 and f_0 in DF for $\varepsilon = 0$ in spin-singlet s -wave superconductor junctions. For $\varepsilon = 0$, $\text{Im}f_3 = 0$ and $\text{Re}f_0 = 0$ are satisfied.

At $\varepsilon = 0$, we denote $\theta(0) = \text{Re}\theta(0) + i\text{Im}\theta(0)$, where $\text{Re}\theta(0)$ and $\text{Im}\theta(0)$ are the real and imaginary part of $\theta(0)$. Then $f_3(0)$ and $f_0(0)$ are given by $\cosh[\text{Im}\theta(0)] \sin[\text{Re}\theta(0)]$ and $i \sinh[\text{Im}\theta(0)] \cos[\text{Re}\theta(0)]$. Thus the following equation is satisfied:

$$\frac{f_3(0)}{f_0(0)} = \frac{\tan \text{Re}\theta(0)}{i \tanh \text{Im}\theta(0)}. \quad (3.25)$$

It is easy to show that $|\text{Re}\theta(0)| < |\text{Im}\theta(0)|$ is satisfied when the crossover occurs, i.e., $\tan \text{Re}\theta(0) = \tanh \text{Im}\theta(0)$. As shown in the previous chapter, this inequality is satisfied when the exchange field is of the order of the minigap energy in DN/S junctions, i.e., $h \sim (R_d/R_b)(E_{Th}/2)$. Therefore the crossover occurs around this value of the exchange field.

3.3.2 Spin-triplet p -wave superconductor junctions

Next we focus on the DF / spin-triplet p -wave superconductor junctions, where we choose $R_d/R_b = 0.1$ and the form factor Ψ_{\pm} is given by $\Psi_{\pm} =$

$\pm \cos \phi$ corresponding to the case of $\alpha = 0$ (see Fig. 3.1). In order to make numerical calculations stable, we introduce a small imaginary number in the quasiparticle energy: $\varepsilon \rightarrow \varepsilon + i\gamma$, with $\gamma = 0.01\Delta$. The real and imaginary parts of f_3 and f_0 at $x = 0$ are plotted in Fig. 3.6 for various h/Δ . Similar to the case of DN/s-wave superconductor junctions, the imaginary part of f_3 and the real part of f_0 vanish at $\varepsilon = 0$. For $h=0$, $f_3 = 0$ and only f_0 is nonzero as shown in Fig. 3.6. The feature of this unusual proximity effect[27] was already discussed in Ref. [25], where OTE pairing state is generated in the DN of DN/ETO superconductor junctions. In this case, the LDOS has a ZEP and odd-frequency component f_0 becomes a purely imaginary number at $\varepsilon = 0$. With increasing h , the amplitude of f_3 is enhanced as shown in Figs. 3.6(a) and 3.6(b), in contrast to the case of DN/spin-singlet s-wave superconductor junctions. At the same time, the magnitude of f_0 near the zero energy is suppressed. Then the features of the proximity effect in DF are the same as in conventional superconductor junctions. The corresponding LDOS normalized by its value in the normal state is plotted as a function of ε in Fig. 3.7. With the increase of h , the magnitude of LDOS at $\varepsilon = 0$ is suppressed and the LDOS peak is splitted. The magnitude of the splitting increases with the increase of h . Note that the peak positions in $\text{Im}f_0$ and LDOS coincide with each other. The spatial dependences of the real part of f_3 and the imaginary part of f_0 at $\varepsilon = 0$ are shown in Fig. 3.8. For $h = 0$, f_3 is absent and the magnitude of the imaginary part of f_0 reaches its maximum at the DF/S interface. With the increase of h , the amplitude of f_0 is drastically reduced. The spatial dependence of f_3 is rather weak and its amplitude is most strongly enhanced for $h = 0.05\Delta$. At the same time, the magnitude of LDOS at $\varepsilon = 0$ is most strongly suppressed (see Fig. 3.7).

Before ending this subsection, we investigate the crossover between singlet and triplet pairing states. Let us plot f_3 and f_0 for $\varepsilon = 0$ as a function of h at (a) $x = 0$, (b) $x = L/2$ and (c) $x = L$ in Fig. 3.9. f_3 has a maximum at a certain value of h . When h exceeds this value, the singlet component becomes dominant as shown in Fig. 3.9. The value of h at the crossover increases with the increase of Z , R_d/R_b and E_{Th} , i.e., with the enhancement of the proximity effect.

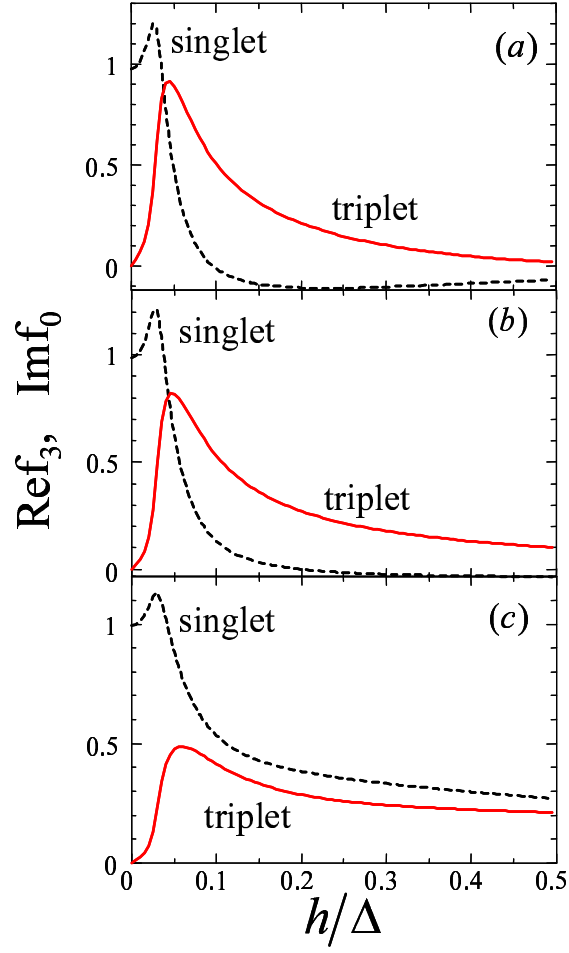


Figure 3.5: The pair amplitudes f_3 and f_0 as a function of h in DF for $\varepsilon = 0$ in spin-singlet s -wave superconductor junctions. (a) $x = 0$. (b) $x = L/2$. (c) $x = L$.

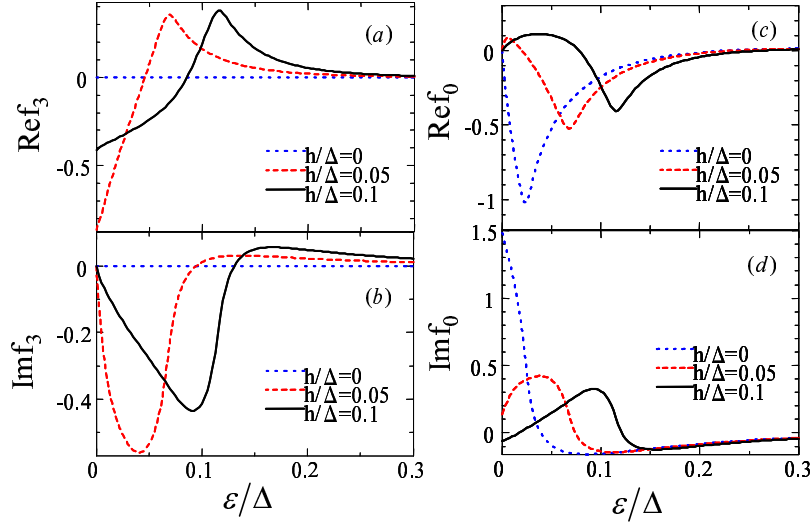


Figure 3.6: Pair amplitudes for DF/ spin-triplet p -wave superconductor junctions. Real (a) and imaginary (b) parts of f_3 . Real (c) and imaginary (d) parts of f_0 . Here we choose $R_d/R_b = 0.1$.

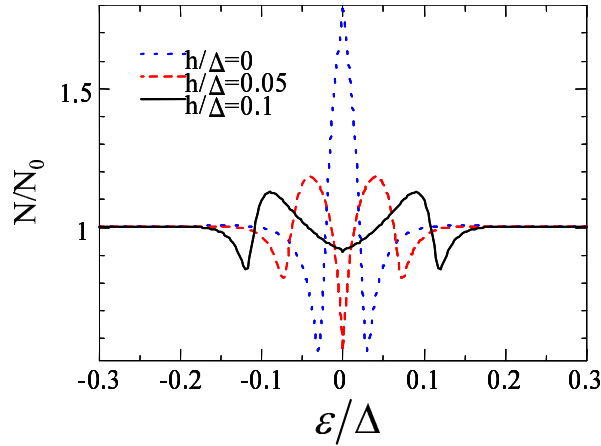


Figure 3.7: Normalized LDOS as a function of ε for $R_d/R_b = 0.1$ and various h/Δ in p -wave superconductor junctions.

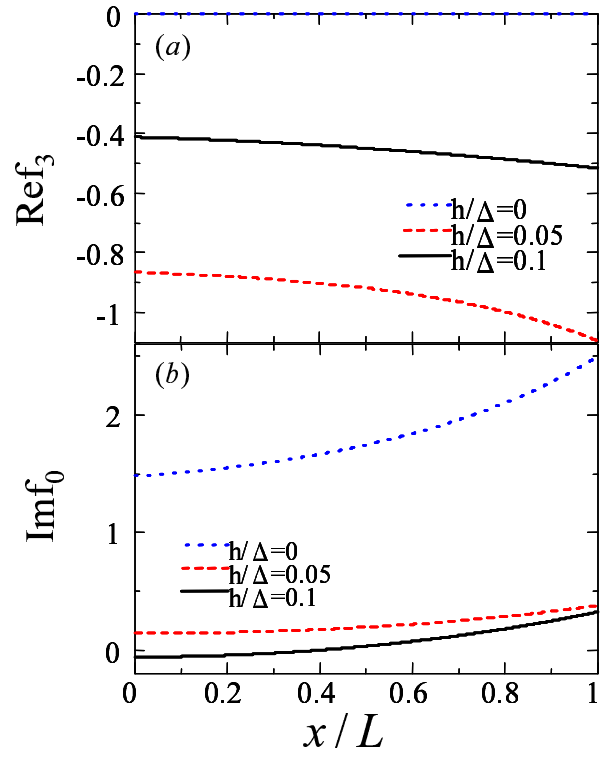


Figure 3.8: Spatial dependence of the pair amplitudes f_3 and f_0 in DF for $\varepsilon = 0$ in p -wave superconductor junctions. For $\varepsilon = 0$, $\text{Im}f_3 = 0$ and $\text{Re}f_0 = 0$ are satisfied.

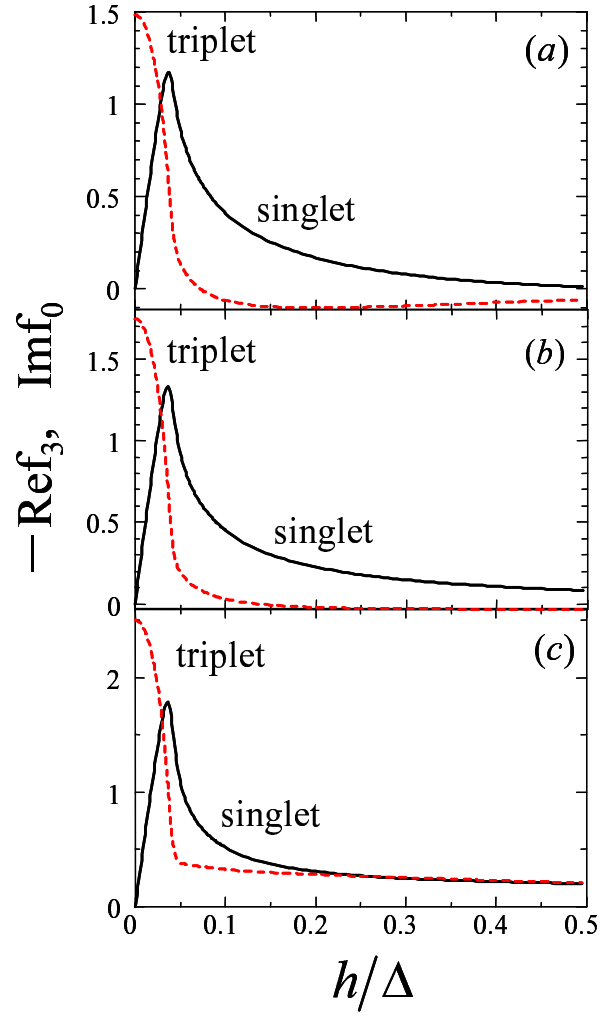


Figure 3.9: The pair amplitudes f_0 and f_3 as a function of h in DF for $\varepsilon = 0$ in p -wave superconductor junctions. (a) $x = 0$. (b) $x = L/2$. (c) $x = L$.

3.3.3 Relevance of the odd-frequency component to ZEP of LDOS

Let us discuss the relation between the generation of the odd-frequency pairing and ZEP in LDOS, using general properties of solutions of the proximity effect problem. Since $\cos \bar{\theta}(\varepsilon) = \cos \theta^*(-\varepsilon)$ are satisfied, the LDOS normalized by its value in the normal state is given by

$$N/N_0 = [\cos \theta(\varepsilon) + \cos \theta^*(-\varepsilon)]/2. \quad (3.26)$$

For $\varepsilon = 0$, the normalized LDOS reads $\cosh[\text{Im}\theta(0)] \cos[\text{Re}\theta(0)]$, while $f_3(0)$ and $f_0(0)$ are given by $\cosh[\text{Im}\theta(0)] \sin[\text{Re}\theta(0)]$ and $i \sinh[\text{Im}\theta(0)] \cos[\text{Re}\theta(0)]$ respectively. As seen from these relations, f_0 becomes zero when the LDOS is zero. In addition, whether the spin-singlet component f_3 dominates the spin-triplet component f_0 or not crucially depends on the value of $\text{Re}\theta(0)$. The most favorable condition where N/N_0 is enhanced is the large magnitude of $\text{Im}\theta(0)$ and the absence of $\text{Re}\theta(0)$, where f_0 dominates f_3 . For the sufficiently large magnitude of $\text{Im}\theta(0)$ and small magnitude of $\text{Re}\theta(0)$, $N/N_0 \sim \cos[\text{Re}\theta(0)] \exp[\text{Im}\theta(0)]/2 \sim \exp[\text{Im}\theta(0)]/2$ and $f_0(0) \sim i \cos[\text{Re}\theta(0)] \exp[\text{Im}\theta(0)]/2 \sim i \exp[\text{Im}\theta(0)]/2$ are satisfied. Then we obtain $N/N_0 \sim -if_0(0)$. This means that the generation of the odd-frequency pair amplitude $f_0(0)$ leads to the enhancement of the density of states at zero energy.

3.4 Conclusions

We have studied the proximity effect in diffusive ferromagnet (DF) / superconductor (S) junctions. Various possible symmetry classes in a superconductor were considered which are consistent with the Pauli's principle: even-frequency spin-singlet even-parity (ESE) state, even-frequency spin-triplet odd-parity (ETO) state, odd-frequency spin-triplet even-parity (OTE) state and odd-frequency spin-singlet odd-parity (OSO) state. As was established in the previous work [25], in the absence of the exchange field the induced pair amplitude in a DF belongs respectively to ESE, OTE, OTE and ESE pairing states. It is shown in the present chapter that, in addition to these states, the OTE, ESE, ESE and OTE pairing states are generated in DF in the presence of the exchange field h .

As a typical example of ESE superconductor, we have chosen spin-singlet s -wave state. We have clarified that when the OTE state dominates the ESE state in the DF, the resulting LDOS has a zero energy peak. At the same time, the amplitude of the OTE pair wave function near the N/DF interface is enhanced at zero energy. As suggested by our findings, the odd-frequency

pairing state was possibly realized in the experiment by Kontos[5], where the ZEP was observed in ferromagnet / s -wave superconductor junctions.

We have also studied spin-triplet p -wave superconductor junctions. In this case, the ZEP in the LDOS splits into two peaks due to the generation of the ESE pairing state by the exchange field. The features of proximity effect specific to spin-triplet p -wave superconductor junctions can be studied in experiments with Sr_2RuO_4 - $\text{Sr}_3\text{Ru}_2\text{O}_7$ eutectic system [40]. Based on general properties of solutions of the proximity effect problem, we have demonstrated that the generation of the odd-frequency pairing state at zero energy leads to the ZEP in LDOS.

Bibliography

- [1] A. I. Buzdin, *Rev. Mod. Phys.* **77**, 935 (2005).
- [2] F. S. Bergeret, A. F. Volkov, and K. B. Efetov, *Rev. Mod. Phys.* **77**, 1321 (2005).
- [3] A. A. Golubov, M. Yu. Kupriyanov, and E. Il'ichev, *Rev. Mod. Phys.* **76**, 411 (2004).
- [4] V. V. Ryazanov, V. A. Oboznov, A. Yu. Rusanov, A. V. Veretennikov, A. A. Golubov, and J. Aarts *Phys. Rev. Lett.* **86**, 2427 (2001); V. V. Ryazanov, V. A. Oboznov, A. V. Veretennikov, and A. Yu. Rusanov *Phys. Rev. B* **65**, 020501(R) (2002); S. M. Frolov, D. J. Van Harlingen, V. V. Bolginov, V. A. Oboznov, and V. V. Ryazanov *Phys. Rev. B* **74**, 020503(R) (2006); V. A. Oboznov, V. V. Bol'ginov, A. K. Feofanov, V. V. Ryazanov, and A. I. Buzdin *Phys. Rev. Lett.* **96**, 197003 (2006).
- [5] T. Kontos, M. Aprili, J. Lesueur, and X. Grisson, *Phys. Rev. Lett.* **86**, 304 (2001); T. Kontos, M. Aprili, J. Lesueur, X. Grisson, and L. Dumoulin, *Phys. Rev. Lett.* **93**, 137001 (2004).
- [6] H. Sellier, C. Baraduc, F. Lefloch, and R. Calemczuk, *Phys. Rev. B* **68**, 054531 (2003).
- [7] Y. Blum, A. Tsukernik, M. Karpovski, and A. Palevski, *Phys. Rev. B* **70**, 214501 (2004).
- [8] C. Surgers, T. Hoss, C. Schonenberger, and C. Strunk, *J. Magn. Magn. Mater.* **240**, 598 (2002).
- [9] C. Bell, R. Loloee, G. Burnell, and M. G. Blamire, *Phys. Rev. B* **71**, 180501(R) (2005).
- [10] V. Shelukhin, A. Tsukernik, M. Karpovski, Y. Blum, K. B. Efetov, A.F. Volkov, T. Champel, M. Eschrig, T. Lofwander, G. Schon, and A. Palevski, *Phys. Rev. B* **73**, 174506 (2006).

- [11] M. Weides, K. Tillmann, and H. Kohlstedt, *Physica C* **437-438**, 349 (2006).
- [12] H. Sellier, C. Baraduc, F. Lefloch, and R. Calemczuk, *Phys. Rev. Lett.* **92**, 257005 (2004).
- [13] F. S. Bergeret, A. F. Volkov, and K. B. Efetov, *Phys. Rev. Lett.* **86**, 4096 (2001).
- [14] A. F. Volkov, A. Anishchanka, and K. B. Efetov, *Phys. Rev. B* **73**, 104412 (2006); A. F. Volkov, Ya. V. Fominov, and K. B. Efetov, *Phys. Rev. B* **72**, 184504 (2005); F. S. Bergeret, A. F. Volkov, and K. B. Efetov *Phys. Rev. B* **68**, 064513 (2003).
- [15] A. Kadigrobov, R. I. Shekter and M. Jonson, *EuroPhys. Lett.* **90**, 394 (2001).
- [16] M. Eschrig, J. Kopu, J. C. Cuevas and G. Schön, *Phys. Rev. Lett.* **90**, 137003 (2003); T. Löfwander, T. Champel, J. Durst, and M. Eschrig, *Phys. Rev. Lett.* **95**, 187003 (2005).
- [17] Y. V. Fominov, A. A. Golubov, and M. Y. Kupriyanov, *JETP Lett.* **77**, 510 (2003).
- [18] M. L. Kubic and M. Endres, *Phys. Rev. B* **62**, 11846 (2000).
- [19] R.S. Keizer, S.T.B. Goennenwein, T.M. Klapwijk, G. Miao, G. Xiao, and A. Gupta, *Nature* **439**, 825 (2006).
- [20] I. Sosnin, H. Cho, V. T. Petrashov, and A. F. Volkov, *Phys. Rev. Lett.* **96**, 157002 (2006).
- [21] V. L. Berezinskii, *JETP Lett.* **20**, 287 (1974).
- [22] A. Balatsky and E. Abrahams, *Phys. Rev. B* **45**, 13125 (1992); E. Abrahams, A. Balatsky, D. J. Scalapino and J. R. Schrieffer, *Phys. Rev. B* **52**, 1271 (1995).
- [23] M. Vojta and E. Dagotto, *Phys. Rev. B* **59**, R713 (1999).
- [24] Y. Fuseya, H. Kohno and K. Miyake, *J. Phys. Soc. Jpn.* **72**, 2914 (2003).
- [25] Y. Tanaka and A. A. Golubov, *Phys. Rev. Lett.* **98**, 037003 (2007).

- [26] C.R. Hu, Phys. Rev. Lett. **72** (1994) 1526; Y. Tanaka, S. Kashiwaya, Phys. Rev. Lett. **74** (1995) 3451; S. Kashiwaya and Y. Tanaka, Rep. Prog. Phys. **63** (2000) 1641 and references therein.
- [27] Y. Tanaka and S. Kashiwaya, Phys. Rev. B **70**, 012507 (2004); Y. Tanaka, S. Kashiwaya, and T. Yokoyama Phys. Rev. B **71**, 094513 (2005); Y. Tanaka, Y. Asano, A. A. Golubov and S. Kashiwaya, Phys. Rev. B **72**, 140503(R) (2005); Y. Asano, Y. Tanaka and S. Kashiwaya, Phys. Rev. Lett. **96**, 097007 (2006).
- [28] A. A. Golubov, M. Yu. Kupriyanov, and Ya. V. Fominov, JETP Lett. **75**, 223 (2002).
- [29] A. Buzdin, Phys. Rev. B **62**, 11377 (2000).
- [30] M. Zareyan, W. Belzig, and Yu. V. Nazarov, Phys. Rev. Lett. **86**, 308 (2001); Phys. Rev. B **65**, 184505 (2002).
- [31] I. Baladie and A. Buzdin, Phys. Rev. B **64**, 224514 (2001).
- [32] F. S. Bergeret, A. F. Volkov, and K. B. Efetov, Phys. Rev. B **65**, 134505 (2002).
- [33] T. Yokoyama, Y. Tanaka, and A. A. Golubov, Phys. Rev. B **72**, 052512 (2005); Phys. Rev. B **73**, 094501 (2006).
- [34] J.W. Serene and D. Rainer, Phys. Rep. **101**, 221 (1983).
- [35] M. Eschrig, Phys. Rev. B **61**, 9061 (2000).
- [36] K.D. Usadel, Phys. Rev. Lett. **25**, 507 (1970).
- [37] Y. Tanaka, A. A. Golubov and S. Kashiwaya, Phys. Rev. B **68**, 054513 (2003).
- [38] A.F. Volkov, A.V. Zaitsev and T.M. Klapwijk, Physica C **210**, 21 (1993).
- [39] S. Yip Phys. Rev. B **52**, 3087 (1995).
- [40] J. Hooper, M. Zhou, Z. Q. Mao, Y. Liu, R. Perry, and Y. Maeno, Phys. Rev. B **73**, 132510 (2006); R. Fittipaldi, A. Vecchione, S. Fusanobori, K. Takizawa, H. Yaguchi, J. Hooper R. S. Perry, and Y. Maeno, J. Crystal Growth, **282**, 152 (2005).

Chapter 4

Odd-frequency pairing state inside the Abrikosov vortex core

4.1 Introduction

Generally, superconducting pairing is classified into even-frequency or odd-frequency state according to a symmetry with respect to time. Due to the Fermi statistics, even-frequency superconductors belong to the symmetry class of spin-singlet even-parity or spin-triplet odd-parity pairing state, while odd-frequency superconductors belong to the spin-singlet odd-parity or spin-triplet even-parity pairing state.

The possibility of the odd-frequency pairing state in various kinds of uniform systems was discussed in Refs. [1, 2, 3, 4, 5], albeit its realization in bulk materials is still controversial. On the other hand, the realization of the odd-frequency pairing state in inhomogeneous superconducting systems has recently been proposed. It is established that odd-frequency pairing is induced due to symmetry breaking in such systems. In ferromagnet/superconductor junctions, odd-frequency pairing emerges due to the broken symmetry in a spin space.[6, 7] It was recently realized that proximity-induced odd-frequency pairing may also be generated near normal metal/superconductor interfaces due to the breakdown of translational symmetry [8] or in a diffusive normal metal attached to a triplet superconductor.[9]

Since an Abrikosov vortex breaks translational symmetry in a superconductor, one may expect the emergence of an odd-frequency unconventional pairing state with higher angular momentum around the vortex core even in a conventional *s*-wave superconductor. This issue is addressed in this chapter.

The study of the mixed state in type-II superconductors, where magnetic flux enters a sample in the form of quantized vortices, has a long history and revealed a variety of physical phenomena.[10, 11, 12, 13, 14, 15] In the clean limit, low-energy bound states, called the Andreev bound states, are generated in the vortex core due to the spatial structure of the superconducting pair potential. [16, 17, 18, 19, 20, 21] One of the manifestations of the bound states is the enhancement of zero-energy quasiparticle density of states (DOS) locally in the core, observable as a zero-bias conductance peak by scanning tunneling spectroscopy (STM).[17, 22]

In this chapter, based on the quasiclassical theory of superconductivity, we study pairing symmetry around an Abrikosov vortex in a clean superconductor. We find that, quite unexpectedly, only odd-frequency spin-singlet chiral p -wave pairing is allowed at the center of the core in s -wave superconductor. That means that the emergence of the odd-frequency pairing is a physical reason of zero energy peak in the local DOS inside the core. Based on these results, we propose the experimental setup to verify the existence of odd-frequency pairing in bulk materials using superconducting STM.

4.2 Formulation

The electronic structure of the vortex core in a single Abrikosov vortex in a clean superconductor is described by the quasiclassical Eilenberger equations.[23, 24] For the calculation of the Green's functions in the vicinity of the vortex, it is necessary to find numerically stable solutions of the Eilenberger equations. For this purpose, we use the Riccati parametrization of the quasiclassical propagator [25]. Along a trajectory $\mathbf{r}(x') = \mathbf{r}_0 + x' \hat{\mathbf{v}}_F$ with unit vector $\hat{\mathbf{v}}_F$ parallel to \mathbf{v}_F , the Eilenberger equations are generally represented in 4×4 matrix form.[26] For the s -wave superconductor with $\hat{\Delta} = \Delta \sigma_y$ (σ_y is a Pauli's matrix in spin space), these equations are reduced to the set of two decoupled differential equations of the Riccati type for the functions $a(x')$ and $b(x')$

$$\begin{aligned} \hbar v_F \partial_{x'} a(x') + [2\epsilon_n + \Delta^\dagger a(x')] a(x') - \Delta &= 0, \\ \hbar v_F \partial_{x'} b(x') - [2\epsilon_n + \Delta b(x')] b(x') + \Delta^\dagger &= 0 \end{aligned} \quad (4.1)$$

where $i\epsilon_n$ are the Matsubara frequencies. For simple case of a cylindrical Fermi surface, the Fermi velocity can be written as $\mathbf{v}_F = v_F(\mathbf{e}_1 \cos \theta + \mathbf{e}_2 \sin \theta)$.

We choose the following form of the pair potential which accurately de-

scribes the behavior around the vortex:

$$\begin{aligned}\Delta(\mathbf{r}) &= \Delta_0 \tanh\left(\frac{\sqrt{x^2 + y^2}}{\xi}\right) \frac{x + iy}{\sqrt{x^2 + y^2}} \\ &\equiv \Delta_0 \tanh\left(\frac{\sqrt{x^2 + y^2}}{\xi}\right) \exp(i\varphi).\end{aligned}\quad (4.2)$$

Here, we introduce the coherence length $\xi = \hbar v_F / \Delta_0$, the center of a vortex is situated at $x = y = 0$ and $\exp(i\varphi)$ is the phase factor which originates from the vortex.

For $\epsilon_n > 0$ the Riccati equations have to be solved using the bulk values as initial values at $x = \pm\infty$. Then, we obtain anomalous Green's function f as

$$f = -\frac{2a}{1 + ab}.\quad (4.3)$$

For the calculation of the normalized local DOS by its value in the normal state, the quasiclassical propagator has to be integrated over the angle θ which defines the direction of the Fermi velocity. The normalized local DOS in terms of functions a and b is given by

$$N(\mathbf{r}_0, E) = \int_0^{2\pi} \frac{d\theta}{2\pi} \operatorname{Re} \left[\frac{1 - ab}{1 + ab} \right]_{i\epsilon_n \rightarrow E + i\delta},\quad (4.4)$$

where E denotes the quasiparticle energy with respect to the Fermi level and δ is an effective scattering parameter that corresponds to an inverse mean free path. In numerical calculations throughout this chapter, we will fix this value as $\delta = 0.1\Delta_0$. Further, in what follows, the origin \mathcal{O} of our coordinate system is placed at the center of the vortex core.

4.3 Results

First, we study local DOS around the vortex at $E = 0$. The results of calculations are shown Fig. 4.1 (a). As is well known, zero energy peak appears in the core. The energy dependence of local DOS at $x = y = 0$ shown in Fig. 4.1 (b) exhibits a strong zero energy peak.

Due to the broken translational symmetry of the system, unconventional pairing states with higher angular momentum are expected to emerge around the vortex. In order to study possible pairing states around the vortex, let

us decompose anomalous Green's function f into various angular momentum components as follows

$$f \cong f_s + f_{px} \cos \theta + f_{py} \sin \theta + f_{dx^2-y^2} \cos 2\theta + f_{dxy} \sin 2\theta + f_{f1} \cos 3\theta + f_{f2} \sin 3\theta + \dots \quad (4.5)$$

Note that all the above pairing components are *singlet*. Their spatial dependencies at $E = 0$ are shown in Figure 4.2. Interestingly, only odd-frequency spin-singlet odd-parity pairings, $\text{Re}f_{px}$ and $\text{Im}f_{py}$, may exist at the center of the core. With the increase of the distance from the core center, the magnitudes of anomalous Green's functions decrease rapidly, except for s -wave one. Note that other angular momentum components not shown in this figure are negligibly small.

Figure 4.3 shows the decomposition of the p -wave pair amplitude at the center of the core $x = y = 0$ as a function of energy. Note that other pairing amplitudes are absent at $x = y = 0$ for all E . The relations $\text{Re}f_{px} = \text{Im}f_{py}$ and $\text{Im}f_{px} = -\text{Re}f_{py}$ are satisfied for all E , as illustrated on the figure. Therefore, the following representation of anomalous Green's function f holds at the center of the core:

$$f = (\text{Re}f_{px} + i\text{Im}f_{px}) (\cos \theta + i \sin \theta) = f_{px} \exp(i\theta). \quad (4.6)$$

We see that anomalous Green's function at the core center has the same angular dependence as the gap function. This fact can be explained as follows. If we consider a pure phase vortex located at $x = y = 0$, then the gap function has the form $\Delta(\mathbf{r}) = \Delta_0 \exp(i\varphi)$. In this case, one can obtain simple analytical solution of the Eilenberger equations at $x = y = 0$ in the form

$$f = -\frac{\Delta_0 \exp(i\varphi)}{\sqrt{\Delta_0^2 + \epsilon_n^2}} = \frac{\Delta_0 \exp(i\theta)}{\sqrt{\Delta_0^2 + \epsilon_n^2}} \quad (4.7)$$

since the relation $\varphi = \theta + \pi$ holds on a trajectory passing through the center of the vortex. The above solution shows that only chiral p -wave pairing state is induced at the vortex center due to the phase winding.

The enhancement of the local DOS in the presence of odd-frequency pairing can be understood by using the normalization condition for the Green's functions $g^2 + f\bar{f} = 1$. Indeed, since for the odd-frequency pairing state the anomalous Green's function $\bar{f} = -2b/(1 + ab)$ at $E = 0$ is given by $\bar{f}(\theta) = -f^*(\theta)$ (see Ref.[26]) and local DOS is given by $N(E) = -\text{Reg}$, one can show that generally $N(E = 0) > 1$. That means that the emergence of the odd-frequency pairing is a physical reason of zero energy peak of the local DOS inside the core.

For a chiral superconductor with angular momentum l and a vortex with vorticity m ($\Delta(\theta) \propto \Delta_0 \exp(il\theta + im\varphi)$), we find that anomalous Green's function is given by $f \propto \exp(i(l+m)\theta)$ at the vortex center, in a similar way. For an odd integer m , in accordance with Fermi statistics, an induced pairing component at the vortex center has different parity and hence different symmetry with respect to frequency from those in the bulk superconductor. Now, let us show example with $l = 1$ (p -wave) and $m = \pm 1$ in Fig. 4.4. As shown in (a), only odd-frequency spin-triplet d -wave pairing can survive at the core center for $l = m = 1$, while only odd-frequency spin-triplet s -wave pairing can survive at the core center for $l = -m = 1$ as shown in (b).

For $l = 0$, *i.e.* in conventional s -wave case, there have been several studies of multi-vortex state with $m \geq 1$ [27, 28]. It was shown that zero energy peak only appears at the vortex center for odd number m [28]. This statement is consistent with our result for $l = 0$ because odd-frequency pairing state is generated only for odd integer m .

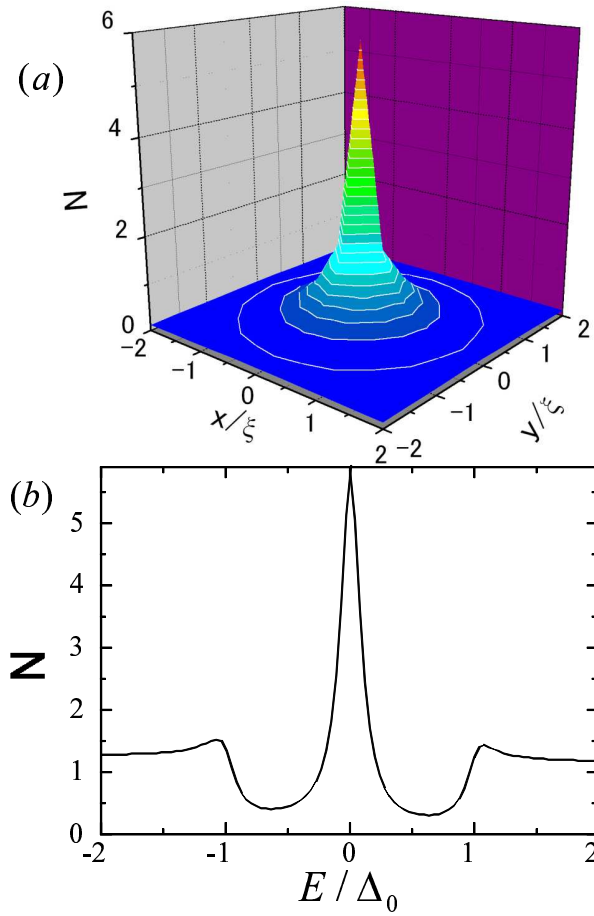


Figure 4.1: (a) Normalized local DOS around the core at $E = 0$. The center of the vortex is situated at $x = y = 0$. (b) The dependence of local DOS on quasiparticle energy at $x = y = 0$. Zero energy peak of the local DOS is seen.

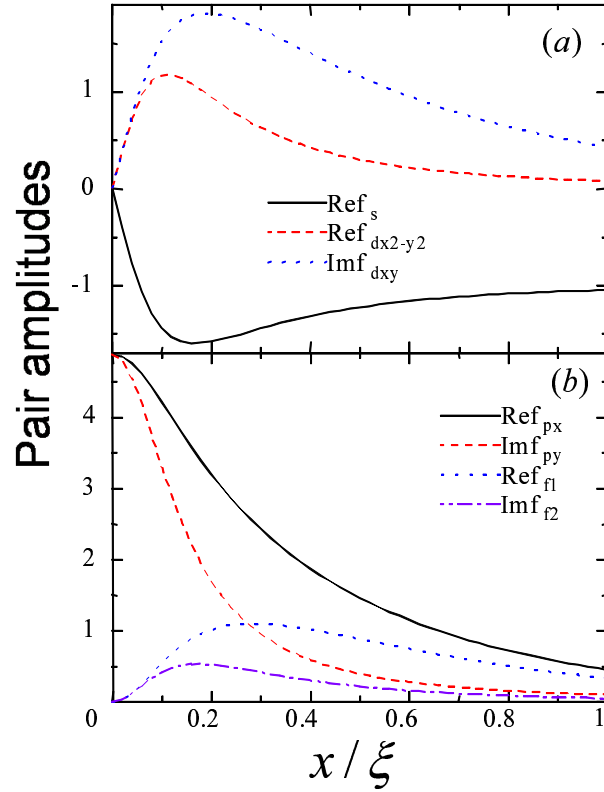


Figure 4.2: Spatial dependencies of various pairing components at $E = 0$. (a) even-frequency spin-singlet even-parity component, (b) odd-frequency spin-singlet odd-parity component. Odd-frequency spin-singlet odd-parity components, Ref_{px} and $\text{Im}f_{py}$, can exist inside the core (near $x = 0$).

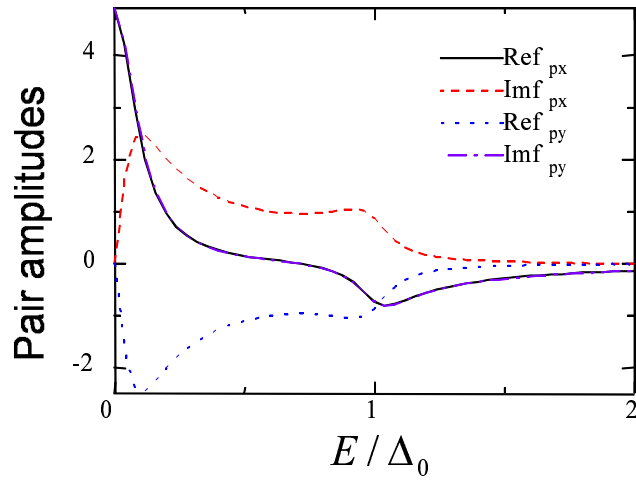


Figure 4.3: p -wave pairing components at $x = y = 0$ as a function of energy E . The relations $\text{Re}f_{px} = \text{Im}f_{py}$ and $\text{Im}f_{px} = -\text{Re}f_{py}$ hold for all E .

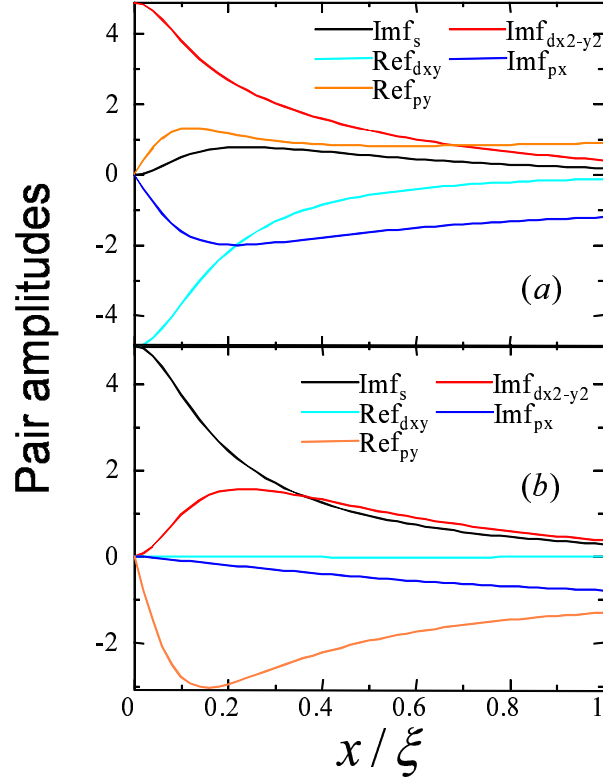


Figure 4.4: Spatial dependencies of various pairing components at $E = 0$ in chiral p -wave superconductors with (a) the same and (b) the opposite chirality with that of the vortex. Odd-frequency spin-triplet even-parity components can exist inside the core (near $x = 0$).

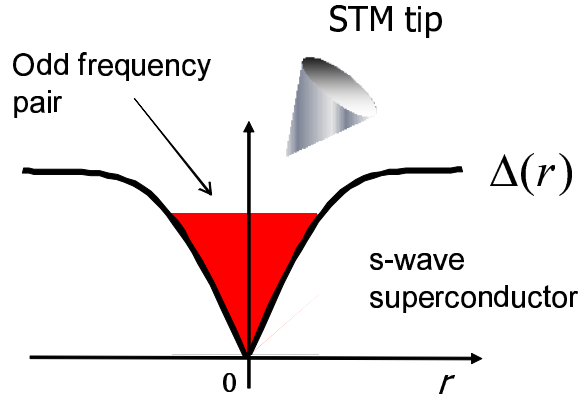


Figure 4.5: Suggested experimental setup to verify the existence of odd-frequency pairing in bulk materials. Nonzero local Josephson current is allowed at the core when superconducting STM tip has odd-frequency spin-singlet odd-parity p -wave pairing. Here, $r = \sqrt{x^2 + y^2}$.

Now, we propose an experimental setup to verify the existence of odd-frequency pairing in bulk materials by using superconducting STM.[29] As discussed above, only odd-frequency spin-singlet odd-parity p -wave pairing state is allowed at the center of the vortex core in s -wave superconductor. Therefore, using a superconductor as an STM tip and investigating its coupling with the vortex state in an s -wave superconductor, one can detect a pairing symmetry of the tip material. Local Josephson current measured in STM experiment with superconducting tip is given by [30]

$$eIR = \pi T \sum_{\theta, \epsilon_n} \text{Im}(f^*(\theta, \epsilon_n) f_S(\theta, \epsilon_n)). \quad (4.8)$$

Here, R is the junction resistance, T is temperature and f_S is anomalous Green's function in the STM tip. It follows from this expression that finite Josephson current is allowed only when superconducting STM has the same symmetry as that of the vortex state in an s -wave superconductor. Otherwise, summation over angle or Matsubara frequency results in zero current. *Therefore, finite Josephson current is allowed at the vortex core only when superconducting STM has odd-frequency spin-singlet odd-parity p -wave pairing.* One can detect the presence of odd-frequency pairing by observing finite current at the core and vanishing current far from the core. If the STM tip is made of a conventional s -wave superconductor, the behavior is opposite: the Josephson current vanishes at the core and is nonzero far from the core.

The experimental setup is illustrated in Fig. 4.5. It was suggested in Refs. [5, 31, 32] that odd-frequency spin-singlet odd-parity state could be realized in CeCu_2Si_2 and CeRhIn_5 , and thus our prediction may help to identify pairing symmetry in these materials.

Finally, we also propose an experimental setup to verify our finding. Our theory predicts that only odd-frequency spin-triplet even-parity s -wave pairing is allowed at the center of the vortex core in chiral p -wave superconductor, realized in Sr_2RuO_4 [35, 36], with a chirality opposite to that of the vortex, as shown in Fig. 4.4 (b). It is established that odd-frequency spin-triplet even-parity s -wave pairing is also generated in half-metal/ s -wave superconductor junctions.[37] Then, using superconducting STM tip made of half-metal attached to an s -wave superconductor, one may confirm the existence of odd frequency pairing at the core by observing finite Josephson current with a similar experimental setup in Fig. 4.5. Note that if we use superconducting STM tip made of conventional s -wave superconductor instead, we cannot observe a zero Josephson current.

4.4 Conclusions

In this chapter, we have studied pairing symmetry inside the Abrikosov vortex core in superconductors. We have shown that only odd-frequency spin-singlet chiral p -wave pairing is allowed at the center of the core in s -wave superconductors as a consequence of the broken translational symmetry. This makes it possible to provide new interpretation of the Andreev bound states inside the core as *the manifestation of the odd-frequency pairing*. This interpretation is consistent with the experimental fact that the observed zero-bias conductance peak by STM at a vortex center is very sensitive to disorder. [33] We have also unveiled the sum rule that for a vortex with vorticity m in a chiral superconductor with angular momentum l , anomalous Green's function at the vortex center has angular momentum $l + m$. Based on these results, we have proposed the experimental setup to verify the existence of odd-frequency pairing in bulk materials by using superconducting STM.

The relation between odd-frequency pairing and zero energy peak of local DOS is quite general feature as already found in normal metal/superconductor junctions[8, 9] or ferromagnet/superconductor junctions.[34] The interpretation of Abrikosov vortex as *a manifestation of the odd-frequency pairs* may become a useful concept to explore new features in the vortex physics.

Bibliography

- [1] V. L. Berezinskii, JETP Lett. **20**, 287 (1974)
- [2] A. Balatsky and E. Abrahams, Phys. Rev. B **45**, 13125 (1992); E. Abrahams, A. Balatsky, D. J. Scalapino and J. R. Schrieffer, Phys. Rev. B **52**, 1271 (1995).
- [3] P. Coleman, E. Miranda, and A. Tsvelik, Phys. Rev. Lett. **70**, 2960 (1993); Phys. Rev. B **49**, 8955 (1994); Phys. Rev. Lett. **74**, 1653 (1995).
- [4] M. Vojta and E. Dagotto, Phys. Rev. B **59**, R713 (1999).
- [5] Y. Fuseya, H. Kohno and K. Miyake, J. Phys. Soc. Jpn. **72**, 2914 (2003).
- [6] F. S. Bergeret, A. F. Volkov, and K. B. Efetov, Phys. Rev. Lett. **86**, 4096 (2001); F. S. Bergeret, A. F. Volkov, and K. B. Efetov, Rev. Mod. Phys. **77**, 1321 (2005).
- [7] A. Kadigrobov, R. I. Shekter and M. Jonson, EuroPhys. Lett. **90**, 394 (2001).
- [8] Y. Tanaka, A. A. Golubov, S. Kashiwaya, and M. Ueda, Phys. Rev. Lett. **99**, 037005 (2007). Y. Tanaka, Y. Tanuma and A. A. Golubov, Phys. Rev. B **76**, 054522 (2007).
- [9] Y. Tanaka and A. A. Golubov, Phys. Rev. Lett. **98**, 037003 (2007).
- [10] A. L. Fetter and P. C. Hohenberg, in *Superconductivity*, edited by R. D. Parks (Marcel Dekker, New York, 1969).
- [11] G. Blatter, M. V. Feigel'man, V. B. Geshkenbein, A. I. Larkin, and V. M. Vinokur, Rev. Mod. Phys. **66**, 1125 (1994).
- [12] E. H. Brandt, Rep. Prog. Phys. **58**, 1465 (1995).
- [13] Y. Morita, K. Kohmoto, and K. Maki, Int. J. Mod. Phys. B **12**, 989 (1998).

- [14] T. Maniv, V. Zhuravlev, I. Vagner, and P. Wyder, *Rev. Mod. Phys.* **73**, 867 (2001).
- [15] G. Blatter and V. B. Geshkenbein, in *The Physics of Superconductors* Vol. 1, edited by K. H. Bennemann, J. B. Ketterson (Springer, 2003)
- [16] C. Caroli, P. G. de Gennes and J. Matricon, *Phys. Lett.* **9**, 307 (1964).
- [17] H. F. Hess, R. B. Robinson, R. C. Dynes, J. M. Valles, Jr., and J. V. Waszczak, *Phys. Rev. Lett.* **62**, 214 (1989).
- [18] Yu. G. Makhlin and G. E. Volovik, *JETP Lett.* **62**, 737 (1995).
- [19] A. I. Larkin and Yu. N. Ovchinnikov, *Phys. Rev. B* **57**, 5457 (1998).
- [20] N. B. Kopnin and G. E. Volovik, *Phys. Rev. Lett.* **79**, 1377 (1997); *Phys. Rev. B* **57**, 8526 (1998).
- [21] G. E. Volovik, *JETP Lett.* **70**, 609 (1999).
- [22] Ø. Fischer, M. Kugler, I. Maggio-Aprile, C. Berthod, and C. Renner, *Rev. Mod. Phys.* **79**, 353 (2007).
- [23] G. Eilenberger, *Z. Phys.* **214**, 195 (1968).
- [24] A. I. Larkin and Yu. N. Ovchinnikov, *Sov. Phys. JETP* **28**, 1200 (1969).
- [25] N. Schopohl and K. Maki, *Phys. Rev. B* **52**, 490 (1995); N. Schopohl, cond-mat/9804064 (unpublished).
- [26] M. Eschrig, *Phys. Rev. B* **61**, 9061 (2000).
- [27] G. E. Volovik, *JETP Lett.* **57**, 244 (1993); S. M. M. Virtanen and M. M. Salomaa, *Phys. Rev. B* **60** 14581 (1999).
- [28] Y. Tanaka, H. Takayanagi and A. Hasegawa, *Solid state Commun.* **85**, 321 (1993); A.S. Mel'nikov and V.M. Vinokur, *Nature* **415**, 60 (2002).
- [29] A. Kohen, Th. Proslier, T. Cren, Y. Noat, W. Sacks, H. Berger, and D. Roditchev, *Phys. Rev. Lett.* **97**, 027001 (2006); J.G. Rodrigo, H. Suderow, and S. Vieira, *Eur. Phys. J. B* **40**, 483 (2004).
- [30] A.V. Zaitsev, *Sov. Phys. JETP* **59**, 1015 (1984).
- [31] S. Kawasaki, T. Mito, Y. Kawasaki, G.-q. Zheng, Y. Kitaoka, D. Aoki, Y. Haga, and Y. Onuki, *Phys. Rev. Lett.* **91**, 137001 (2003).

- [32] Guo-qing Zheng, N. Yamaguchi, H. Kan, Y. Kitaoka, J. L. Sarrao, P. G. Pagliuso, N. O. Moreno, and J. D. Thompson, Phys. Rev. B **70**, 014511 (2004).
- [33] C. Renner, A. D. Kent, P. Niedermann, Ø. Fischer, and F. Lévy, Phys. Rev. Lett. **67**, 1650 (1991).
- [34] V. Braude and Yu. V. Nazarov, Phys. Rev. Lett. **98**, 077003 (2007); T. Yokoyama, Y. Tanaka, and A. A. Golubov, Phys. Rev. B **75**, 134510 (2007); Y. Asano, Y. Tanaka and A. A. Golubov, Phys. Rev. Lett. **98**, 107002 (2007).
- [35] Y. Maeno, H. Hashimoto, K. Yoshida, S. Nishizaki, T. Fujita, J. G. Bednorz, and F. Lichtenberg, Nature (London) **372**, 532 (1994).
- [36] A. P. Mackenzie and Y. Maeno, Rev. Mod. Phys. **75**, 657 (2003).
- [37] R. S. Keizer, S.T.B. Goennenwein, T.M. Klapwijk, G. Miao, G. Xiao, and A. Gupta, Nature **439**, 825 (2006).

Chapter 5

Chirality sensitive effect on surface state in chiral p -wave superconductors

5.1 Introduction

Up to now, much attention has been paid to unconventional superconductors, because they can exhibit a sign change of their gap function as a function of momentum. This property induces many interesting phenomena, which can be observed directly by so-called phase sensitive experiments providing powerful tools to test the symmetry of the gap function [1]. One important consequence of the sign change of the gap function is the possible existence of Andreev bound states at the surface of the superconductor [2, 3, 4, 5, 6]. The formation of Andreev bound states increases the local zero-energy quasiparticle density of states (DOS) at the surface, leading to a pronounced zero-bias conductance peak in the tunneling conductance observable both in singlet d -wave superconductors like the cuprates and in triplet p -wave superconductors like Sr_2RuO_4 [6, 7, 8, 9, 10, 11]. For the case of d -wave superconductors it is well-known, that an applied magnetic field or an applied electric current result in a split of this zero-bias conductance peak, since the zero-energy spectral weight of the bound states is effectively Doppler shifted towards higher energies. The same effect also appears in the absence of external magnetic fields for the scenario of an Abrikosov vortex, which is pinned not far from the boundary. Here, the zero-energy DOS is suppressed in a shadow-like region "behind" the vortex [12, 13].

Another important aspect of unconventional superconductors is that they can have a chirality of the pair potential. For example, Sr_2RuO_4 is known to

have a chiral p -wave symmetry: $d = (0, 0, k_x + ik_y)$. [14, 15, 16, 18, 17] The vortices in chiral p -wave superconductors have been intensively studied. The interplay between vorticity and chirality in the vicinity of the vortex core is discussed in Ref. [19]. However, the study to explore phenomena which directly reflect the characteristics of the chirality is insufficient, while spin or phase sensitive phenomena have been intensively investigated.

In this chapter, we study the DOS in chiral p -wave superconductor in the presence of an Abrikosov vortex in front of a specular surface, based on the quasiclassical theory of superconductivity. We clarify that the DOS at the shadow region of the vortex is sensitive to its chirality. When the chirality is the same as (opposite to) that of the superconductor, the zero energy peak (gap) of the DOS at the shadow region emerges. This is because the DOS at the shadow region has a linear term of the vector potential. Based on the results, we propose a chirality sensitive test on superconductors. In contrast to spin sensitive test on superconductors (e.g., Knight shift [15]) or phase one (e.g., SQUID [18, 20]), chirality sensitive test has not yet been established. We think that our results contribute to the development of physics of unconventional superconductors with chirality.

5.2 Formulation

For the calculation of the local DOS in the vicinity of the boundary, it is necessary to find numerically stable solutions of the Eilenberger equations [21, 22] that satisfy the appropriate boundary conditions at the specular surface. For this purpose, we use the Riccati parametrization of the quasiclassical propagator [23]. Along a trajectory $\mathbf{r}(x) = \mathbf{r}_0 + x \hat{\mathbf{v}}_F$ with unit vector $\hat{\mathbf{v}}_F$ parallel to \mathbf{v}_F , the Eilenberger equations are generally represented in 4×4 matrix form. [24] For the chiral p -wave superconductor with $\hat{\Delta} = \Delta \sigma_x$ (σ_x is a Pauli's matrix in spin space), these equations are reduced to be a set of two decoupled differential equations of the Riccati type for the functions $a(x)$ and $b(x)$ [26]

$$\begin{aligned} \hbar v_F \partial_x a(x) + [2\tilde{\epsilon}_n + \Delta^\dagger a(x)] a(x) - \Delta &= 0, \\ \hbar v_F \partial_x b(x) - [2\tilde{\epsilon}_n + \Delta b(x)] b(x) + \Delta^\dagger &= 0 \end{aligned} \quad (5.1)$$

where $i\tilde{\epsilon}_n = i\epsilon_n + \mathbf{v}_F \cdot \frac{e}{c} \mathbf{A}$ are shifted Matsubara frequencies. For the simple case of a cylindrical Fermi surface, the Fermi velocity can be written as $\mathbf{v}_F = v_F(\mathbf{e}_1 \cos \theta + \mathbf{e}_2 \sin \theta)$. The θ - and \mathbf{r} -dependence of the pairing potential Δ can be factorized in the form

$$\Delta(\mathbf{r}, \theta) = \Delta_0 \exp(i\theta) \Psi(\mathbf{r}). \quad (5.2)$$

Here, Ψ is a phase factor which originates from the vortex. Near the boundary and the center of the vortex, the pair potential has a spatial dependence in general. However, it is known from the previous theories [12, 13] that if we want to know the qualitative aspects of DOS in a shadow-like region, we can assume that the magnitude of the gap is constant throughout the superconductor.

With the condition that there are no currents flowing across the boundary, we have the pairing potential around a vortex as $\Psi(\mathbf{r}) = e^{i\Phi(\mathbf{r})}$. [25] By considering a vortex-antivortex pair, in analogy with the mirror method, the phase $\Phi(\mathbf{r})$ is obtained as $\Phi(\mathbf{r}) = \arg(\mathbf{r} - \mathbf{r}_V) - \arg(\mathbf{r} - \bar{\mathbf{r}}_V)$ where $\bar{\mathbf{r}}_V = \mathbf{r}_V - 2\hat{\mathbf{n}}\langle\hat{\mathbf{n}}, \mathbf{r}_V\rangle$ with the position of the vortex \mathbf{r}_V and unit vector $\hat{\mathbf{n}}$ normal to the surface. The vortex chosen here corresponds to a pure phase vortex. For our purpose, to obtain qualitative results of DOS of chiral p -wave superconductor in the presence of the vortex, this simplification is reasonable. [12, 13]

For $\epsilon_n > 0$ the Riccati equations have to be solved using the bulk values as initial values at $x = \pm\infty$

$$\begin{aligned} a(-\infty) &= \frac{\Delta(-\infty)}{\epsilon_n + \sqrt{\epsilon_n^2 + |\Delta(-\infty)|^2}}, \\ b(+\infty) &= \frac{\Delta^\dagger(+\infty)}{\epsilon_n + \sqrt{\epsilon_n^2 + |\Delta(+\infty)|^2}}. \end{aligned} \quad (5.3)$$

For the calculation of the normalized local DOS, the imaginary part of the quasiclassical propagator has to be integrated over the angle θ that defines the direction of the Fermi velocity. In terms of a and b , we have

$$N(\mathbf{r}_0, E) = \int_0^{2\pi} \frac{d\theta}{2\pi} \text{Re} \left[\frac{1 - ab}{1 + ab} \right]_{i\epsilon_n \rightarrow E + i\delta} \quad (5.4)$$

where E denotes the quasiparticle energy with respect to the Fermi level and δ is an effective scattering parameter that corresponds to an inverse mean free path. Throughout this chapter, we fix this value as $\delta = 0.1\Delta_0$.

The sign change in the order parameter during the reflection at the surface induces Andreev bound states and hence zero energy DOS on the surface are enhanced. [5, 6, 26] The same sign change occurs on a trajectory passing near the center of a vortex and therefore leads to similar localized Andreev bound states inside the vortex core. The suppression of the amplitude of the pairing potential around the vortex center does not change the calculated result of the trapped state qualitatively. [27] The influence of the boundary for anisotropic superconductors is included within the quasiclassical theory by

the nonlinear boundary conditions for the quasiparticle propagator [28, 29]. For the Riccati parametrization, a substantial simplification occurs and an explicit solution of the nonlinear boundary conditions can be found [30].

In the following, the origin \mathcal{O} of our coordinate system is placed at the boundary right between the vortex and the image vortex. The y -axis is orientated parallel to the boundary. x_V denotes the vortex position on the x -axis and also measures the vortex to boundary distance. Furthermore it is useful to introduce the coherence length $\xi = \hbar v_F / \Delta_0$ as the unit of a general length scale.

5.3 Results

In what follows, we consider two cases: (a) chirality of p -wave superconductor is the same as that of the vortex. (b) chirality of p -wave superconductor is opposite to that of the vortex. In order to study the case (b), we have to just replace Ψ by Ψ^* in Eq. (5.2).

We study DOS at $E = 0$ in the presence of the vortex with (a) the same chirality and (b) the opposite chirality in Fig. 5.1. A phase vortex is situated at a distance of two coherence lengths $x_V = 2\xi$ from the surface. We find that Andreev bound states formed at $x = 0$ are strongly modified by the presence of the vortex: In (a), a sharpe peak appears at the shadow region on the surface while a sharpe dip appears at the shadow region as shown in (b). These features can be understood by the Doppler shift [5, 7, 31], which is most remarkable in the shadow region. [12]

Let us explain this chirality sensitive phenomenon as follows. Now, we consider the surface DOS of chiral p -wave superconductors in the presence of a nearly homogeneous vector potential. Since we assume that the magnitude of the gap is constant throughout the superconductor, solving differential equations of the Riccati type numerically for given $\hat{\mathbf{v}}_F$ -direction is unnecessary in this case. We can calculate DOS on the surface analytically in a straightforward way. Noting that a (b) is spatially independent for the incoming (outgoing) trajectory [23], we obtain

$$N(E) = 2\text{Re} \left\langle \frac{1}{1 + a_{in} b_{out}} \right\rangle_{i\epsilon_n \rightarrow E+i\delta} - 1 \quad (5.5)$$

with $a_{in} = s\Delta_0 e^{i(\pi-\theta)}$, $b_{out} = s\Delta_0 e^{-i\theta}$ and the abbreviation $s = 1/(\tilde{\epsilon}_n + \sqrt{\tilde{\epsilon}_n^2 + \Delta_0^2})$. Furthermore, $\langle \dots \rangle$ denotes angular averaging, which we may restrict to outgoing angles $-\pi/2 \leq \theta \leq \pi/2$ only. Therefore, we have

$$N(E) = 2\text{Re} \left\langle \frac{1}{1 + (1 - 2\tilde{\epsilon}_n c) e^{-2i\theta}} \right\rangle_{i\epsilon_n \rightarrow E+i\delta} - 1. \quad (5.6)$$

Expanding the DOS at $E = 0$ in the vector potential A , we obtain in the limit of $\delta \rightarrow +0$

$$N(E = 0) = 1 + \frac{ev_F}{c\Delta_0}A_y + \dots \quad (5.7)$$

An interesting aspect is that a linear term of the vector potential A survives. This is because this term remains after angular averaging while, for s -, d - or p -wave superconductors without chirality, we get similarly

$$N = C + \langle F(\theta) \sin \theta \rangle A_y + \dots \quad (5.8)$$

with a constant C and a function F which satisfies $F(\theta) = F(-\theta)$. The coefficient of the linear term is an odd function of the angle and hence vanishes by angular averaging. The absence of odd order term in A_y reflects the presence of inversion symmetry with respect to the x - y plane for these pairings. Since the magnetic field is related to the vector potential as $B_z = \frac{\partial A_y}{\partial x}$, the zero energy DOS depends on the sign of the magnetic field. Applying magnetic field in a certain direction leads to the zero energy peak of the surface DOS, while applying it in the opposite direction leads to the gap structure. Note that the reversal of the magnetic field corresponds to that of the chirality of the vortex.

Next, we study the DOS at $x = 0$ and $E = 0$ as a function of y in the presence of the vortex with (a) the same chirality and (b) the opposite chirality in Fig. 5.2. As x_V increases, zero energy peak in (a) and zero energy gap in (b) are suppressed, while the widths of them increase because the effect of the vortex becomes weak.

Figure 5.3 exhibits the local DOS at the point $x = y = 0$ for different vortex to boundary distances x_V as a function of energy. If the Abrikosov vortex is placed near the boundary, a remarkable zero energy peak and zero energy gap emerge as shown in (a) and (b), respectively. With increasing distance between vortex and boundary, these zero-energy anomalies are suppressed. However, even for large distance $x_V = 10\xi$ apart from the surface, these zero-energy anomalies are still visible.

Now, we investigate pairing symmetry on the surface of the superconductor. Near the surface, odd-frequency spin-triplet *even-parity* pairing is expected to be generated due to the broken translational symmetry. [32] Here, we study the chirality effect on the odd- and even-frequency pairings at the shadow region. Figure 5.4 shows imaginary part of the odd-frequency spin-triplet even-parity pairing f_{ep} and real part of the even-frequency spin-triplet odd-parity pairing f_{op} at the shadow point $x = y = 0$ and $E = 0$ as a function of θ with (a) the same chirality and (b) the opposite chirality. f_{ep} and f_{op} are obtained as an even and odd part of anomalous Green's functions

f which is given by $f = -2ia/(1 + ab)$ with respect to the transformation $\theta \rightarrow \theta + \pi$. As shown in (a), imaginary part of the even-parity pairing f_{ep} dominates while real part of the odd-parity pairing f_{op} is dominant in (b). Note that real part of f_{ep} and imaginary part of f_{op} are negligibly small. Since anomalous Green's function $\bar{f} = 2ib/(1 + ab)$ is given by $\bar{f}(\theta) = -f^*(\theta + \pi)$ at $E = 0$, we obtain $\bar{f}_{ep}(\theta) = -f_{ep}^*(\theta)$ and $\bar{f}_{op}(\theta) = f_{op}^*(\theta)$. Thus, we can understand that the local DOS is enhanced (reduced) by the presence of $f_{ep}(f_{op})$ by using normalization condition $g^2 + f\bar{f} = 1$. Therefore, large magnitude of the even-parity pairing f_{ep} (odd parity pairing f_{op}) is responsible for the zero energy peak (gap) at the shadow region. See also Appendix.

To understand this result, we again analytically calculate anomalous Green's functions f on the surface in the presence of a nearly homogeneous vector potential in a similar way of the calculation of the DOS by choosing $\Psi = 1$ in Eq. (5.2). Expanding them at $E = 0$ with respect to the vector potential, we obtain for $0 < \theta < \pi/2, 3\pi/2 < \theta < 2\pi$ (region A)

$$f_{ep}(\theta \in A) = -2i \cos \theta + \frac{2iev_F A_y}{c\Delta_0} \cos^2 \theta, \quad (5.9)$$

$$f_{op}(\theta \in A) = \frac{\cos 2\theta}{\sin \theta} - \frac{ev_F A_y}{c\Delta_0} \frac{\cos 2\theta}{\tan \theta} \quad (5.10)$$

with $\delta \rightarrow +0$. For $\theta \sim 0$ we cannot take the limit $\delta \rightarrow +0$ from the first. For $\theta \rightarrow 0$, we obtain $f_{ep} = \frac{-2i}{1-q}$ and $f_{op} = \frac{2\theta}{(1-q)^2} \left(2 + \frac{ev_F A_y}{c\Delta_0} \right)$ with $q = 1 - 2\delta/\Delta_0$ ($\delta \rightarrow +0$). Note that these pairings are all triplet. We find that a linear term of the vector potential survives, which indicates that applied magnetic field in a certain direction enhances the anomalous Green's functions, while the magnetic field in the opposite direction reduces them. Therefore, we understand the dependence of imaginary part of f_{ep} and real part of f_{op} on the chirality of the vortex in Figs. 5.4 (a) and (b).

Based on our results, we can propose a chirality sensitive test on superconductors. It is expected that we can observe the enhancement (or suppression) of the DOS on the surface applying a weak magnetic field on the surface of a superconductor, by using, e.g., a low-temperature scanning-tunneling spectroscopy (STS) [33, 34]. If we can observe the suppression (or enhancement correspondingly) of the DOS on the surface by STS by reversing the direction of the applied magnetic field, we can conclude that the superconductor has a chirality. This unusual reversal effect does not appear in non-chiral superconductors. Moreover, the experiment allows us to detect the chirality and possibly even the domains of different chirality, if domain walls reach the surface. This idea is very promising since zero energy peak due to the Andreev bound state has been observed by STS [6].

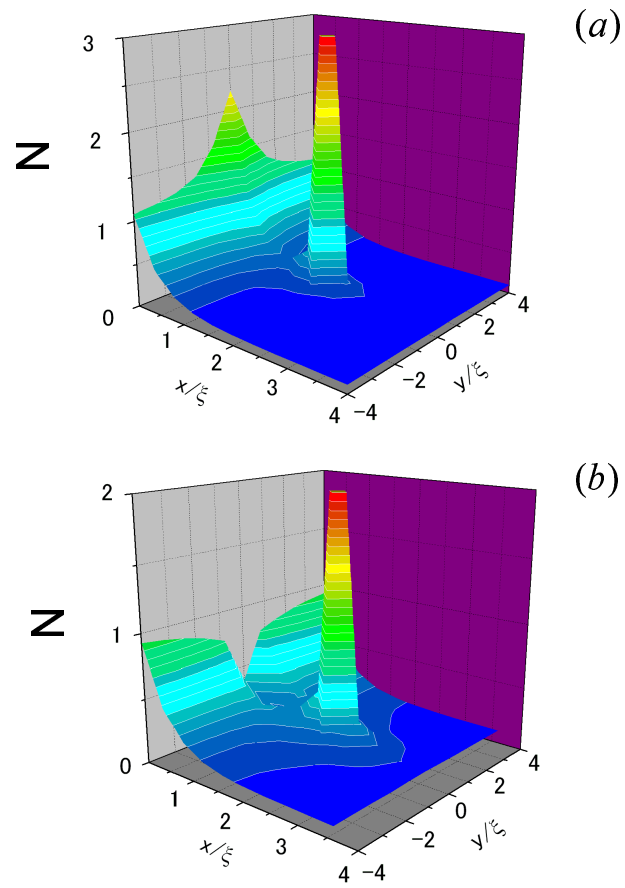


Figure 5.1: DOS at $E = 0$ in the presence of the vortex with (a) the same chirality and (b) the opposite chirality. The single Abrikosov vortex can be found at a distance of two coherence lengths $x_V = 2\xi$ in front of the surface. Andreev bound states are formed at $x = 0$.

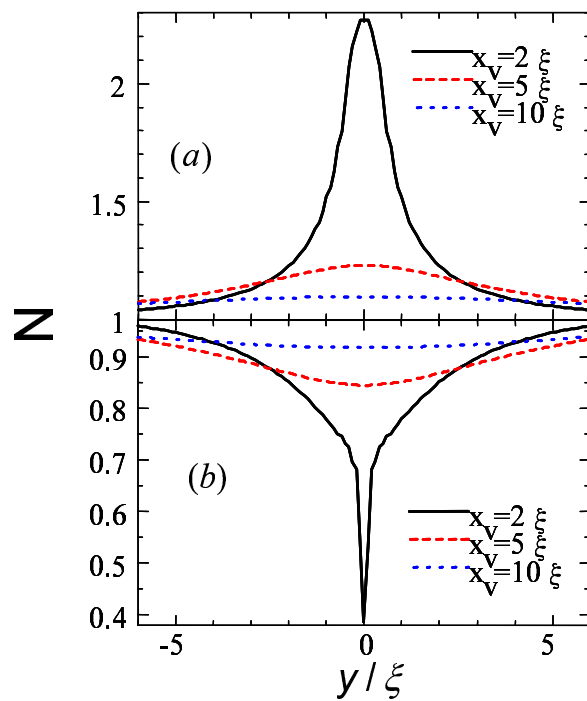


Figure 5.2: DOS at $x = 0$ and $E = 0$ for different vortex to boundary distances x_v in the presence of the vortex with (a) the same chirality and (b) the opposite chirality.

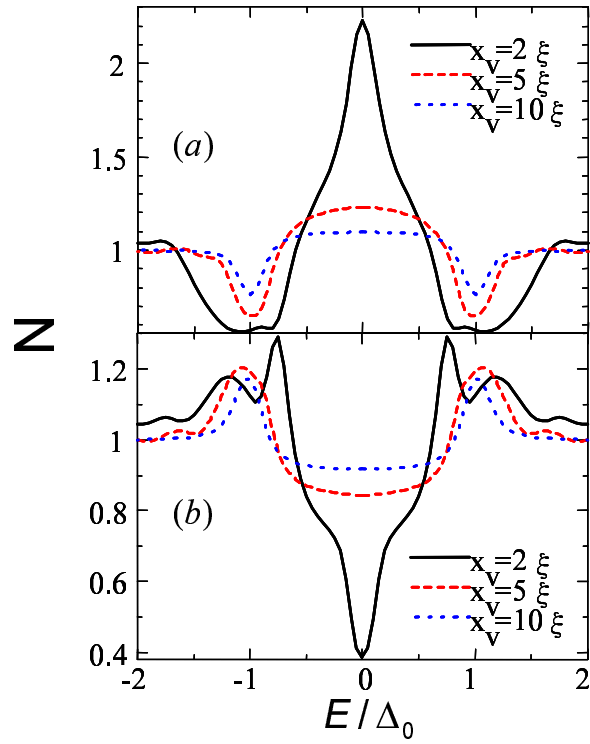


Figure 5.3: Local DOS at the point $x = y = 0$ for different vortex to boundary distances x_V as a function of energy in the presence of the vortex with (a) the same chirality and (b) the opposite chirality.

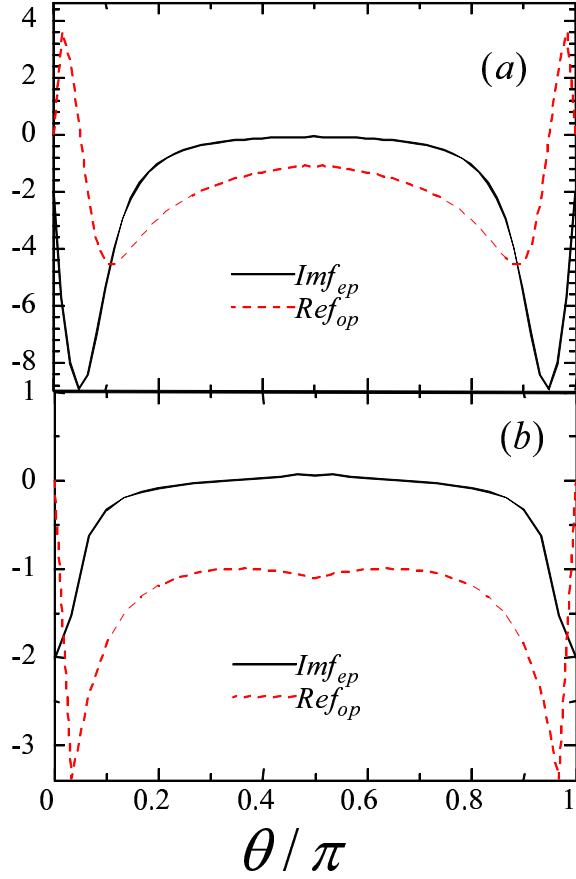


Figure 5.4: Imaginary part of odd frequency spin-triplet even parity pairing f_{ep} and real part of even frequency spin-triplet odd parity pairing f_{op} at the point $x = y = 0$ as a function of θ in the presence of the vortex with (a) the same chirality and (b) the opposite chirality.

5.4 Conclusions

In this chapter, we have studied the DOS in chiral p -wave superconductor in the presence of an Abrikosov vortex in front of a specular surface, based on the quasiclassical theory of superconductivity. We clarified that the DOS at the shadow region of the vortex is sensitive to its chirality. When the chirality is the same as (opposite to) that of the superconductor, the zero energy peak (gap) of the DOS at the shadow region emerges. This is because the DOS at the shadow region has a linear term of the vector potential. Based on the results, we proposed chirality sensitive test on superconductors.

It is also worth noting that the modification of the surface quasiparticle states due to the presence of vortices has an effect on the force acting on vortices near the surface. An increase of the DOS leads to a repulsion of the vortex from the boundary towards the bulk, whereas a decrease results in an attraction towards the boundary. Thus, in both cases the Bean-Livingston barrier would be modified, which influences the escape and entrance of vortices to the superconductor [35, 36].

5.5 Appendix: Basic properties of Riccati parameters from the Eilenberger equations

Here, we discuss basic properties of Riccati parameters a and b from the Eilenberger equations, which impose a relation between f and \bar{f} . Eilenberger equations read

$$v_F \partial_x a + (2(-iE + \delta) + \Delta^* a) a - \Delta = 0, \quad (5.11)$$

$$v_F \partial_x b - (2(-iE + \delta) + \Delta b) b + \Delta^* = 0. \quad (5.12)$$

With the transtormation $a(E + i\delta, k, r) \rightarrow -a^*(-E + i\delta, -k, r)$ in the first equation, we obtain

$$-v_F \partial_x a^* + (2(-iE + \delta) - \Delta^* a^*) a^* + \Delta^* = 0 \quad (5.13)$$

with wave vector k and position r , because $\Delta(k) = -\Delta(-k)$. Hence, we have $b(E + i\delta, k, r) = -a^*(-E + i\delta, -k, r)$. Anomalous Green's functions are given by

$$f = \frac{-2ia}{1 + ab} = \frac{-2ia}{1 - aa^*(-E + i\delta, -k, r)}, \quad (5.14)$$

$$\bar{f} = \frac{2ib}{1 + ab} = \frac{-2ia^*(-E + i\delta, -k, r)}{1 - aa^*(-E + i\delta, -k, r)}. \quad (5.15)$$

This results in $\bar{f}(E + i\delta, k, r) = -f^*(-E + i\delta, -k, r)$ and hence we get $\bar{f}_{ep}(E + i\delta, k, r) = -f_{ep}^*(-E + i\delta, k, r)$ and $\bar{f}_{op}(E + i\delta, k, r) = f_{op}^*(-E + i\delta, k, r)$. Therefore, we have at $E = 0$

$$f\bar{f} = (f_{ep} + f_{op})(-f_{ep}^* + f_{op}^*) = |f_{op}|^2 - |f_{ep}|^2 + 2i\text{Im}(f_{ep}f_{op}^*) \quad (5.16)$$

and finally the DOS

$$-\text{Reg} = \sqrt{\frac{1}{2} \left(1 + |f_{ep}|^2 - |f_{op}|^2 + \sqrt{\left(1 + |f_{ep}|^2 - |f_{op}|^2 \right)^2 + 4 \left(\text{Im}(f_{ep}f_{op}^*) \right)^2} \right)} \quad (5.17)$$

Bibliography

- [1] M. Sigrist and K. Ueda, *Rev. Mod. Phys.* **63**, 239 (1991).
- [2] C. R. Hu, *Phys. Rev. Lett.* **72**, 1526 (1994).
- [3] Y. Tanaka and S. Kashiwaya, *Phys. Rev. Lett.* **74**, 3451 (1995).
- [4] L. J. Buchholtz, M. Palumbo, D. Rainer, and J. A. Sauls, *J. Low Temp. Phys.* **101**, 1099 (1995).
- [5] Y. Asano, Y. Tanaka and S. Kashiwaya, *Phys. Rev. B* **69**, 13450 (2004).
- [6] S. Kashiwaya and Y. Tanaka, *Rep. Prog. Phys.* **63**, 1641 (2000).
- [7] M. Fogelström, D. Rainer, and J. A. Sauls, *Phys. Rev. Lett.* **79**, 281 (1997).
- [8] M. Covington, M. Aprili, E. Paraoanu, L.H. Greene, F. Xu, J. Zhu, and C.A. Mirkin, *Phys. Rev. Lett.* **79**, 277 (1997).
- [9] M. Yamashiro, Y. Tanaka, and S. Kashiwaya *Phys. Rev. B* **56**, 7847 (1997).
- [10] C. Honerkamp and M. Sigrist, *J. Low Temp. Phys.* **111**, 895 (1998).
- [11] T. Yokoyama, Y. Tanaka, and J. Inoue, *Phys. Rev. B* **72**, 220504(R) (2005).
- [12] S. Graser, C. Iniotakis, T. Dahm, and N. Schopohl, *Phys. Rev. Lett.* **93**, 247001 (2004)
- [13] C. Iniotakis, S. Graser, T. Dahm, and N. Schopohl, *Phys. Rev. B* **71**, 214508 (2005)
- [14] Y. Maeno, H. Hashimoto, K. Yoshida, S. Nishizaki, T. Fujita, J. G. Bednorz, and F. Lichtenberg, *Nature (London)* **372**, 532 (1994).

- [15] K. Ishida, H. Mukuda, Y. Kitaoka, K. Asayama, Z. Q. Mao, Y. Mori, and Y. Maeno, *Nature (London)* **396**, 658 (1998).
- [16] G. M. Luke, Y. Fudamoto, K. M. Kojima, M. I. Larkin, J. Merrin, B. Nachumi, Y. J. Uemura, Y. Maeno, Z. Q. Mao, Y. Mori, H. Nakamura, and M. Sgrist, *Nature (London)* **394**, 558 (1998).
- [17] A. P. Mackenzie and Y. Maeno, *Rev. Mod. Phys.* **75**, 657 (2003).
- [18] K. D. Nelson, Z. Q. Mao, Y. Maeno, and Y. Liu, *Science* **306**, 1151 (2004); Y. Asano, Y. Tanaka, M. Sgrist, and S. Kashiwaya, *Phys. Rev. B* **67**, 184505 (2003); *Phys. Rev. B* **71**, 214501 (2005).
- [19] N. Hayashi and Y. Kato, *Phys. Rev. B* **66** 132511 (2002); N. Hayashi and Y. Kato, *J. Low Temp. Phys.* **131** 893 (2003).
- [20] D. A. Wollman, D. J. Van Harlingen, W. C. Lee, D. M. Ginsberg, and A. J. Leggett *Phys. Rev. Lett.* **71**, 2134 (1993).
- [21] G. Eilenberger, *Z. Phys.* **214**, 195 (1968).
- [22] A. I. Larkin and Yu. N. Ovchinnikov, *Zh. Eksp. Teor. Fiz.* **55**, 2262 (1968) [*Sov. Phys. JETP* **28**, 1200 (1969)].
- [23] N. Schopohl and K. Maki, *Phys. Rev. B* **52**, 490 (1995); N. Schopohl, cond-mat/9804064 (unpublished).
- [24] M. Eschrig, *Phys. Rev. B* **61**, 9061 (2000).
- [25] O. V. Dolgov and N. Schopohl, *Phys. Rev. B* **61**, 12389 (2000).
- [26] M. Matsumoto and M. Sgrist, *J. Phys. Soc. Jpn.* **68**, 994 (1999).
- [27] T. Dahm, S. Graser, C. Iniotakis, and N. Schopohl, *Phys. Rev. B* **66**, 144515 (2002).
- [28] L. J. Buchholtz and D. Rainer, *Z. Phys. B* **35**, 151 (1979).
- [29] A. V. Zaitsev, *Zh. Eksp. Teor. Fiz.* **86**, 1742 (1984) [*Sov. Phys. JETP* **59**, 1015 (1984)].
- [30] A. Shelankov and M. Ozana, *Phys. Rev. B* **61**, 7077 (2000).
- [31] Y. Tanaka, Y. Tanuma, K. Kuroki and S. Kashiwaya, *J. Phys. Soc. Jpn.* **71**, 2102 (2002).

- [32] Y. Tanaka, A. A. Golubov, S. Kashiwaya, and M. Ueda, *Phys. Rev. Lett.* **99**, 037005 (2007).
- [33] H. F. Hess, R. B. Robinson, R. C. Dynes, J. M. Valles, Jr., and J. V. Waszczak, *Phys. Rev. Lett.* **62**, 214 (1989).
- [34] Ø. Fischer, M. Kugler, I. Maggio-Aprile, C. Berthod, and C. Renner, *Rev. Mod. Phys.* **79**, 353 (2007).
- [35] C. P. Bean and J. D. Livingston, *Phys. Rev. Lett.* **12**, 14 (1964).
- [36] C. Iniotakis, T. Dahm, and N. Schopohl, *cond-mat/0705.1819*.

Chapter 6

Summary and outlook

In this thesis, we studied superconducting systems with broken symmetry. The presence of ferromagnet, vortex and surface breaks symmetry in spin space and translational symmetry. These broken symmetry is an important ingredient of the emergence of odd frequency superconductivity which hardly appears in bulk materials –it has been a huge obstacle for the development of the study of odd frequency superconductivity. By considering these symmetry breaking systems, we elucidated how this exotic pairing state arises and influences observable quantities, especially density of states, which will provide a new insight on the physics of the odd frequency superconductivity.

In chapter 2, we studied the conditions for the appearance of the peak in the density of states of diffusive ferromagnet in normal metal / diffusive ferromagnet / superconductor junctions. A detailed theoretical study of the tunneling conductance and the density of states in these junctions is presented.

In chapter 3, we investigated the proximity effect and pairing symmetry in diffusive ferromagnet / superconductor junctions. Various possible symmetry classes in a superconductor were considered which are consistent with the Pauli's principle: even-frequency spin-singlet even-parity state, even-frequency spin-triplet odd-parity state, odd-frequency spin-triplet even-parity state and odd-frequency spin-singlet odd-parity state. The relevance of the odd-frequency to the density of states is discussed.

In chapter 4, we studied pairing symmetry inside the Abrikosov vortex core in superconductors. We showed that only odd-frequency spin-singlet chiral p -wave pairing is allowed at the center of the core in s -wave superconductors as a consequence of the broken translational symmetry. This makes it possible to provide a new interpretation of the Andreev bound states inside the core as *the manifestation of the odd-frequency pairing*. We also unveiled the sum rule behind this phenomenon. Based on these results, we proposed

the experimental setup to verify the existence of odd-frequency pairing in bulk materials by using superconducting scanning tunneling spectroscopy.

In chapter 5, we studied the density of states in chiral p -wave superconductor in the presence of an Abrikosov vortex in front of a specular surface. We clarified that the density of states at the shadow region behind the vortex is sensitive to its chirality. When the chirality is the same as (opposite to) that of the superconductor, the zero energy peak (gap) of the density of states at the shadow region emerges. This is because the density of states at the shadow region has a linear term of the vector potential. Based on the results, we proposed chirality sensitive test on superconductors.

Since phase transitions involving pairing of fermions form centerpieces of physics, our prediction could make a widespread impact on such disparate subdisciplines as cosmology, astrophysics, condensed matter physics, physics of extremely dilute ultra-cold atomic gases, and physics of quantum liquids. Extending the possible pairing states compatible with the Pauli-principle will influence all these disciplines.

Finally, we will comment on future problems. In chapters 2 and 3, we investigated the proximity effect and pairing symmetry in diffusive ferromagnet / superconductor junctions, assuming a uniform magnetization of the ferromagnet. An interesting problem is to study the proximity effect in a similar junction by considering nonuniform magnetization (domain structure) or antiferromagnetism, instead of the uniform magnetization. Also, to generalize the formalism to take into account arbitrary impurity concentration of the ferromagnet, arbitrary magnitude of the exchange field including half-metallicity or spin-active interface is an important future study. In chapter 5, we found that the surface density of states in chiral p -wave superconductor in the presence of an Abrikosov vortex in front of a specular surface is sensitive to the chirality. This effect may influence the Bean-Livingston barrier, which influences the escape and entrance of vortices to the superconductor. To study how the Bean-Livingston barrier would be modified by this chirality sensitive effect is a remaining but intriguing problem.

Acknowledgement

First of all, I would like to thank Prof. Yukio Tanaka. He has led me to an interesting subject for my thesis, which was full of surprises. I wish to express my thanks to Prof. Junichiro Inoue, who has advised on my works and presentations despite his overloaded works. Dr. Alexander A. Golubov, I have learned very much from you. I always enjoy discussions with you and respect your wide-ranged knowledge of physics!

I appreciate valuable discussions and collaborations with Dr. Seiichiro Onari, Dr. Shiro Kawabata, Prof. Takeo Kato, Dr. Yasuhiro Asano, Dr. Yakov V. Fominov, Prof. Manfred Sigrist, Dr. Christian Iniotakis, Jacob Linder, Dr. Tatsushi Akazaki and Prof. Hideaki Takayanagi.

I also acknowledge support by JSPS Research Fellowships for Young Scientists.

List of Publications

1. *Influence of magnetic impurities on charge transport in diffusive-normal-metal/superconductor junctions*,
T. Yokoyama, Y. Tanaka, A. A. Golubov, J. Inoue, and Y. Asano
Phys. Rev. B **71**, 094506 (2005).
2. *Theory of enhanced proximity effect by midgap Andreev resonant state in diffusive normal-metal/triplet superconductor junctions*,
Y. Tanaka, S. Kashiwaya, and T. Yokoyama
Phys. Rev. B **71**, 094513 (2005).
3. *Resonant peak in the density of states in normal-metal/diffusive-ferromagnet/superconductor junctions*,
T. Yokoyama, Y. Tanaka, and A. A. Golubov
Phys. Rev. B **72**, 052512 (2005).
4. *Theory of thermal and charge transport in diffusive normal metal/superconductor junctions*,
T. Yokoyama, Y. Tanaka, A. A. Golubov, and Y. Asano
Phys. Rev. B **72**, 214513 (2005).
5. *Intrinsically s-wave-like property of triplet superconductors with spin-orbit coupling*,
T. Yokoyama, Y. Tanaka, and J. Inoue
Phys. Rev. B **72**, 220504(R) (2005).
6. *Resonant proximity effect in normal metal / diffusive ferromagnet / superconductor junctions*,
T. Yokoyama, Y. Tanaka, and A. A. Golubov
Phys. Rev. B **73**, 094501 (2006).

7. *Nonmonotonic temperature dependence of critical current in diffusive d-wave junctions*,
T. Yokoyama, Y. Tanaka, A. A. Golubov, and Y. Asano
Phys. Rev. B **73**, 140504(R) (2006).
8. *Charge transport in two-dimensional electron gas/insulator/superconductor junctions with Rashba spin-orbit coupling*,
T. Yokoyama, Y. Tanaka, and J. Inoue
Phys. Rev. B **74**, 035318 (2006)
9. *Josephson current through superconductor/diffusive-normal-metal/superconductor junctions: Interference effects governed by pairing symmetry*,
Y. Asano, Y. Tanaka, T. Yokoyama and S. Kashiwaya,
Phys. Rev. B **74**, 064507 (2006)
10. *Angular dependence of Josephson currents in unconventional superconducting junctions*,
T. Yokoyama, Y. Sawa, Y. Tanaka, and A. A. Golubov,
Phys. Rev. B **75**, 020502(R) (2007)
11. *Theory of the Josephson effect in unconventional superconducting junctions with diffusive barriers*,
T. Yokoyama, Y. Tanaka, and A. A. Golubov,
Phys. Rev. B **75**, 094514 (2007)
12. *Quasiclassical Green's function theory of the Josephson effect in chiral p-wave superconductor/diffusive normal metal/chiral p-wave superconductor junctions*,
Y. Sawa, T. Yokoyama, Y. Tanaka, and A. A. Golubov,
Phys. Rev. B **75**, 134508 (2007)
13. *Manifestation of the odd-frequency spin-triplet pairing state in diffusive ferromagnet/superconductor junctions*,
T. Yokoyama, Y. Tanaka, and A. A. Golubov,
Phys. Rev. B **75**, 134510 (2007)
14. *Theory of the tunneling spectroscopy of ferromagnetic superconductors*,
T. Yokoyama and Y. Tanaka,
Phys. Rev. B **75**, 132503 (2007)

15. *Enhanced triplet superconductivity in noncentrosymmetric systems*,
T. Yokoyama, S. Onari and Y. Tanaka,
Phys. Rev. B **75**, 172511 (2007)
16. *Quantitative model for the $I_C R$ product in d -wave Josephson junctions*,
T. Yokoyama, Y. Sawa, Y. Tanaka, A. A. Golubov, A. Maeda, and A. Fujimaki,
Phys. Rev. B **76**, 052508 (2007)
17. *Andreev bound states and tunneling characteristics of a non-centrosymmetric superconductor*,
C. Iniotakis, N. Hayashi, Y. Sawa, T. Yokoyama, U. May, Y. Tanaka
and M. Sigrist,
Phys. Rev. B **76**, 012501 (2007)
18. *Theory of Macroscopic Quantum Tunneling in High- T_C c -Axis Josephson Junctions*,
T. Yokoyama, S. Kawabata, T. Kato and Y. Tanaka,
Phys. Rev. B **76**, 134501 (2007)
19. *Fulde-Ferrell-Larkin-Ovchinnikov state of superconductors with and without inversion symmetry: Hubbard model approach*,
T. Yokoyama, S. Onari and Y. Tanaka,
submitted to Phys. Rev. B
20. *Identifying the odd-frequency pairing state of superconductors by a field-induced Josephson effect*,
J. Linder, T. Yokoyama, and A. Sudbø,
submitted to Phys. Rev. Lett.
21. *Quantum transport in a normal metal/odd-frequency superconductor junction*,
J. Linder, T. Yokoyama, Y. Tanaka and A. Sudbø,
submitted to Phys. Rev. B
22. *Odd-frequency pairing state inside the Abrikosov vortex core*,
T. Yokoyama, Y. Tanaka, and A. A. Golubov,
submitted to Phys. Rev. Lett.

23. *Chirality sensitive effect on surface states in chiral p-wave superconductors*,
T. Yokoyama, C. Iniotakis, Y. Tanaka, and M. Sigrist,
submitted to Phys. Rev. Lett.
24. *Spin-polarized proximity effect in superconducting junctions*,
T. Yokoyama and Y. Tanaka
Comptes Rendus Physique Volume **7**, 2006, Pages 136-149.
25. *Wiedemann-Franz law in proximity bilayers*,
T. Yokoyama, Y. Tanaka, A. A. Golubov, J. Inoue and Y. Asano
Journal of Physics and Chemistry of Solids Volume **66**, Issues 8-9, 2005,
Pages 1398-1400.
26. *Meissner effect in diffusive normal metal / d-wave superconductor junctions*,
T. Yokoyama, Y. Tanaka, A. A. Golubov, J. Inoue and Y. Asano
Journal of Physics and Chemistry of Solids Volume **66**, Issues 8-9, 2005,
Pages 1395-1397.
27. *Meissner effect in diffusive normal metal / s-wave superconductor junctions*,
T. Yokoyama, Y. Tanaka, A. A. Golubov, J. Inoue and Y. Asano
Physica C: Superconductivity Volumes **426-431**, 2005, Pages 262-267.
28. *Charge transport in the normal metal / diffusive ferromagnet / s-wave superconductor junctions*,
T. Yokoyama, Y. Tanaka, A. A. Golubov, J. Inoue and Y. Asano
Physica E: Low-dimensional Systems and Nanostructures Volume **29**,
Issues 3-4 , 2005, Pages 520-524.
29. *Theory of charge transport in diffusive normal metal / superconductor point contacts in the presence of magnetic impurity*,
T. Yokoyama, Y. Tanaka, A. A. Golubov, J. Inoue and Y. Asano
Journal of Physics and Chemistry of Solids Volume **67**, 2006, Pages 68-71

30. *Josephson current between p-wave superconductors*,
T. Yokoyama, Y. Tanaka, A. A. Golubov and Y. Asano
Physica C Volumes **445-448**, 2006, Pages 963-966
31. *Theory of charge transport in high- T_C superconductor junctions from the view point of the mid gap Andreev resonant state*,
Y. Tanaka, S. Kashiwaya, Y. Asano and T. Yokoyama
Physica C Volume **435**, 2006, Pages 1-7
32. *Thermal broadening effect on the tunneling conductance in diffusive normal metal / superconductor junctions*,
I. Shigeta, T. Yokoyama, Y. Asano and Y. Tanaka
AIP Conference Proceedings, Vol. **850**, 2006, pp.999-1000
33. *Charge transport in 2DEG/s-wave superconductor junction with Dresselhaus-type spin-orbit coupling*,
Y. Sawa, T. Yokoyama, and Y. Tanaka
Journal of Magnetism and Magnetic Materials, Volume **310**, 2007,
Pages 2277-2279
34. *Theory of tunneling conductance in normal metal/triplet superconductor junctions without inversion symmetry*,
T. Yokoyama, Y. Tanaka and J. Inoue
Journal of Magnetism and Magnetic Materials, Volume **310**, 2007,
Pages 660-662
35. *Theory of Josephson effect in d-wave superconductor/diffusive ferromagnet/d-wave superconductor junctions*,
T. Yokoyama, Y. Tanaka and A.A. Golubov
Journal of Magnetism and Magnetic Materials, Volume **310**, 2007,
Pages 498-500
36. *Proximity effect in NS junctions in the presence of Anderson impurities*,
T. Yokoyama, Y. Tanaka and A. A. Golubov
Pages 266-268 in "Frontiers of Computational Science" edited by Y. Kaneda and M. Sasai, Springer, 2007

37. *Wiedemann-Franz law in diffusive normal metal /p-wave superconductor junctions*
 T. Yokoyama, Y. Tanaka, A. A. Golubov and Y. Asano
 Pages 269-272 in "Frontiers of Computational Science" edited by Y. Kaneda and M. Sasai, Springer, 2007
38. *Theory of Josephson Effect in Sr₂RuO₄/Diffusive Ferromagnet/Sr₂RuO₄ Junctions*
 Y. Sawa, T. Yokoyama, Y. Tanaka and A. A. Golubov
 Journal of Low Temperature Physics **148**, 887 (2007)
39. *Dependence of Josephson Current on Orientational Angle in Diffusive p -Wave Superconductor Junctions*
 Y. Sawa, T. Yokoyama, Y. Tanaka and A. A. Golubov
 Journal of Low Temperature Physics **148**, 881 (2007)
40. *Theory of Josephson effect in Sr₂RuO₄/diffusive normal metal/Sr₂RuO₄ junctions*
 Y. Sawa, T. Yokoyama, Y. Tanaka and A. A. Golubov
 Physica C: Superconductivity, Volumes **463-465**, 2007, Pages 997-1000
41. *Theory of macroscopic quantum coherence in d-wave superconductor junctions*
 T. Umeki, T. Kato, T. Yokoyama, Y. Tanaka, S. Kawabata and S. Kashiwaya
 Physica C: Superconductivity, Volumes **463-465**, 2007, Pages 157-160
42. *Temperature dependence of tunneling conductance in diffusive normal metal/triplet superconductor junctions*
 I. Shigeta, T. Yokoyama, Y. Asano, F. Ichikawa and Y. Tanaka
 Physica C: Superconductivity, Volumes **460-462**, 2007, Pages 1319-1320